NASA CONTRACTOR REPORT

NASA CR-2049

THE GEOMETRY AND PHYSICAL PROPERTIES OF EXHAUST CLOUDS GENERATED DURING THE STATIC FIRING OF S-IC AND S-II ROCKET ENGINES

by Richard E. Forbes, Michael R. Smith, and Ralph R. Farrell

Prepared by
INSTITUTE OF ENVIRONMENTAL SCIENCES
MISSISSIPPI STATE UNIVERSITY
State College, Miss.
for

NATIONAL AERONAUTICS AND SPACE ADMINISTRATION • WASHINGTON, D. C. • JUNE 1972

TECHNICAL REPORT STANDARD TITLE PAGE

1. REPORT NO.	2. GOVERNMENT ACCESSION NO.	3. RECIPIENT'S CATALOG NO.
NASA CR-2049		

4. TITLE AND SUBTITLE	5. REPORT DATE
THE GEOMETRY AND PHYSICAL PROPERTIES OF EXHAUST CLOUDS GENERATED DURING THE STATIC FIRING OF S-IC AND S-II ROCKET ENGINES	June 1972
	6. PERFORMING ORGANIZATION CODE

7. AUTHOR(S)	8. PERFORMING ORGANIZATION REPORT #
Richard E. Forbes, Michael R. Smith, and Ralph R. Farrell	IES-7-10-2

9. PERFORMING ORGANIZATION NAME AND ADDRESS	10. WORK UNIT NO.
Institute of Environmental Sciences Mississippi State University State College, Mississippi	11. CONTRACT OR GRANT NO. NGL 25-001-32
	13. TYPE OF REPORT & PERIOD COVERED
12. SPONSORING AGENCY NAME AND ADDRESS	CONTRACTOR REPORT
NASA Washington, D. C. 20546	14. SPONSORING AGENCY CODE

15. SUPPLEMENTARY NOTES

16. ABSTRACT

An experimental program was conducted at the NASA Mississippi Test Facility at Bay Saint Louis, Mississippi during the static firing of the S-IC-13, -14, and -15 rocket engines and the S-II-13, -14, and -15 rocket engines. The data compiled during the experimental program consisted of photographic recordings of the time-dependent growth and diffusion of the exhaust clouds, the collection of meteorological data in the ambient atmosphere, and the acquisition of data on the physical structure of the exhaust clouds which were obtained by flying instrumented aircraft through the clouds.

A new technique was developed to verify the previous measurements of evaporation and entrainment of blast deflector cooling water into the cloud. Small hollow glass spheres (approximately 10 microns in diameter) were injected into the cooling water at the pumping station. These particles were subsequently detected on all passes through the clouds by using an impact-type sampler. The particles are clearly identifiable under a microscope and are also sufficiently small that they may be injected into natural clouds at the updrafts near the base of the clouds.

The results of this experimental program indicates that at the lower altitudes the rocket exhaust cloud or plume closely resembles a free-jet type of flow. At the upper altitudes, where the cloud is approaching an equilibrium condition, the structure is very similar to a natural cumulus cloud.

17. KEY WORDS	18. DISTRIBUTION STATEMENT
Cloud growth Mass-Energy conditions Mass-Energy flux Diffusion	

19. SECURITY CLASSIF. (of this report)	20. SECURITY CLASSIF. (of this page)	21. NO. OF PAGES	22. PRICE
Uncl	Uncl	104	$3.00

*For sale by the National Technical Information Service, Springfield, Virginia 22151

TABLE OF CONTENTS

LIST OF FIGURES

LIST OF FIGURES (Continued)

LIST OF FIGURES (Concluded)

INTRODUCTION

The prediction of the growth and diffusion characteristics of natural and man-made clouds and exhaust plumes has been the object of much research during the past fifty years. Most of this work has been of an empirical nature and involved the prediction of the trajectory of the cloud or plume axis under fairly uniform meteorological conditions and other associated restrictive assumptions. During the past two years a research team from Mississippi State University has been attempting to develop numerical simulation techniques which will permit the prediction of the growth and diffusion of exhaust clouds which are generated during the static firing of various size rockets under arbitrary meteorological conditions. The verification of the numerical simulation model required the acquisition of various experimental data to test the reliability and accuracy of the prediction scheme under various meteorological conditions.

The experimental program was conducted at the NASA Mississippi Test Facility at Bay Saint Louis, Mississippi during the static firing of the S-IC-13,-14 and -15 rocket engines and the S-II-13,-14, and -15 rocket engines. The data compiled during the experimental

program consisted of photographic recordings of the time-dependent growth and diffusion of the exhaust clouds, the collection of meteorological data in the ambient atmosphere, and the acquisition of data on the physical structure of the exhaust clouds which were obtained by flying instrumented aircraft through the clouds.

The results of this experimental program indicates that at the lower altitudes the rocket exhaust cloud or plume closely resembles a free-jet type of flow. At the upper altitudes, where the cloud is approaching an equilibrium condition, the structure is very similar to a natural cumulus cloud. The photographic records of the cloud growth have been normalized through the use of an image rectifier to give a true shape of the normalized cloud. The condensation of the water vapor at the upper altitudes gives indication of the general structure and shape of the exhaust cloud; however, it was noted, through the use of infrared color film, it was possible to differentiate between the exhaust product cloud and the water vapor cloud and that the water vapor cloud did not necessarily define the true extent of the exhaust products cloud. The distribution of dry bulb temperature and relative humidity throughout the exhaust clouds during the various stages of development and dissipation are shown graphically in text. In addition a mass-energy balance was established for the S-IC rocket

exhaust cloud and the results indicate that approximately 100% of the cooling water supplied to the exhaust gas deflector is vaporized and entrained in the exhaust jet.

DESCRIPTION OF EXPERIMENTAL PROGRAM

Photographic records of the time dependent growth and dissipation of the rocket exhaust cloud were made utilizing 16 mm movie film recording at 12 frames per second, and both color and infrared color film in a K-17B camera. The K-17B (9.5 inch film) was actuated with an intravelometer which was set to fire every five seconds. In addition, 35 mm and 4½ x 5 cameras were used to obtain photographs of the cloud from fixed wing aircraft. The ground-based cameras were mounted on top of the Central Control Building (Building 1200) which was located approximately 3700 meters (12,200 feet) from the S-IC test stand and approximately 3000 meters (10,000 feet) from the A-2 test stand. (Figure 1).

Meteorological data on the temperature structure of the atmosphere and the magnitude and direction of the upper winds was obtained from the U. S. Weather Bureau located at MTF. On the day of a static firing, meteorologists released radiosonde equipped balloons every three hours for approximately 12 hours prior to the scheduled static firing in order to assure that rapid changes in the upper atmosphere did not occur which would lead to undesirable acoustic

reflections. An additional sounding was made one hour prior to the scheduled firing. A radiosonde and balloon were released at engine ignition in order to map the structure of the atmosphere during the time the rocket engine was actually firing. In most cases only minor changes of the structure of the atmosphere occurred during the several hours preceding the static firing; therefore, the meterological data taken during the static firing was actually used to compare with the data acquired by the aircraft.

A compact, lightweight airborne data acquisition system (ADAS) was constructed by the research team to be installed in a single engine aircraft to make probings through the exhaust cloud during its growth and dissipation. The system was installed in a Piper PA-24 aircraft and had the capability of recording all the airborne data on analog tape or of telemetering the data directly to the Data Handling Center at the Mississippi Test Facility. In all tests the data were recorded on-board and at the same time telemetered to the DHC for real-time processing. In this manner the data were available for immediate review.

The normal mode of data acquisition was to telemeter the data directly from the aircraft to the data handling center at NASA-MTF. An omni-directional antenna mounted on the roof of the Data Handling Center was utilized for data acquisition. At the test recording

station, the acquired data were simultaneously recorded on analog tape and also processed through an analog-digital converter. The digital information was run through a calibration routine to convert the digital index value to a true engineering unit (TEU). The TEU data was then stored in a digital format on magnetic tape and this provided the basis for all future data reduction processes. The data reduction system was so designed that oscillograph plots of all the variables could be presented simultaneously with data reduction.

Due to the large updrafts which occurred in the clouds, the aircraft gained several hundred feet during a typical pass though the cloud, such that the measurement of temperature had little significance if it was referenced to the temperature at the point of penetration. In order to correct for this deficiency the temperature in the cloud was referenced to the ambient temperature at the same altitude. A calibration curve for the atmospheric temperature was composed from the pre-test and post test calibration data. Thus at a given altitude, an undisturbed temperature could be obtained from the calibration curve. If the aircraft climbed during the test run it was possible to reference the temperature at any particular instance and time to the undisturbed temperature at the same altitude outside the cloud. In this manner, a temperature difference ΔT was defined such that the temperature difference was zero outside

the cloud, and the shape of the temperature distribution curve was an indication of the temperature distribution at some mean altitude which occurred during the test run.

Pre-test and post-test calibrations were made on the airborne data system and these calibrations were checked against the meteorological data to ensure good correlation.

REDUCTION OF PHOTOGRAPHIC RECORDS

The 9½ inch film from the K-17B camera was utilized to obtain the time-dependent growth and dissipation histories of the rocket exhaust clouds. The film was installed in a Weston photographic image rectifier and the correct elevation and azimuth angles of the camera were set into the device so that a normalized view of the exhaust cloud was projected upon the recording plane. The edge of the exhaust jet and the condensation cloud were traced upon the drafting paper which was attached to the normalized plane. By repeating the tracings at various time intervals, a time sequence and history of the cloud growth was obtained. In order to check the accuracy of the normalized view of the cloud and assure that the proper elevation and azimuth angle were utilized, the height of the cloud at various time intervals was noted from the various aircraft that were used during the experiment. These heights and times were then used to cross reference the altitude of the cloud at the

identical times as it was shown in the normalized plane. In all instances the final projection in the normalized plane agreed within less than two and one half percent of that observed by the aircraft.

METEOROLOGICAL DATA

The meteorological data obtained from the radiosonde released at the time of engine ignition was utilized to define the temperature distributions and wind velocity field in the region immediately above and adjacent to the test stands. Complete tabulation of the meteorological data obtained during these tests is presented in Appendix I. Plots of the temperature distribution and the relative humidity distribution in the atmosphere are presented as functions of altitude for each test condition.

ACQUISITION OF AIRBORNE DATA

At the beginning of this project it was anticipated that the photographic records would yield good time-dependent history of the growth and dissipation of the water vapor cloud and that the exhaust products would be encompassed in this cloud. Analysis of photographic records from an S-IC static firing indicated that the boundary of the exhaust products cloud could possibly be quite different from that of the water vapor cloud due to the difference in density and molecular weight of the two gases. At this point

it was deemed desirable to equip an aircraft with adequate instrumentation to delineate the temperature and liquid water content distributions in the cloud, such that the predictions from the numerical simulation program could be correlated with the physical structure of the cloud. In addition, the properties of such an exhaust cloud have not previously been defined and it was anticipated that a cloud could possibly be utilized for weather modification research. Utilizing a surplus S-IB telemetry package and spare components located on the test facility, the research team assembled a compact, lightweight airborne data acquisition system which was installed in a single engine aircraft. The total self-contained package weighed approximately 250 pounds including approximately 100 pounds of NI-CAD batteries.

The temperature sensors for the airborne package were developed utilizing thermistors mounted in a cylindrical housing with one of the thermistors moistened continuously to provide a wet bulb temperature reading. The temperature head was calibrated using an improvised flow chamber which simulated the flow velocities that were being encountered during the test program. It was felt that the care utilized in the design of the flow chamber and in the calibration of the temperature sensors was such that the final data were extremely reliable. The airborne temperature data compared very favorably with that obtained from the radiosonde.

Prior to the acquisition of test data during a static firing, a pre-test calibration was run by flying the aircraft at various airspeeds at a mean altitude that was thought to be representative of that at which the predominance of test runs would be made. In addition, the aircraft was flown at some mean airspeed at three or four different altitudes in order to establish a good temperature versus altitude calibration. During the static firing, the pilot of the aircraft waited until the exhaust cloud approached its equilibrium altitude before penetrating the cloud. Extreme turbulence and updrafts were encountered in several of the firings; however, the aircraft was always operated to prevent over-stressing its structure. In most cases moderate to severe turbulence was encountered as the aircraft penetrated the condensation cloud; however, the core of the cloud appeared tc be fairly laminar such that the pilot experienced almost no turbulence during the time he was passing through the center of the cloud. During eacn run the aircraft was flown on a more or less north to south path such that the aircraft data were obtained in the same plane as the photographic data. In this manner a cross correlation of cloud thicknesses could be obtained. Immediately following the static firing and after the exhaust cloud dissipated, the aircraft conducted a post-test calibration in order to determine the possibility of calibration drift during the test run. In most cases it was not necessary to

make corrections in the data due to the stable design of the amplifiers.

REDUCTION OF AIRBORNE DATA

Data obtained by the airborne data acquisition system included dry and wet bulb temperatures, aircraft airspeed, pressure altitude, and an event marker to indicate cloud penetration and exit. The event marker was manually activated by the pilot upon entry and exit of the cloud. Due to the importance of obtaining valid measurements with the dry and wet bulb thermistors, this system was duplicated in order that these variables could be recorded on two independent systems. Following a flight the raw data were transformed, using appropriate calibration factors, into true engineering units. Upon obtaining the true engineering units data, an analysis was undertaken to determine the best manner in which the data should be presented to give a physically realistic description of events in and surrounding the cloud.

Radiosonde data were available for each firing from a sounding beginning at the time of engine ignition. It was felt that, wherever possible, the data acquired by the aircraft should be compared with that obtained from the radiosonde sounding. Dry bulb temperatures obtained by the aircraft could be compared directly with

ambient temperature readings recorded by the radiosonde at a given altitude. In addition, conversion of the aircraft dry and wet bulb readings into relative humidity would allow a comparison of this variable with that obtained by the radiosonde at a given altitude. Measurements within the cloud would indicate the deviation of relative humidity and temperature from ambient at a given altitude. Since it was impossible to maintain aircraft altitude in the rapidly developing cumulus clouds, it was necessary that all measurements be referred to the undisturbed or ambient conditions at a given altitude. The instantaneous value of relative humidity within the cloud has direct meaning since it represents the moisture content in the cloud as compared to ambient conditions surrounding the cloud. However, when analyzing temperatures within the cloud one must account not only for the measured value compared to ambient but any changes induced by climbing or driving of the aircraft.

The following procedures were utilized in converting the dry and wet bulb temperatures into relative humidity and temperature deviations from ambient within the cloud (disturbed temperature).

The instantaneous aircraft altitude was indicated by a sensitive calibrated altimeter set to 1013.2 millibars (29.92 inches of mercury) prior to take off. It is assumed, in all calculations, that the altitude as measured by the altimeter is the correct value of

this variable.

In order to calculate relative humidity values from dry and wet bulb temperatures, one must account for the ambient pressure at which the readings were taken. The standard psychrometric chart is, in general, referenced to a sea level pressure of 1013.2 millibars and is not usable for our purpose. However, if one knows the altitude (and thus pressure) at which the aircraft is flying, psychrometric relations may be developed from basic thermodynamic considerations which will give the correct value of relative humidity at that altitude when the dry and wet bulb temperatures are known. Altitudes measured by the aircraft were converted to pressure using the I.C.A.N. (International Commission for Air Navigation) atmosphere:

$$P = 1013.2 \left[\frac{1 - 0.0065Z}{288} \right]^{5.2568}$$

where P is in millibars and Z in meters. Since the altimeter was set to 1013.2 millibars prior to take off, it was felt that this procedure provided sufficient accuracy for purposes of calculating relative humidity at a given altitude. Pressures thus calculated were utilized along with dry and wet bulb temperatures to calculate the relative humidity at a given altitude. The psychrometric routine used to perform these calculations was developed from basic thermodynamic considerations and gave good results when compared to

the variable pressure psychrometric chart given by Berry, Bollay, and Beers (1). A documented copy of the psychrometric routine is on file with the Data Handling Center at NASA Mississippi Test Facility. Recorded relative humidity as calculated from this procedure should be nearly instantaneous, possessing only the time lags inherent in the thermistors and the altitude (of order one tenth second).

It is a recognized fact that the earth's atmosphere is not homogenous and that one may measure spatial variations of some property even when flying at a fixed altitude. This factor was readily apparent when attempts were made to indicate cloud temperatures in useable form. Temperatures indicated within the clouds were influenced by two factors; the variation due to the presence of the cloud and the changes produced by climbing and diving of the aircraft while in the cloud. Both factors must be accounted for in an analysis of temperature disturbances (relative to ambient) produced by the clouds.

The following procedure was utilized to provide the most meaningful indication of the temperature disturbances created by the clouds. Dry bulb temperatures, as measured outside the clouds, were used along with altitude to obtain a relationship between altitude and dry bulb temperature when these variables were not under the influence of a cloud. Standard least squares techniques

were used to obtain a relationship giving the best temperature (in the least squares sense) when the altitude was known. It was determined that a linear relationship of the form:

$$T_{calc.} = a + bZ$$

gave sufficient accuracy for our purposes since the altitude change of the aircraft was generally less than 500 meters for successive passes through the cloud on a given firing. $T_{calc.}$ is the expected temperature at a given altitude Z if one is outside the influence of the cloud. Although this relationship was obtained by fitting data outside clouds, it could now be used to calculate the temperature one would expect to measure in the cloud at a given altitude if the cloud had no influence on the temperature. A comparison of $T_{calc.}$ and the actual dry bulb temperature measured at a given altitude would indicate the disturbance in temperature produced by the cloud presence. This temperature difference, where

$$\Delta T = T_{meas.} - T_{calc.}$$

indicates heating in the cloud (relative to ambient) if ΔT is greater than zero or cooling if ΔT is less than zero. Calculations have been performed using the data from both dry bulb systems.

As was expected, there were slight differences in the absolute

magnitudes of relative humidity and disturbed temperature as measured by the two independent dry-wet systems on the aircraft. These differences were, in general, negligible and more importantly the trend as indicated by the two systems was similar in all cases. This will be discussed in more detail when considering the analysis of the data.

At this point, consideration will be directed to the analysis of data as obtained for particular firings. Meaningful data were recorded for the following four static firings:

S-IC-13	6 February 1970
S-IC-15	30 September 1970
S-II-14	31 July 1970
S-II-15	30 October 1970

The S-IC stage is fueled by a LOX-RP1 system whereas the S-II is a LOX-Liquid Hydrogen system. The fuel flow, heat release, and firing duration of the two stages differ significantly and thus one would not expect the cloud geometry and composition to be similar for the two stages. In addition, meteorological parameters will significantly affect the growth and dissipation of the clouds. These factors will be considered in the following discussion.

DATA FOR SIC ROCKET EXHAUST CLOUDS

S-IC-13 6 February 1970

The data to be discussed will be similar for each of the four firings. These will include a listing of the pertinent radiosonde meteorological parameters, typical photographs from which the rectified cloud images were traced, typical rectified cloud geometry, relative humidity profiles within the clouds, and disturbed temperature profiles in the clouds. Complete radiosonde soundings are presented in the appendices along with the entire set of rectified cloud images and typical tabulated data recorded in the clouds by the airborne data acquisition system.

For cloud S-IC-13, airborne data were recorded by a research aircraft from Pennsylvania State University in addition to the data recorded by the Mississippi State aircraft. The Penn. State aircraft operated independently of the MSU task, funding being provided by the MITRE Research Corporation of Bedford, Massachusetts. The duplication of effort on firing S-IC-13 was indeed fortunate since the magnetic tape containing the data from the MSU aircraft was misplaced or erased prior to the recording of a hard copy of the data. In general, the Penn. State aircraft penetrated the S-IC cloud in the vicinity of 4500 meters (15,000 feet) MSL while the penetrations made by the MSU aircraft were in the vicinity of 3000 meters (10,000 feet) MSL.

Radiosonde soundings of ambient temperature and relative humidity have been plotted versus altitude in meters in Figures 2 and 3. These figures are presented first in order that subsequent measurements and observations may be analyzed in light of the prevailing meteorological conditions. The temperature inversion in the vicinity of 1000-2000 meters in Figure 2 should be expected to affect the cloud geometry as will be shown later. The relative humidity profile may be used as a cross check on humidities recorded by the aircraft outside the clouds when aircraft altitude is known.

In general, several penetrations of each cloud were made by the aircraft for a particular static firing. In the following discussion, these penetrations will be referred to in chronological order as Pass 1, Pass 2, etc.

Rectified cloud geometry was determined from the 9.5 inch photographic plates by the method previously discussed. Prints of typical photographs for firing S-IC-13 are shown in Figures 4, 5, and 6 at 20, 60, and 160 seconds after engine ignition. The test stand and other physical characteristics of the Mississippi Test Facility are clearly evident in the photographs and were used in developing the appropriate length scales and angles necessary to produce the rectified images. The prints shown in Figures 4, 5, and 6 are necessarily shown in black and white, however, it should be emphasized that the original plates from which the rectified clouds were produced

were in color. The color film gave superior resolution of the cloud geometry against the background as compared to black and white photography and this characteristic cannot be adequately shown in the black and white prints.

Several interesting features of the cloud are evident in Figures 4, 5, and 6. The cloud is well defined against the background since the LOX-RP1 system produces a dark gray exhaust emission. Figure 4 indicates that the initial phase of cloud development is predominately a free jet type of flow since the cloud angle to the horizontal is approximately 30 degrees. The angle between the blast deflector axis and the horizontal is 30 degrees and this factor dominates the cloud geometry during the early stages of development. Figure 5 shows that free convection or buoyancy has become important in the growth process since the angle between the cloud axis and the ground is now approximately 45 degrees. Engine cut off for S-IC-13 was at approximately 125 seconds after ignition. Figure 6 indicates that the lower portion of the cloud had begun to detach from the test stand at 160 seconds with a small residual dark cloud in the vicinity of the test stand.

The color negative from which Figure 6 was printed showed that the cloud underwent a condensation process at a specific altitude. The white portion of the cloud in which condensation was occuring could be clearly delineated from the gray non-condensible exhaust

products in the cloud. The altitude at which condensation was first observed has been indicated on the rectified images which were traced from the color negatives.

The time dependent cloud geometry for cloud S-IC-13 is shown in Figures 7 and 8. The 300 meter length scale provides a reference from which cloud dimensions may be determined. The K-17 cameras provided only 205 seconds of coverage for this particular firing, however Figure 8 shows that the vertical development of the cloud had exceeded the field of view of the camera at this time. The cloud top is approximately 4000 meters above the ground at 160 seconds after engine ignition and moves out of the field of view prior to the next photograph (5 seconds between photographs).

The approximate vertical growth rate of the cloud may be determined by making measurements between successive traces on Figures 7 and 8. The maximum vertical growth rate for firing S-IC-13 occurred between 130 and 160 seconds where the height increased approximately 1200 meters in 30 seconds, giving an average growth rate of 40 meters per second. The maximum rate of climb as measured by the Penn. State aircraft while in the S-IC cloud was approximately 38 meters per second which compares favorably with the growth rates measured from the cloud geometry.

The dashed horizontal line on Figure 8 (approximately 1740 meters above the surface) indicates the altitude at which condensation was

first observed in the cloud photographs. The condensation process begins in the vicinity of the temperature inversion in the vicinity of 1000-1700 meters as indicated by the radiosonde data of Figure 2. The latent heat released in the condensation process provides the heat input to the cloud to continue the cumulus development to higher altitudes after engine cut off.

Three passes were made through cloud S-IC-13 by the Penn. State aircraft. Engine ignition was at 1546:41 Central Standard Time with entry into the cloud first made at 1555:33; or approximately nine minutes after engine ignition. Aircraft elevation at entry into the cloud was approximately 4250 meters for all three passes.

The relative humidity profiles of the cloud are shown in Figures 9, 10 and 11 where relative humidity has been plotted versus time. The dashed vertical lines indicate cloud penetration on the left and cloud exit on the right. Figures 9,10, and 11 indicate good comparison between the aircraft data and radiosonde data for relative humidity when the aircraft is outside the cloud; the value being of order 80% at the penetration altitude. Figure 9 indicates that relative humidities of approximately 125% are encountered half way through the cloud, this value decreasing back to ambient conditions prior to exit from the cloud. The super-saturated conditions indicate the unstable nature of the cloud at this point in time. The relative humidity measurements were made through a reverse flow

psychrometer, thus there is no possibility of water droplet impact affecting the measurement. Maximum relative humidities encountered on pass 2 through the cloud were approximately 100% indicating a saturated condition near the center of the cloud.

A sharp decline in relative humidity was noted near the center of the cloud during pass 3 as shown in Figure 11. This decrease was caused by a decrease in aircraft altitude near the center of the cloud during pass 3. The aircraft entered the cloud at 4200 meters, descended to 3900 meters at the center of the cloud, and exited the cloud at 4100 meters. Reference to the radiosonde sounding (Figure 3) shows that one would expect the relative humidity to vary as shown in Figure 11 if, in the latter stages of cloud development, the ambient conditions were impressed on the cloud during the dissipation phase.

Cloud disturbed temperature has been plotted versus time in Figures 12, 13, and 14. Reference to these figures indicates that, statistically, the cloud has reached temperature equilibrium with the ambient atmosphere at the time of the first pass. Passes two and three indicate temperature equilibrium with the ambient atmosphere; local temperature deviations of order ½ degree centigrade being the maximum recorded in the cloud.

Figures 15 and 16 contain temperature and relative humidity histories of the ambient atmosphere recorded by radiosonde at ignition time for firing S-IC-15. The measured temperature lapse rate is significantly less than the adiabatic lapse rate in the vicinity of 1500 - 3000 meters. The average relative humidity is approximately 20 - 40% which is considerably less than that recorded for firing S-IC-13. Cloud photographs are shown in Figures 17 and 18 at 65 seconds and 200 seconds after ignition, respectively. The effect of wind on the cloud geometry is apparent in the preceeding figures, showing that the cloud has been displaced to directly above the test stand at 200 seconds after ignition. Complete wind profiles are shown in Appendix I.

Rectified cloud images in Figures 19, 20, and 21 show the cloud geometry from 50 to 325 seconds after ignition. The cloud detaches from the vicinity of the test stand between 125 and 155 seconds and continues the growth process while drifting to the south. Condensation was first observed at an altitude of approximately 1680 meters as shown on Figure 20. It will be recalled that this is in the vicinity of the region of constant temperature lapse rate.

Engine ignition for S-IC-15 was at 1817:05 Central Daylight Time. Four passes were made through the cloud by the MSU aircraft while the Penn. State aircraft made 3 passes. The entry and exit altitudes for each aircraft on each pass are shown in Table 1.

Table 1. Cloud Entry and Exit Altitudes S-IC-15

MSU			PENN. STATE		
	IN	OUT		IN	OUT
Pass 1	3120 m.	3480 m.	Pass 1	3635 m.	3489 m.
Pass 2	3140 m.	2930 m.	Pass 2	3518 m.	3459 m.
Pass 3	2460 m.	2490 m.	Pass 3	3424 m.	3276 m.
Pass 4	2600 m.	2600 m.			

The Penn. State aircraft first entered the cloud approximately 6 minutes after engine ignition whereas the MSU aircraft made pass 1 approximately 3 minutes after ignition. To preserve the chronology of events the MSU cloud data will be discussed first, however one

should be aware that during the latter passes both aircraft may have been in the cloud at the same time. The times of entry and exit may be determined from the figures.

Relative humidity histories in the cloud as measured by System 1 on the MSU aircraft are shown in Figures 22, 23, 24, and 25. The data will only be shown for System 1 since it was determined that data recorded were essentially the same for both systems.

Figure 22 is perhaps the most interesting data recorded during this work. The relative humidity rises sharply to 100% on entry into the cloud, decreases near the center of the cloud and again rises to around 100% after passing the center of the cloud. The vortex nature of the cloud is evidenced in this data, the relative humidity at the center being lower than 100% because of entrainment of ambient air into the center of the vortex. The response of the system is seen to be good as indicated by the rapid return to ambient on cloud exit.

Subsequent figures indicate that the cloud relative humidity is only slightly disturbed from ambient for passes 2, 3, and 4. Pass 2 was begun approximately 7 minutes after ignition, indicating that the cloud rapidly reaches equilibrium with the surrounding atmosphere.

Disturbed temperature is given in Figures 26, 27, 28, and 29 for the four passes through the cloud.

The first pass through the cloud produced unexpected results in the disturbed temperature measurement as shown in Figure 26. The data (System 1) recorded on pass 1 are shown in Table 2.

Table 2: Recorded Data - MSU Aircraft

TIME (SEC.)	T_D (°F)	T_W (°F)	ALTITUDE (FEET)	RELATIVE HUMIDITY (%)
1820:12	49.2	31.5	10279	16
:13	47.4	31.7	10234	17
:14	44.1	32.6	10194	28
:15	39.6	33.2	10237	45
:16	36.4	33.5	10301	70
:17	35.5	33.4	10277	77
:18	34.5	33.6	10396	89
:19	36.1	34.4	10388	84
:20	36.6	35.0	10438	84
:21	35.7	35.1	10451	92
:22	34.2	34.8	10478	104
:23	35.0	34.2	10553	95
:24	35.0	33.8	10587	87
:25	35.8	33.2	10642	77
:26	36.8	32.9	10746	68
:27	38.9	33.6	10772	57
:28	39.8	34.5	10827	56
:29	39.3	35.0	10890	62
:30	39.0	35.2	10930	66
:31	38.6	35.3	10937	71
:32	38.4	35.5	10982	74
:33	38.4	35.4	11034	73
:34	38.5	35.6	11144	74
:35	37.8	35.7	11164	76
:36	36.8	35.7	11318	88
:37	36.5	35.5	11329	88
:38	36.1	35.6	11341	95
:39	36.0	35.5	11475	95
:40	35.9	35.0	11478	91
:41	36.1	34.6	11483	88
:42	37.7	33.9	11495	73
:43	40.0	32.9	11435	50
:44	41.4	32.4	11452	40
:45	42.1	31.7	11423	34
:46	42.7	31.2	11442	30
:47	43.2	30.7	11407	27
:48	43.7	30.3	11401	24
:49	44.0	30.0	11398	22
:50	44.2	29.7	11374	21
:51	44.3	29.4	11357	20
:52	44.5	29.3	11383	19
:53	44.7	29.1	11317	18

Data presented are time (seconds), dry bulb temperature (^{o}F), wet bulb temperature (^{o}F), aircraft altitude (feet), and relative humidity (%). These data are typical, however the complete set would also contain the dry and wet bulb temperatures as recorded on System 2 and the second calculated relative humidity.

The relative humidity increased rapidly from 15 - 20% to approximately 100% as entry was made into the cloud. In the areas of high relative humidity the dry and wet bulb readings are essentially identical; for example at time 1820:21 T_D = 35.7^{o}F and T_W= 35.1^{o}F. This indicates a significant cooling of the cloud relative to the ambient surroundings since the cloud temperature is indicated both by the wet bulb and dry bulb when the relative humidity is 100%. No liquid water content (rain) was observed by the pilot during the first pass, indicating that the dry bulb temperature suppression was not produced by "wet bulbing" on the dry thermometer.

The reduced temperature in the cloud can only be explained by adiabatic expansion of the cloud which produces the cooling effect. The momentum of the exhaust jet is sufficient to transport the cloud to altitude and the resulting expansion process, when assumed adiabatic, will produce significant reductions in the cloud temperature. This produces a highly unstable situation and the cloud must

be penetrated during the early stages of development to observe this phenomenon. For example, Figure 27 shows that approximately 4 minutes later the cloud has areas that are above as well as below ambient temperature. Pass 3 (in Figure 28) indicates that the temperature depression is completely absent and the cloud has attained a central temperature which is approximately 4° Centigrade above ambient. Figure 29 indicates that the cloud is tending to approach equilibrium with the surroundings, the central heated region being much smaller and the disturbed temperature around 3°C. above ambient.

The relative humidity and disturbed temperature traces recorded by the Penn. State aircraft in cloud S-IC-15 are shown in Figures 30 through 35. The first pass was made through the cloud approximately 4 minutes after engine ignition. Figure 30 indicates relative humidities of 30% above ambient for the first pass; a slight rise above ambient near the cloud center for pass 2 (Figure 31) and little or no change for pass 3 (Figure 32).

Figure 33 indicates that the Penn. State aircraft also experienced a cooling effect upon entering the cloud for the first pass. The temperature at the cloud center was measured at approximately 5°C. below ambient. Pass 2 (Figure 34) indicated that the cloud was still cooler than ambient, but only near the center of the cloud.

Pass 3 (Figure 35) indicated only slight deviations in the cloud temperature with slight cooling (1°C.) either side of the cloud center and near ambient conditions near the entrance, center, and exit.

DATA FOR SII ROCKET EXHAUST CLOUDS

S-II-14 31 July 1970

Radiosonde soundings of relative humidity and temperature are shown for firing S-II-14 in Figures 36 and 37. The weather conditions were hot and humid at the time of firing with numerous small cumulus clouds in the area. The bases of the cumulus were generally around 1100 meters MSL with tops measured at 3000 meters MSL. Several light rain showers were observed in the area at the time of firing.

Engine ignition was at 1400:27 Central Daylight Time with the first penetration made approximately 17 minutes after engine ignition.

Figures 38 and 39 are photographs of the cloud at 50 seconds after ignition (Figure 38) and 110 seconds after ignition (Figure 39). The numerous natural cumulus clouds in the area at the time of firing can be seen in these photographs. The cloud produced by the second stage (S-II) firings is white in appearance and does not have the "smoky" appearance of the S-IC clouds. Thus the clouds produced a much sharper contrast on the color film making it very easy to distinguish the rocket cloud from any natural clouds which may appear in the photographs. Total firing duration for the second stage is approximately 6 minutes.

The time dependent cloud traces are shown in Figures 40 and 41. These traces depict the cloud geometry from 50 seconds after ignition to 450 seconds after ignition. The cloud height at 450 seconds is approximately 3400 meters. It can be seen that the cloud vertical growth rate is much smaller than for the S-IC clouds. This is to be expected since the mass, momentum and heat input rates to the cloud are much smaller for the second stage.

Relative humidity profiles of the cloud are given for the two passes in Figures 42 and 43. Pass 1 was made at an altitude of 4000 meters MSL while pass 2 was at an altitude of 2900 meters MSL. The average humidity is approximately 100% for all of pass 1 while this value exists only for a small portion of the cloud during pass 2.

Figures 44 and 45 present the disturbed temperature versus time. The statistical fit for $T_{calc.}$ presented a problem for this particular firing since it was impossible to remain entirely clear of natural cumulus during the calibration runs.

Figure 44 indicates a decrease in temperature of approximately 2.5°C shortly after entry into the cloud and the temperature remains at this value for the entire pass. The disturbed temperature does not return to zero upon exiting the cloud, however the data indicated the return to near undisturbed conditions approximately 20 seconds after cloud exit. At the time of the first pass the cloud had begun to merge with the natural cumulus clouds in the area making it

difficult to clearly determine the extent of the rocket cloud.

The disturbed temperature trace for the second pass is shown in Figure 45. The central temperature of the cloud is around 5°C below ambient with the disturbed temperature at entrance and exit being essentially zero.

S-II-15 30 October 1970

Relative humidity and temperature soundings as given by the radiosonde for firing S-II-15 are shown in Figures 46 and 47. The significiant factor for this firing is the particularly low value of relative humidity at all altitudes above 1000 meters MSL (approximately 10%). There also exists a weak temperature inversion in the vicinity of 1000 meters MSL as shown in Figure 47.

Figure 48 presents the cloud photograph at 50 seconds after ignition and Figure 49 depicts the cloud 200 seconds after ignition. At 200 seconds after ignition the cloud has begun to separate into two distinct clouds at a point approximately 750 meters above the ground.

Cloud traces covering the period from 50 seconds after ignition to 550 seconds after ignition are shown in Figures 50, 51, and 52. A comparison of Figure 50 and Figure 40 indicates that the clouds for S-II-14 and S-II-15 have essentially the same height at 200 seconds. Meteorological factors however, play an important role in the final development of the cloud. This factor is particularly noticeable when one compares the cloud geometry for these two firings at 450 seconds. Cloud S-II-14 (Figure 41) attained a height of approximately

3360 meters in 450 seconds while S-II-15 only reached a height of 1200 meters in the same period (Figure 52). The geometry dependence of the cloud on the ambient relative humidity is thus graphically demonstrated in these two firings. These results also indicate the futility of attempting to produce reasonable results with empirically based cloud growth formulas when the pertinent meteorological parameters are not included.

Although firing S-II-15 produced a well defined cloud photographically, this was not evidenced on the three passes through the cloud. The relative humidity traces for the entire flight, including the three passes through the cloud, produced a constant value of relative humidity at approximately 20%. This value is perhaps more indicative of the actual atmospheric value of relative humidity than the 10% produced by the radiosonde, since the 10% is approximately the lower limit of measurement for the sonde.

A comprehensive study of the relative humidity and disturbed temperature data for the three passes, and for periods outside the cloud, indicated that the aircraft data system was operating properly. Dry bulb temperatures from the aircraft compare (within 2°C) to those measured by the sonde at a given altitude and, as previously mentioned, the relative humidity values as measured by the sonde and the aircraft compare very favorably. Based on these arguments we must conclude that the relative humidity trace (Figure 53) and the disturbed temperature

trace (Figure 54) are correct for this firing. It can be seen that there is no significant change in relative humidity for the pass through the cloud and that, statistically, there is no deviation of the cloud temperature from ambient. These data are only shown for pass 1 since subsequent passes (2 and 3) produced essentially identical results. Ignition for S-II-15 occurred at 1515:43 Central Daylight Time with pass 1 being made through the cloud approximately 4 minutes after ignition. Evidently the atmosphere was so dry on this particular day that the firing produced no perturbations on the atmosphere even in the interior of the cloud.

CONCLUSIONS

The time dependent geometry and physical cloud properties have been presented for four static rocket firings, including two S-I-C firings and two S-II firings. Pertinent meteorological parameters have been presented for each firing and the prevailing weather conditions were seen to have a strong influence on the growth of the clouds. Although the maximum aircraft penetration altitude in the S-I-C clouds was approximately 4200 meters, the pilots estimated that on several occasions the maximum cloud tops appeared to reach 7500 meters.

A new technique was developed to verify the previous measurements of evaporation and entrainment of blast deflector cooling water into the cloud. Small hollow glass spheres (approximately 10 microns in diameter) were injected into the cooling water at the pumping station. These particles were subsequently detected on all passes through the clouds by using an impact type sampler. The particles are clearly identifiable under a microscope and are also sufficiently small that they may be injected into natural clouds at the updrafts near the base of the clouds.

Perhaps the most interesting data recorded were the reduced temperatures during the first passes through the developing clouds.

This is evidently a result of the very rapid vertical development of the clouds. Data presented in this report will provide input to an analytical model which will attempt to predict, using known numerical techniques, the time dependent geometry and properties of the cloud.

Appendix I

Tabulated Radiosonde Data

S-IC-13

HEIGHT	TEMP C	VTEMP C	PRESSURE	REL HUM	W DIR	W SPD M/SEC	DEW PT
0	147	156	10260	490	950	50	42
132	127	135	10100	486	1170	56	22
291	113	121	9910	582	1151	52	34
444	99	107	9730	647	1186	55	35
616	88	96	9530	658	1177	52	28
765	73	80	9360	657	1014	41	13
925	64	70	9180	540	920	50	-21
1087	52	57	9000	497	926	59	-43
1150	46	51	8930	522	932	60	-42
1261	50	55	8810	468	943	62	-53
1354	52	55	8710	265	921	50	-124
1420	52	53	8640	100	898	41	-238
1467	49	50	8590	100	865	31	-240
1592	59	62	8460	265	421	8	-117
1689	59	67	8360	612	3291	11	-8
1778	53	59	8270	525	3068	20	-35
1957	40	48	8090	730	3073	33	-3
1988	37	45	8060	728	3090	30	-6
2140	31	38	7910	643	3227	20	-28
2316	23	27	7740	493	204	4	-71
2495	8	12	7570	474	914	9	-90
2677	-2	2	7400	650	1656	13	-60
2852	-14	-12	7240	196	1892	32	-216
3029	-24	-22	7080	245	2065	29	-199
3199	-36	-35	6930	100	2725	24	-307

Radiosonde Data: S-IC-13

S-IC-13

HEIGHT	TEMP C	VTEMP C	PRESSURE	REL HUM	W DIR	W SPD M/SEC	DEW PT
3371	-47	-47	6780	131	2956	36	-288
3500	-57	-56	6670	146	2832	35	-284
3535	-57	-56	6640	132	2798	36	-295
3630	-57	-56	6560	132	2763	39	-295
3714	-64	-63	6490	103	2737	43	-326
3921	-72	-70	6320	384	2696	63	-189
4108	-93	-90	6170	639	2701	81	-148
4285	-105	-102	6030	715	2899	80	-146
4400	-112	-108	5940	770	2971	69	-144
4491	-121	-118	5870	637	3047	61	-175
4676	-134	-131	5730	720	2914	67	-173
4769	-144	-142	5660	749	2932	80	-179
4877	-144	-142	5580	633	2948	95	-198
4973	-144	-143	5510	493	2963	97	-227
5069	-152	-150	5440	514	2977	99	-229
5252	-169	-167	5310	536	2962	86	-240
5452	-181	-179	5170	511	3035	73	-257
5627	-193	-191	5050	516	3125	68	-267
5821	-205	-203	4920	585	3152	71	-264
6018	-219	-218	4790	577	3032	109	-280
6064	-221	-219	4760	577	3012	117	-281

Radiosonde Data: S-IC-13

S-IC-15

HEIGHT	TEMP C	VTEMP C	PRESSURE	REL HUM	W DIR	W SPD M/SEC	DEW PT
0	267	284	10140	420	49	15	128
385	229	243	9703	430	247	60	96
488	218	231	9590	433	237	60	88
761	191	204	9288	480	209	60	79
1134	155	167	8892	553	182	65	66
1302	139	150	8720	591	218	71	60
1508	122	132	8508	524	254	79	28
1676	109	117	8340	472	316	87	1
1807	111	117	8210	323	357	94	-47
1907	108	114	8112	320	384	100	-51
2170	100	105	7860	311	446	98	-62
2356	100	106	7685	302	490	98	-65
2762	102	107	7320	283	440	78	-72
2834	97	102	7256	279	428	75	-78
2922	92	97	7180	275	383	70	-85
3062	96	101	7060	253	298	63	-92
3250	87	91	6900	246	158	57	-103
3641	67	71	6581	232	3539	54	-127
3693	65	68	6540	230	3532	55	-130
4033	39	44	6271	326	3495	64	-109
4380	13	19	6010	465	3468	68	-88
4430	10	15	5972	449	3464	69	-95
4860	-17	-14	5660	331	3387	81	-158
4902	-20	-17	5630	321	3388	84	-164
5059	-25	-22	5520	284	3390	92	-182
5263	-38	-35	5378	301	3392	104	-187
5671	-64	-61	5105	338	3363	133	-196
6078	-90	-87	4846	382	3304	159	-206

Radiosonde Data: S-IC-15

S-II-14

HEIGHT	TEMP C	VTEMP C	PRESSURE	REL HUM	W DIR	W SPD M/SEC	DEW PT
0	331	361	10130	500	2800	10	213
143	303	330	9970	532	3222	9	197
233	297	325	9870	562	3447	11	200
315	287	314	9780	594	3342	12	200
407	279	306	9680	608	2861	8	196
508	271	298	9570	622	2726	12	192
601	261	287	9470	640	2817	11	188
705	252	277	9360	645	2755	10	180
818	242	266	9240	650	2888	8	172
933	229	252	9120	656	3495	9	161
1077	218	241	8970	673	180	12	155
1224	204	225	8820	684	283	6	144
1382	192	212	8660	682	3078	0	132
1542	182	200	8500	681	1678	3	122
1695	173	191	8350	678	1408	9	113
1829	162	178	8220	676	1333	14	102
1975	158	174	8080	647	1354	16	92
2124	155	170	7940	614	1258	17	81
2243	152	164	7830	488	1302	11	45
2362	148	159	7720	439	2334	2	27
2473	139	150	7620	472	169	3	28
2595	126	139	7510	593	622	7	49
2765	120	133	7360	618	850	6	49

Radiosonde Data: S-II-14

S-II-14

HEIGHT	TEMP C	VTEMP C	PRESSURE	REL HUM	W DIR	W SPD M/SEC	DEW PT
2925	110	123	7220	621	465	5	41
3065	101	112	7100	584	614	13	23
3267	93	101	6930	434	769	15	-24
3448	78	86	6780	493	834	18	-20
3645	63	72	6620	542	748	30	-21
3820	48	57	6480	639	539	22	-13
3985	43	51	6350	600	379	9	-27
4153	34	40	6220	501	296	7	-59
4298	28	34	6110	492	117	4	-67
4418	18	24	6020	495	2955	0	-75
4553	6	12	5920	509	312	3	-82
4662	2	7	5840	437	254	3	-106
4801	0	3	5740	381	283	3	-125
4899	-13	-9	5670	381	509	4	-137
5040	-23	-19	5570	364	3017	2	-151
5170	-27	-24	5480	298	2840	10	-179
5286	-32	-30	5400	254	2692	13	-202
5404	-41	-40	5320	138	2465	18	-276
5508	-46	-45	5250	181	2425	22	-252
5629	-53	-52	5170	232	2308	19	-230
5736	-60	-59	5100	126	2090	22	-302
5859	-70	-69	5020	214	2172	13	-253
6016	-80	-78	4920	308	2557	11	-221

Radiosonde Data: S-II-14

S-II-15

HEIGHT	TEMP C	VTEMP C	PRESSURE	REL HUM	W DIR	W SPD M/SEC	DEW PT
0	226	235	10180	270	3300	31	27
85	213	218	10080	153	3404	32	-60
171	202	207	9980	161	3498	34	-62
318	186	191	9810	177	26	40	-62
494	171	175	9610	185	29	46	-69
664	154	158	9420	220	3599	63	-61
863	134	139	9200	260	34	64	-56
1010	121	124	9040	158	101	57	-130
1048	129	131	9000	100	114	54	-178
1198	134	136	8840	100	178	43	-175
1246	136	138	8790	100	270	38	-173
1361	129	131	8670	100	582	32	-178
1547	118	120	8480	100	393	37	-187
1736	110	112	8290	100	47	44	-193
1786	108	110	8240	100	17	43	-194
1908	108	110	8120	100	3538	40	-194
2001	108	110	8030	100	3391	38	-194
2084	102	104	7950	100	3252	38	-199
2242	94	96	7800	100	2921	55	-205
2403	79	81	7650	100	2815	76	-217
2576	65	67	7490	100	2686	86	-228
2742	59	61	7340	100	2537	89	-232

Radiosonde Data: S-II-15

S-II-15

HEIGHT	TEMP C	VTEMP C	PRESSURE	REL HUM	W DIR	W SPD M/SEC	DEW PT
2922	51	52	7180	100	2524	70	-239
3105	43	44	7020	100	2771	58	-245
3164	45	46	6970	100	2817	59	-244
3269	37	38	6880	100	2895	60	-249
3435	21	22	6740	100	2891	55	-262
3605	11	12	6600	100	2854	63	-270
3776	-2	-1	6460	100	2779	72	-281
3951	-14	-13	6320	100	2672	80	-290
4129	-23	-23	6180	100	2603	92	-297
4285	-33	-32	6060	100	2606	101	-305
4455	-49	-48	5930	100	2620	103	-317
4629	-65	-65	5800	100	2570	95	-330
4792	-83	-83	5680	100	2528	82	-344
4943	-98	-98	5570	100	2581	84	-356
5125	-116	-115	5440	100	2648	99	-370
5295	-130	-130	5320	100	2672	96	-381
5468	-146	-145	5200	100	2566	84	-393
5615	-156	-156	5100	100	2483	104	-401
5779	-169	-169	4990	100	2513	102	-412
5915	-182	-182	4900	100	2557	96	-422
6054	-193	-193	4810	100	2559	111	-431

Radiosonde Data: S-II-15

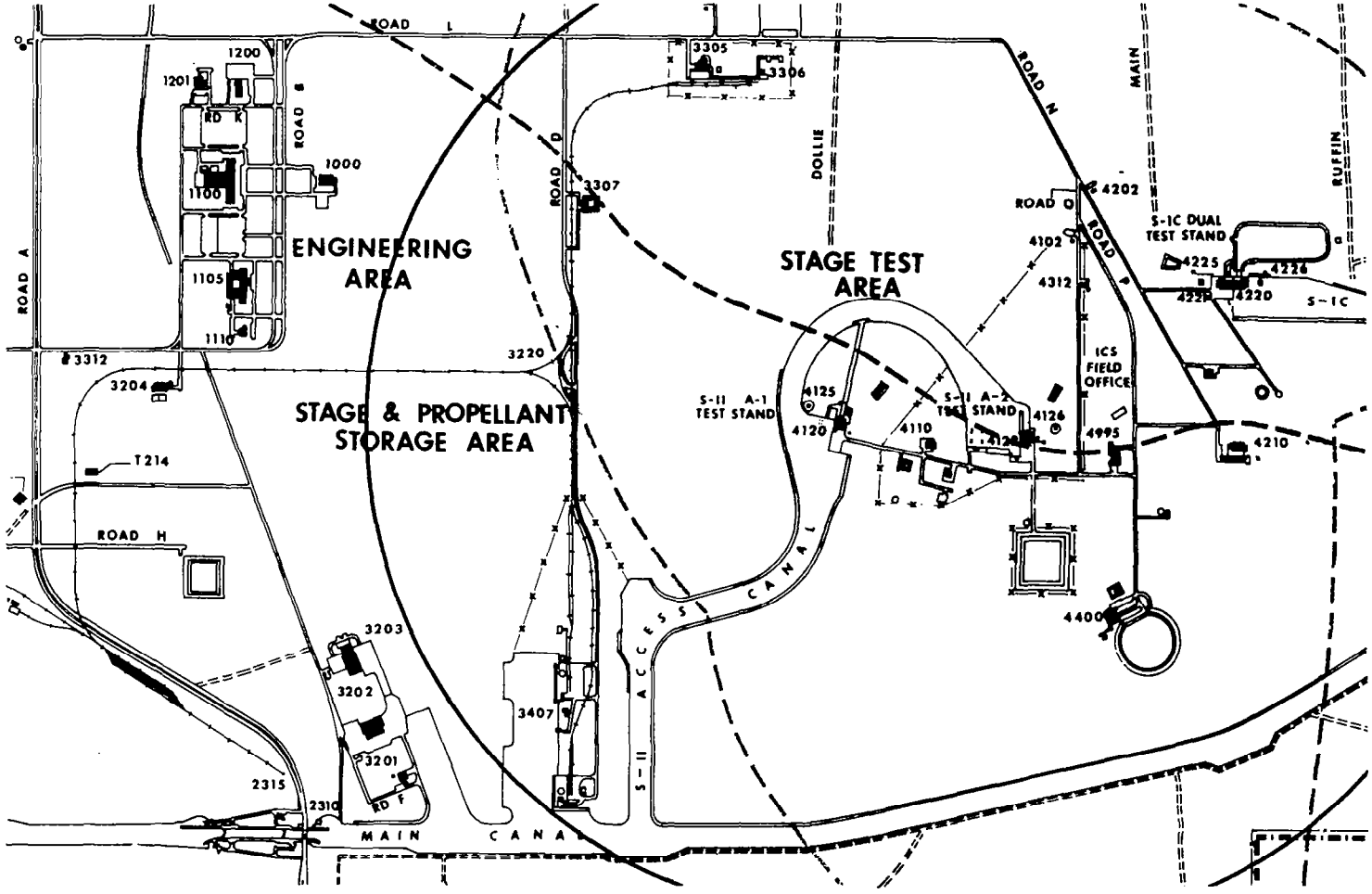

Figure 1. Map of Mississippi Test Facility.

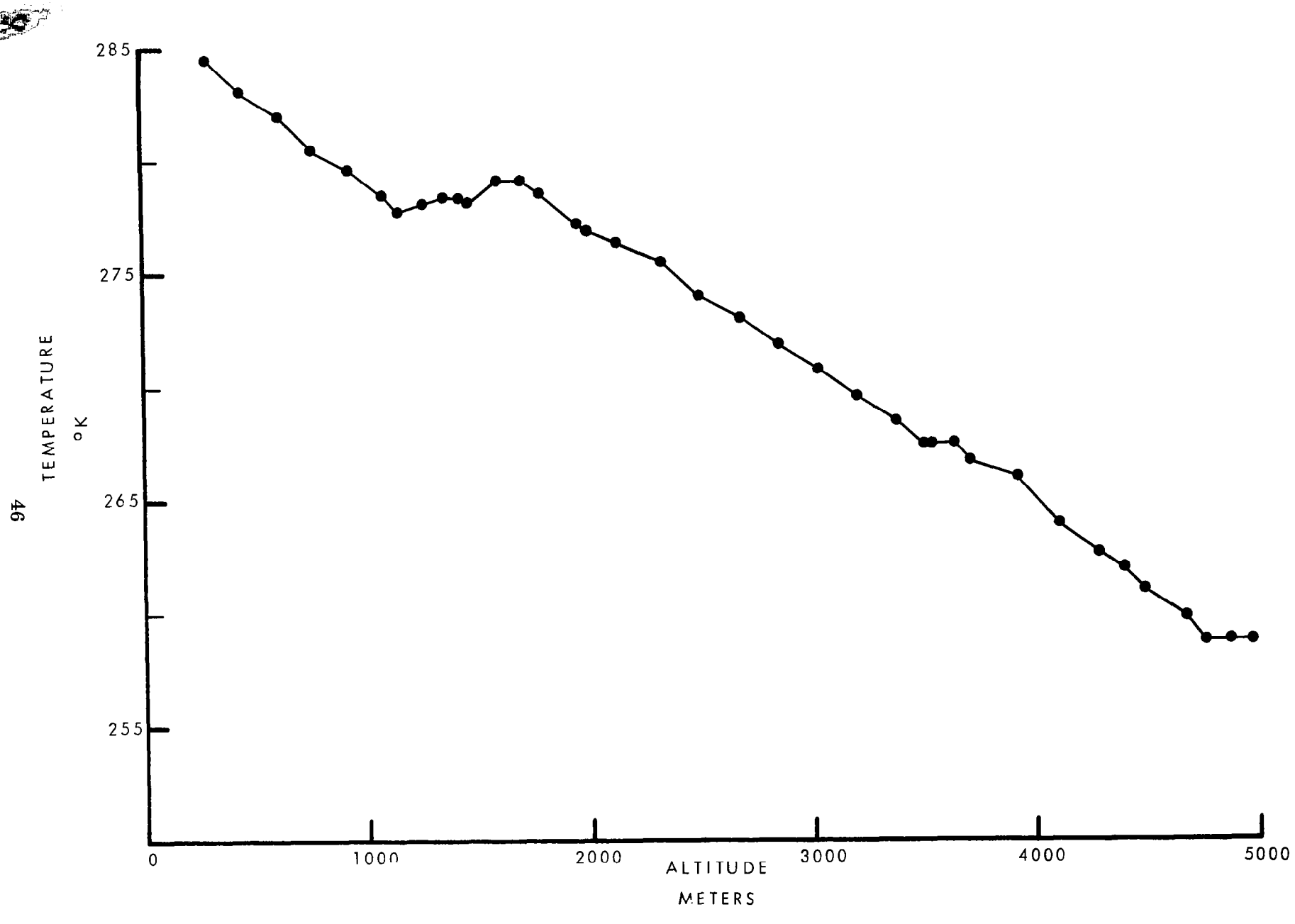

Figure 2. Radiosonde Temperature Sounding.
Firing S-IC-13.

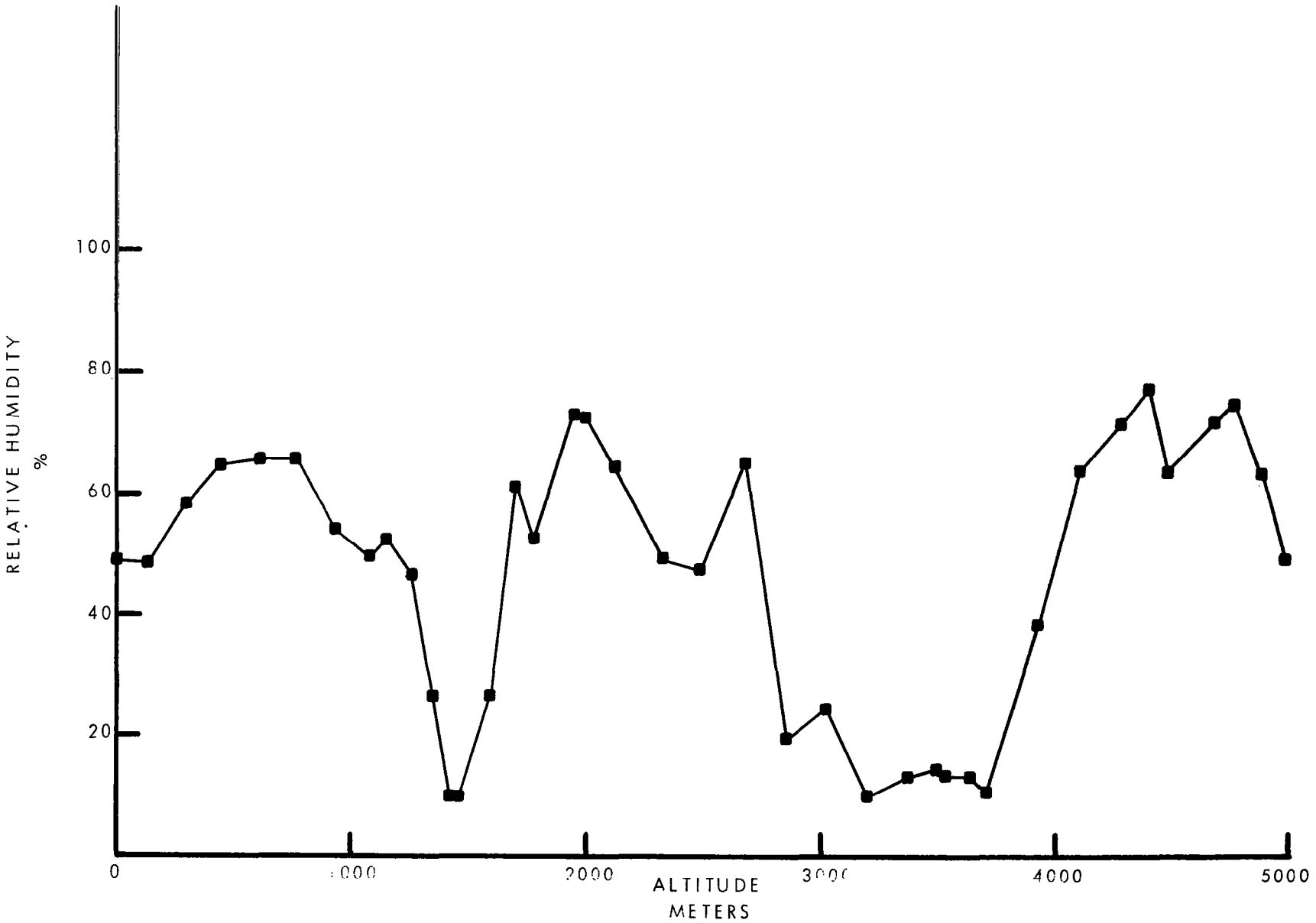

Figure 3. Radiosonde Relative Humidity Sounding.
Firing S-IC-13.

Figure 4. Cloud Photograph 20 Seconds After Ignition. Firing S-IC-13.

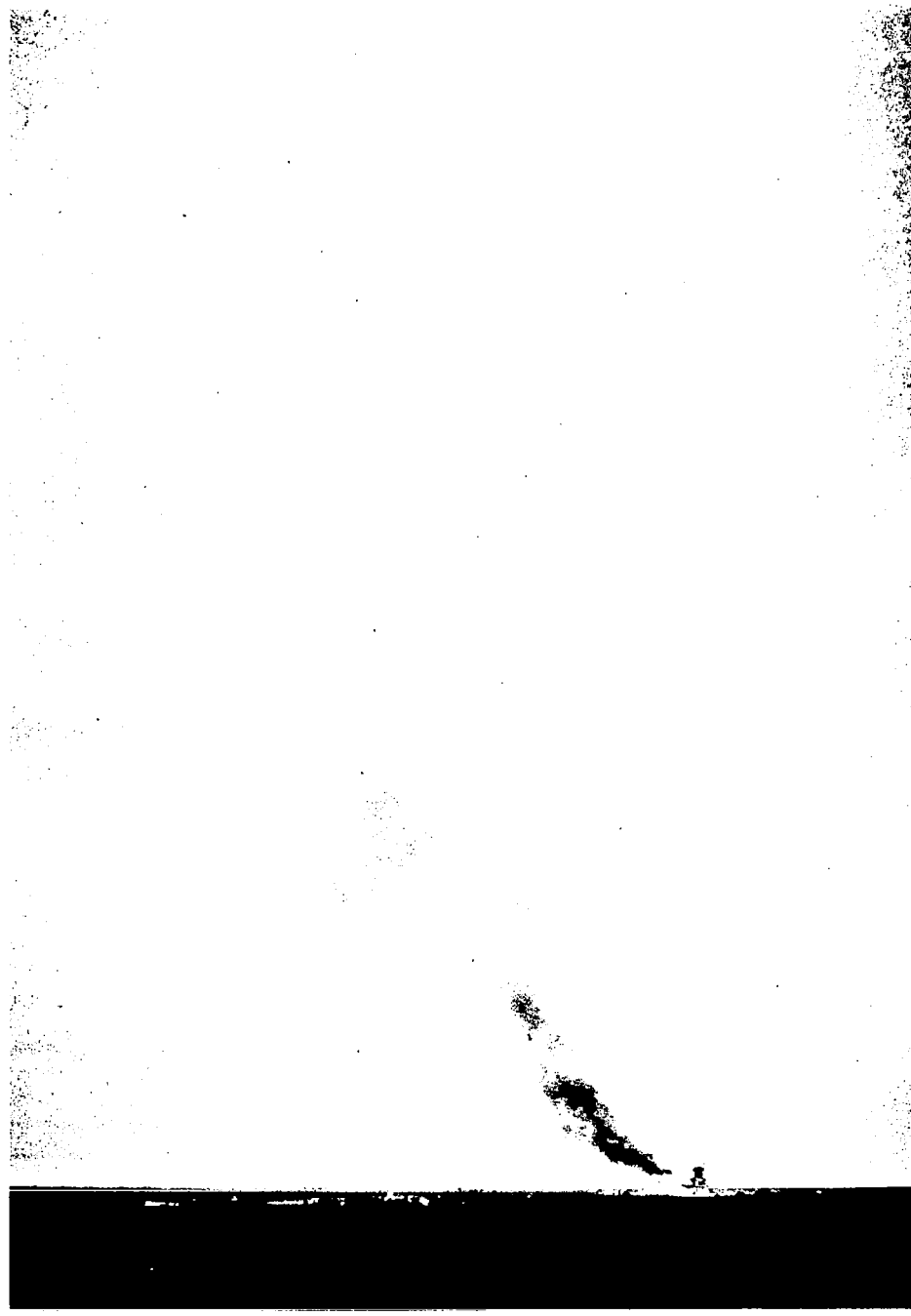

Figure 5. Cloud Photograph 60 Seconds After Ignition. Firing S-IC-13.

Figure 6. Cloud Photograph 160 Seconds After Ignition. Firing S-IC-13.

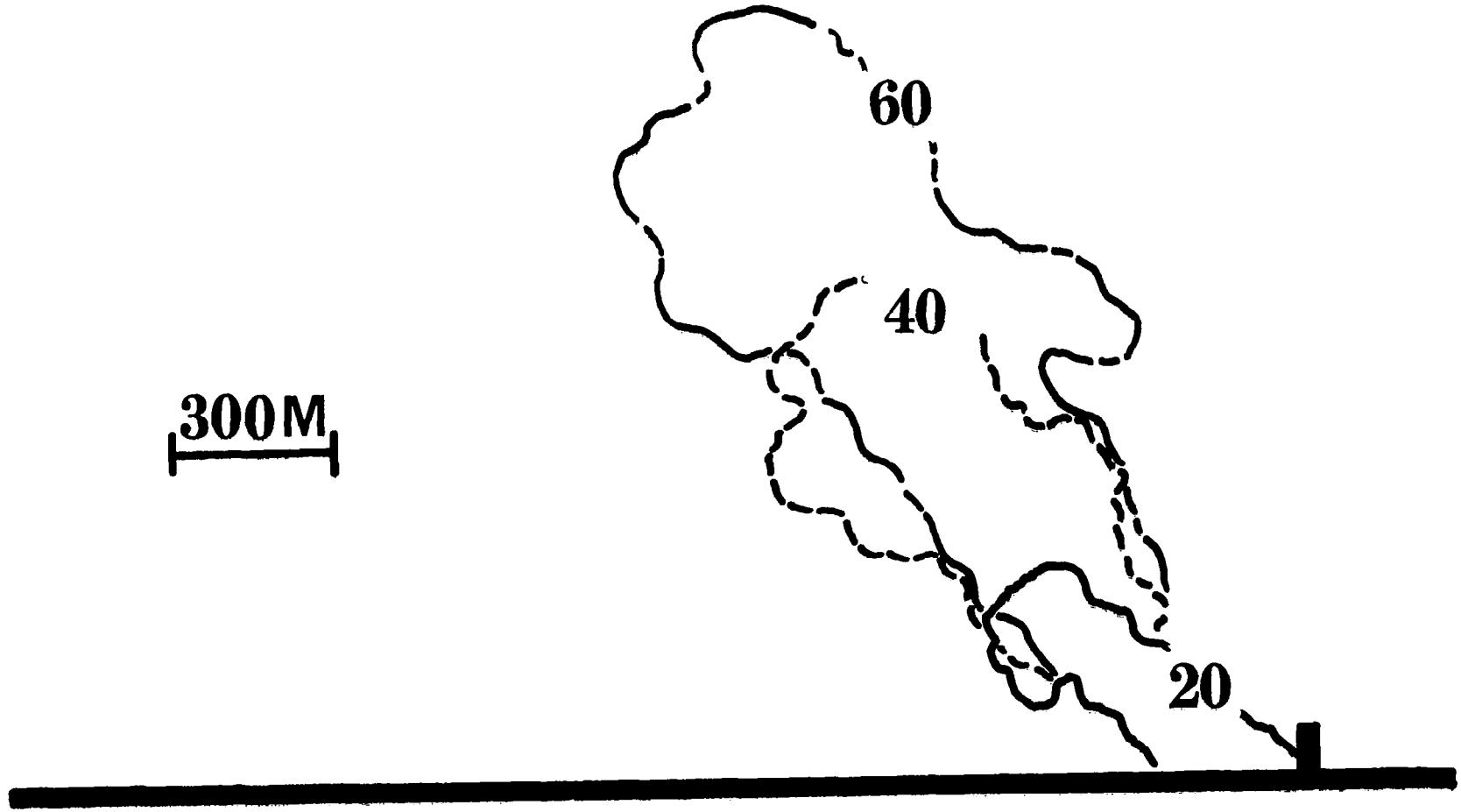

Figure 7. Rectified Cloud Geometry. Firing S-IC-13.

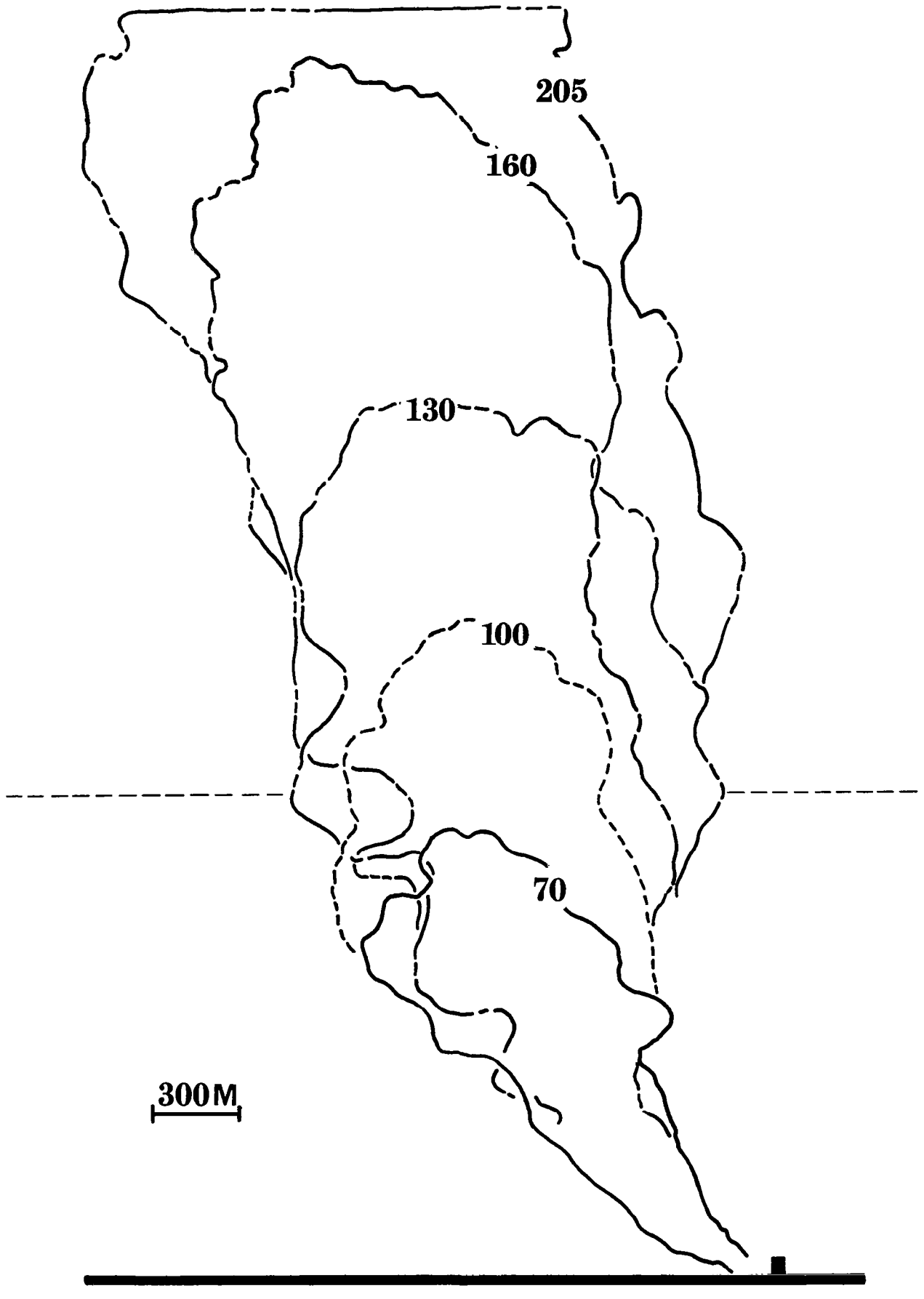

Figure 8. Rectified Cloud Geometry. Firing S-IC-13.

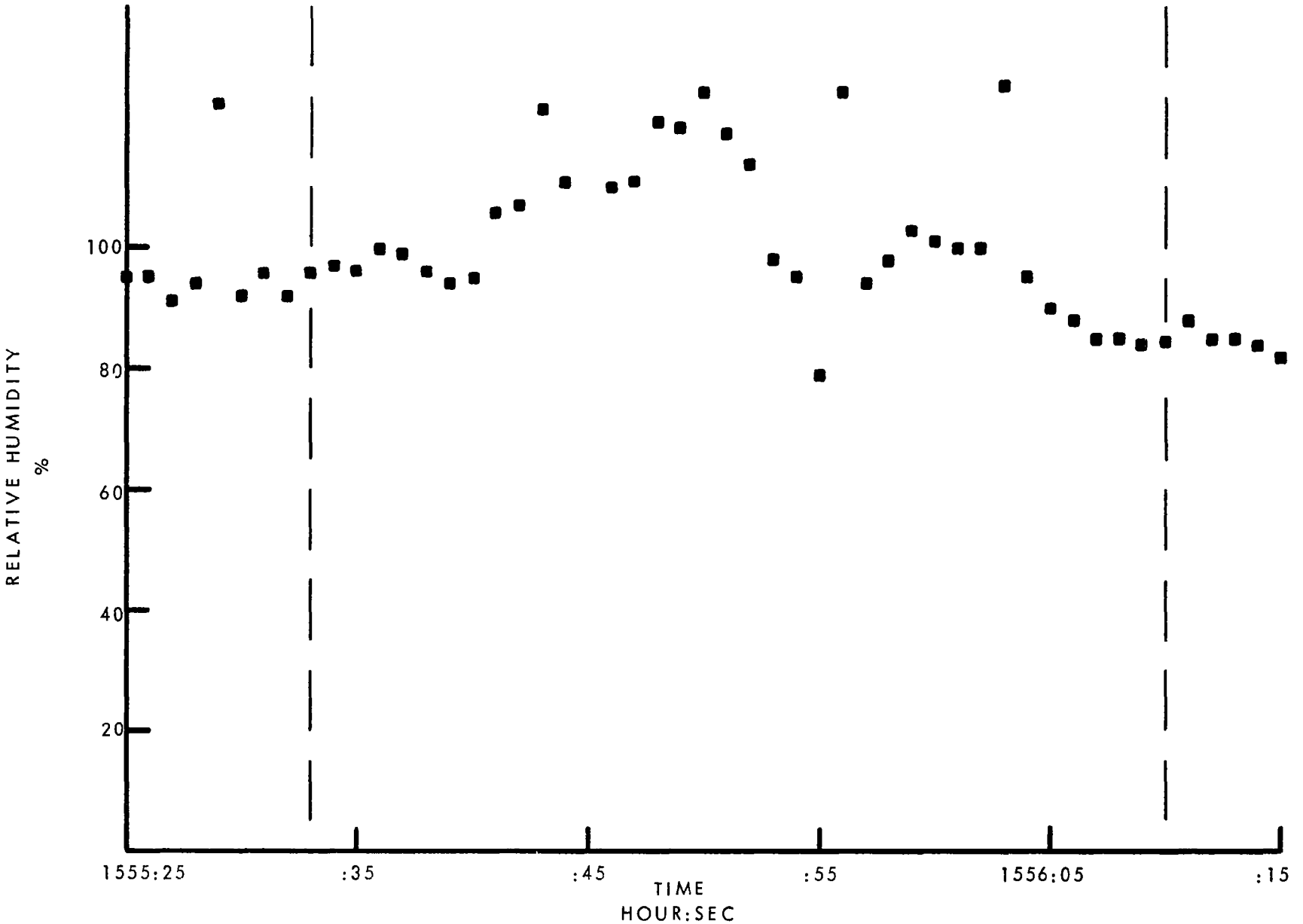

Figure 9. Relative Humidity In Cloud. Pass 1.
Firing S-IC-13. Penn. State Aircraft.

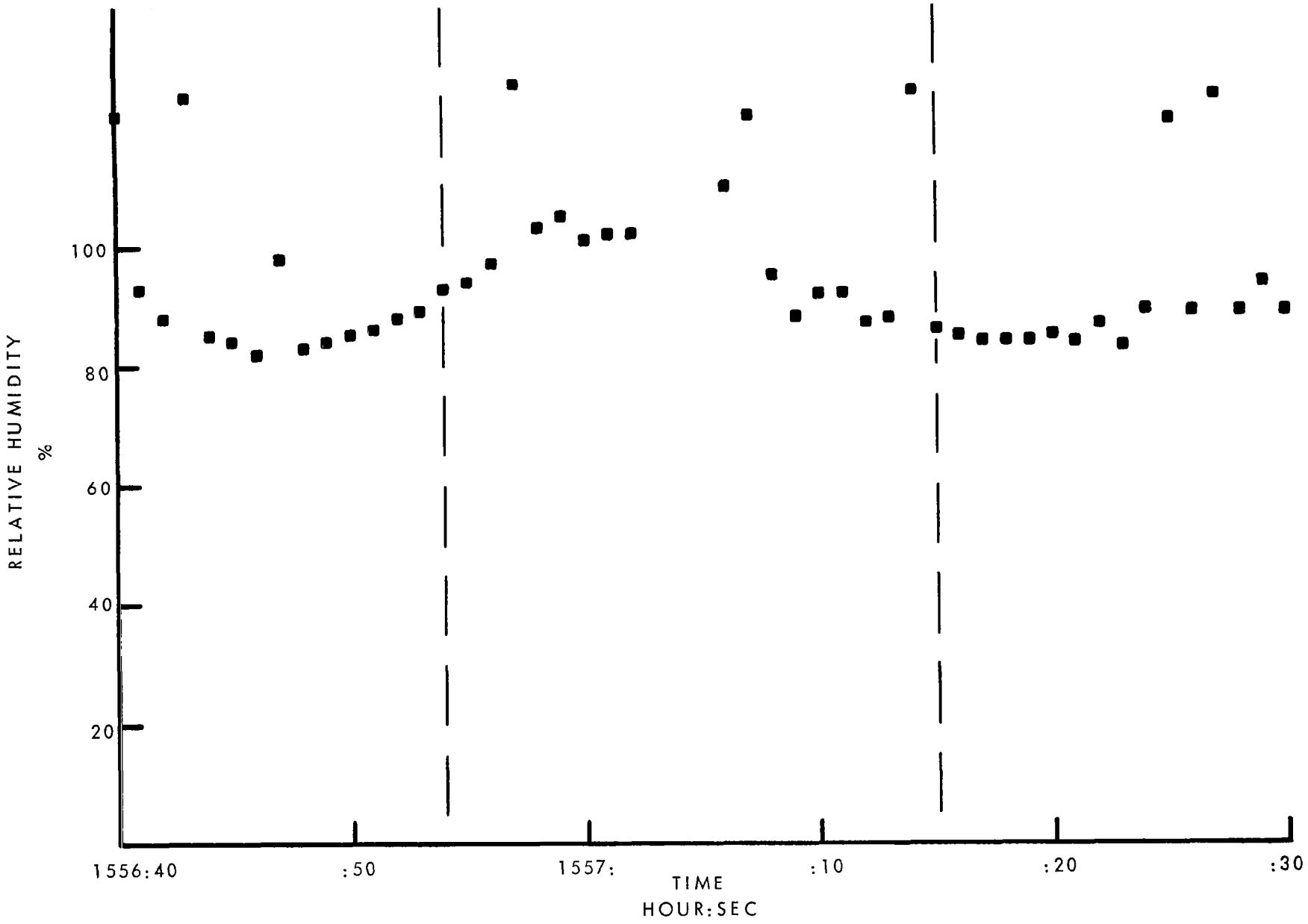

Figure 10. Relative Humidity In Cloud. Pass 2.
Firing S-IC-13. Penn. State Aircraft.

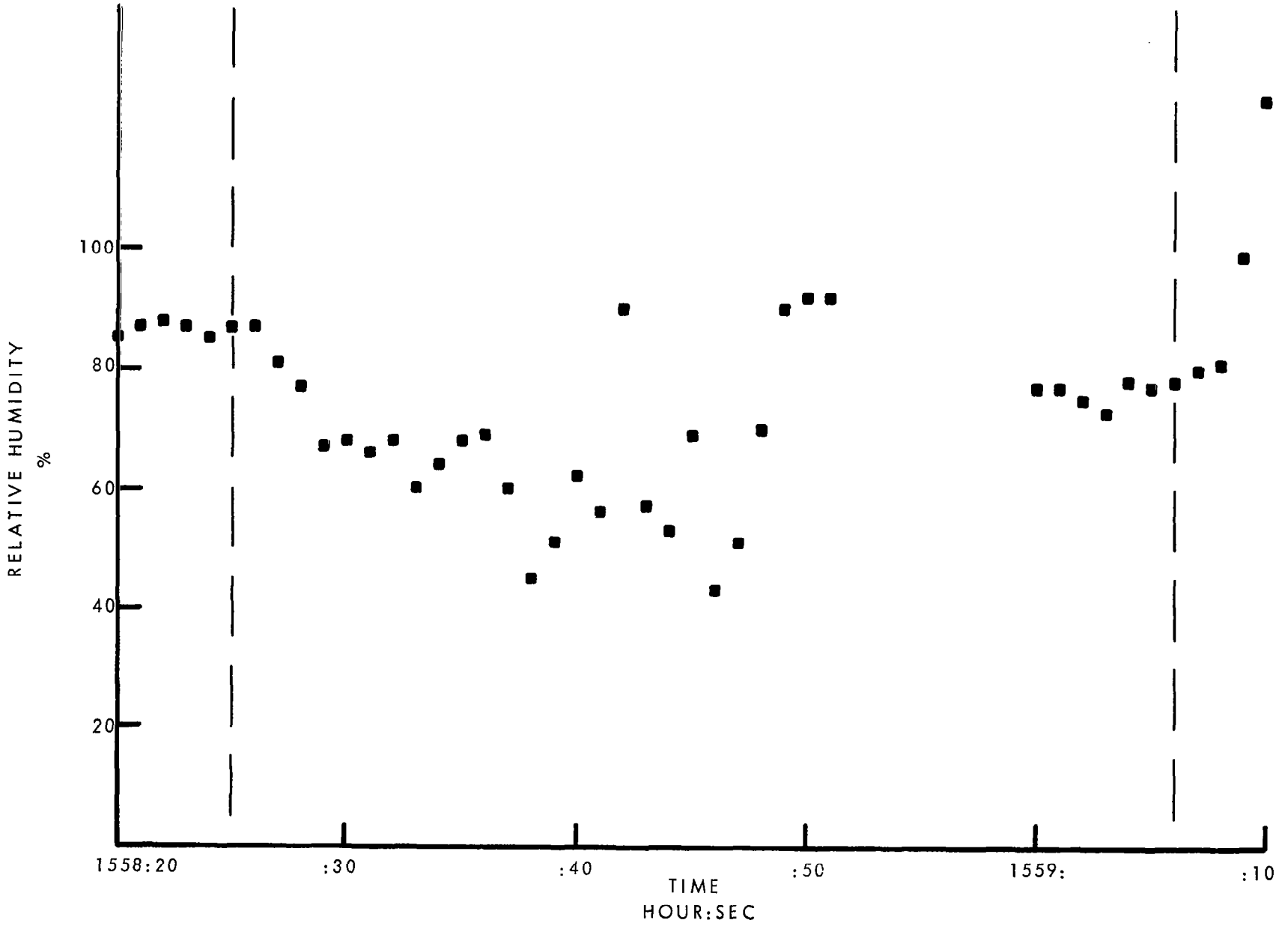

Figure 11. Relative Humidity In Cloud. Pass 3.
Firing S-IC-13. Penn. State Aircraft.

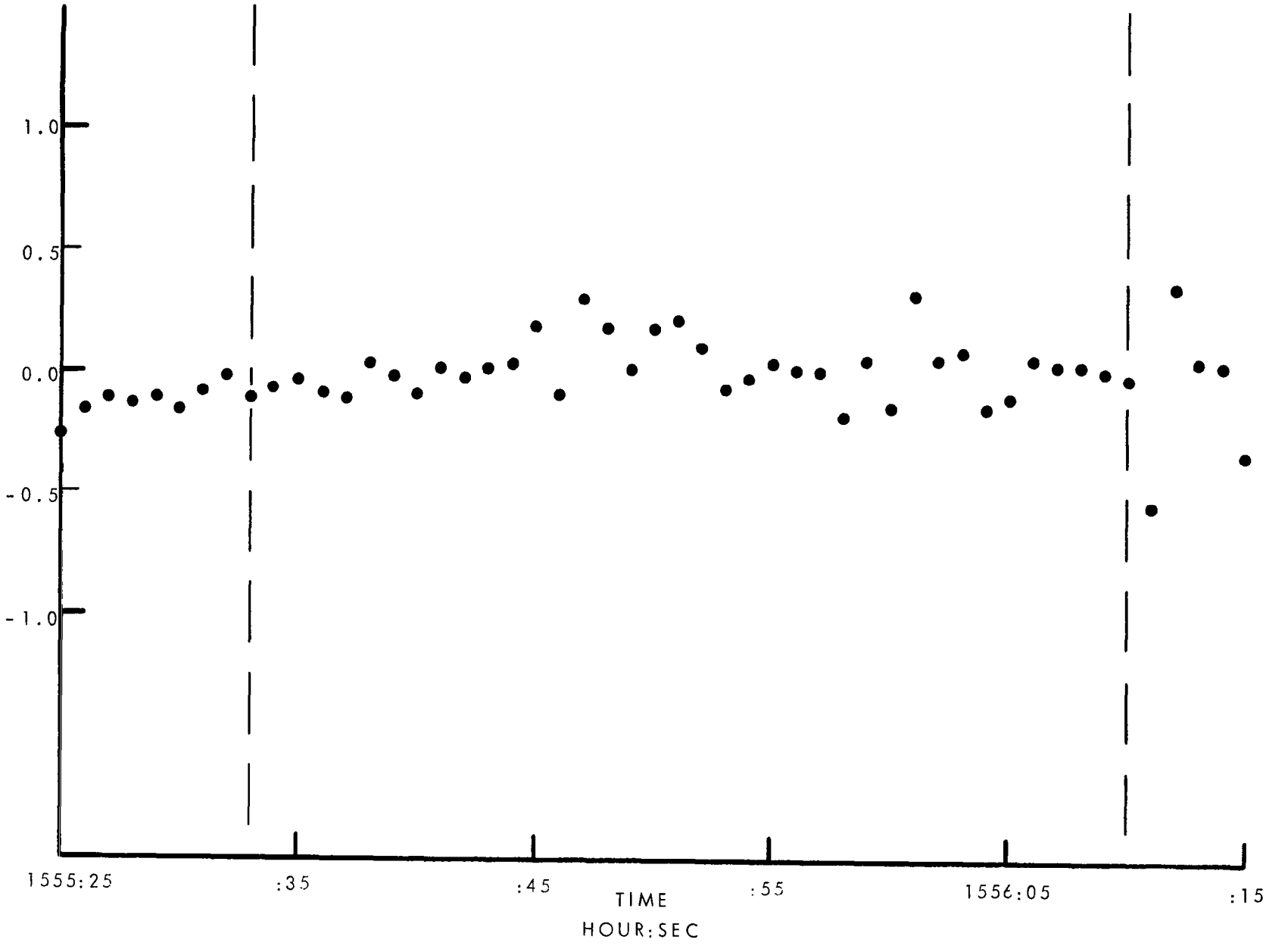

Figure 12. Disturbed Temperature In Cloud. Pass 1.
Firing S-IC-13. Penn. State Aircraft.

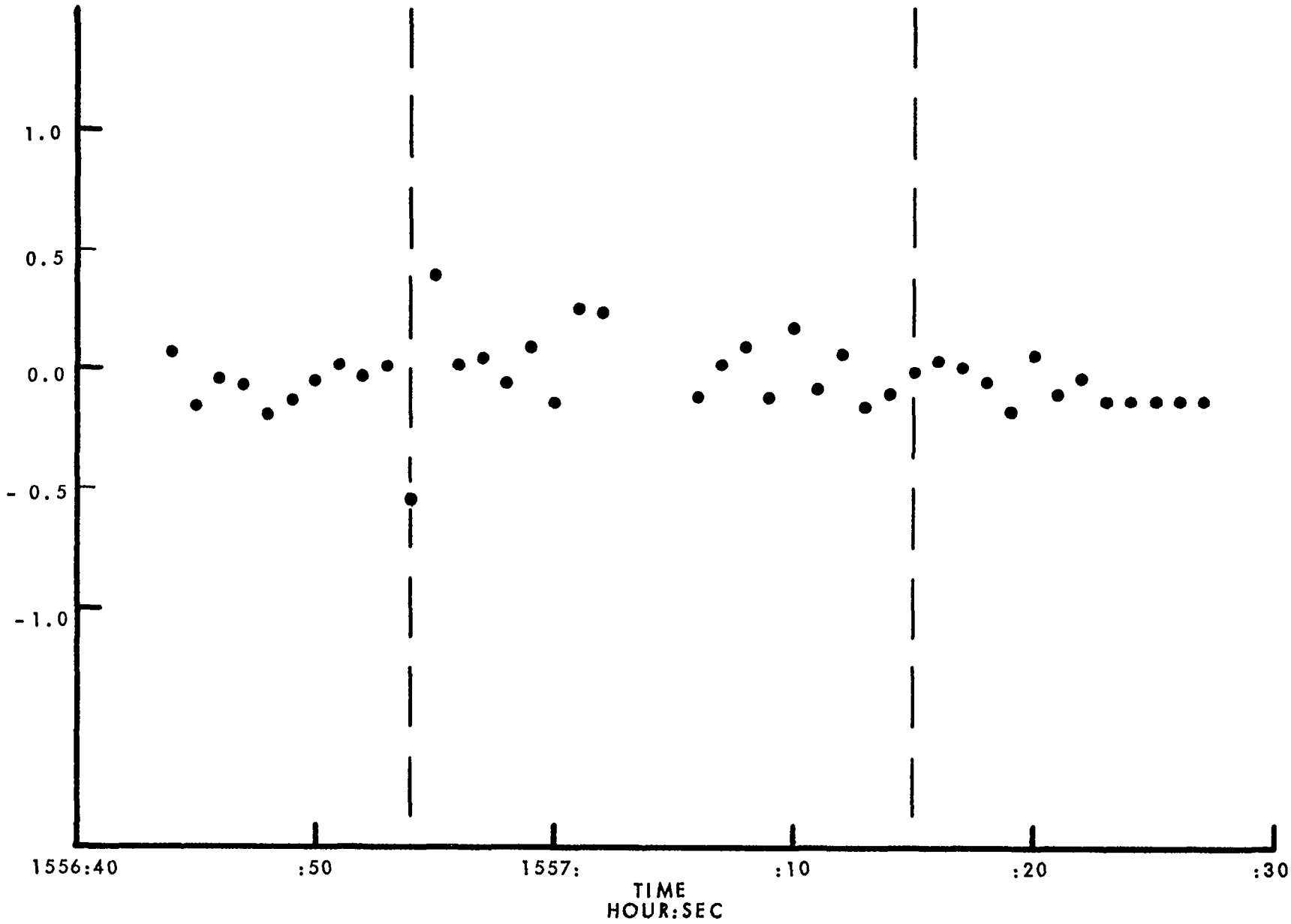

Figure 13. Disturbed Temperature In Cloud. Pass 2. Firing S-IC-13. Penn. State Aircraft.

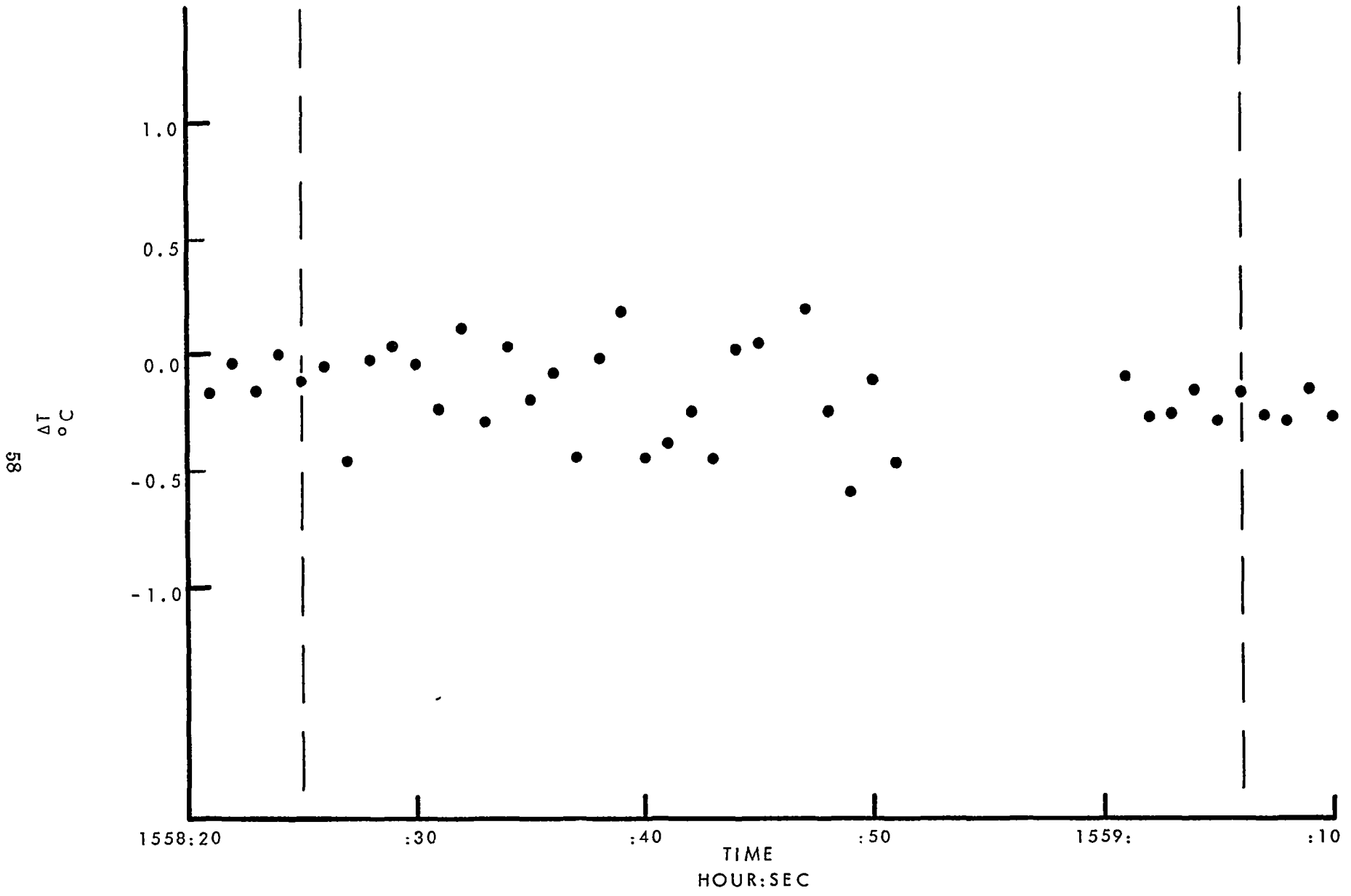

Figure 14. Disturbed Temperature In Cloud. Pass 3.
Firing S-IC-13. Penn. State Aircraft.

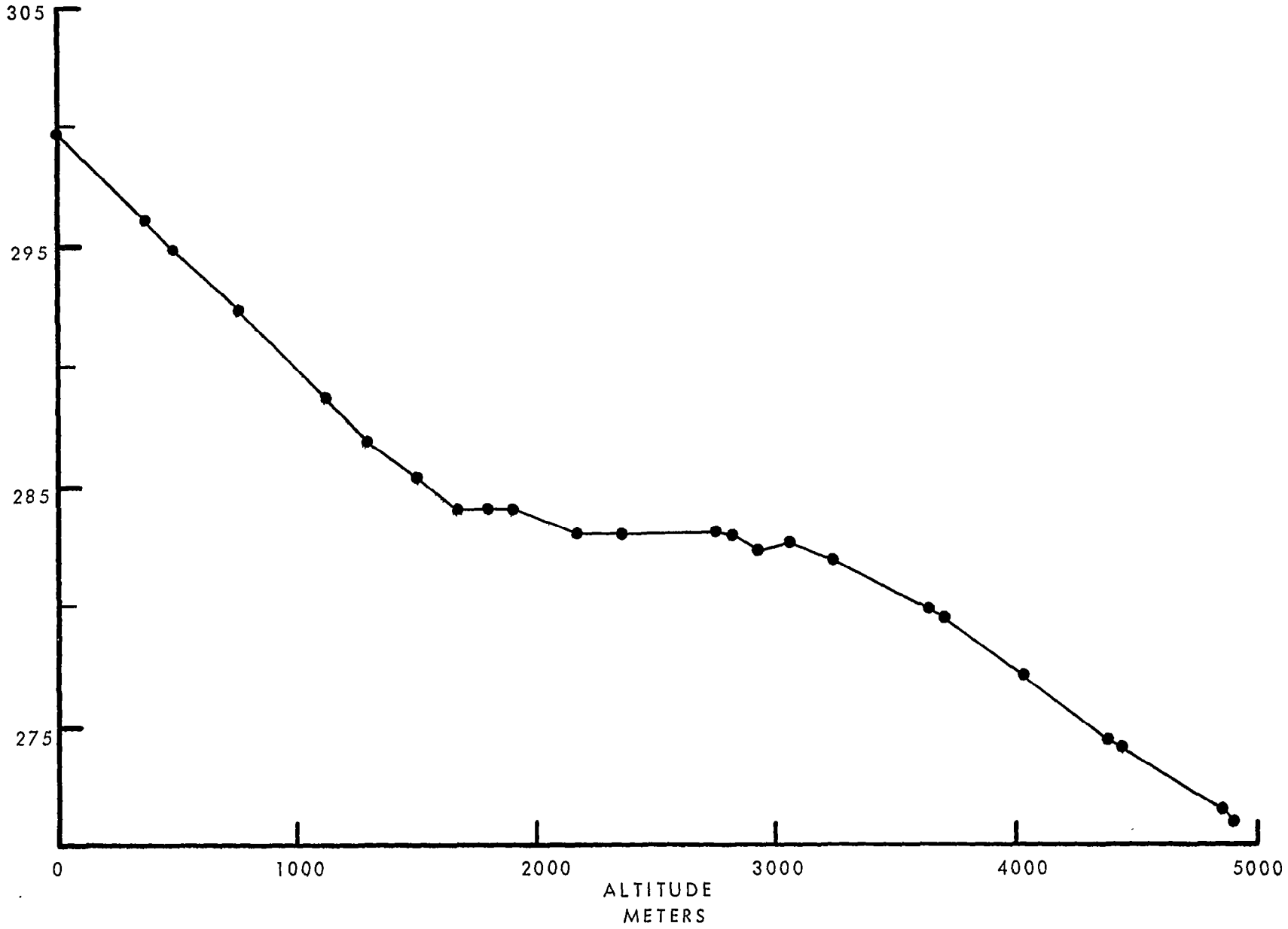

Figure 15. Radiosonde Temperature Sounding. Firing S-IC-15.

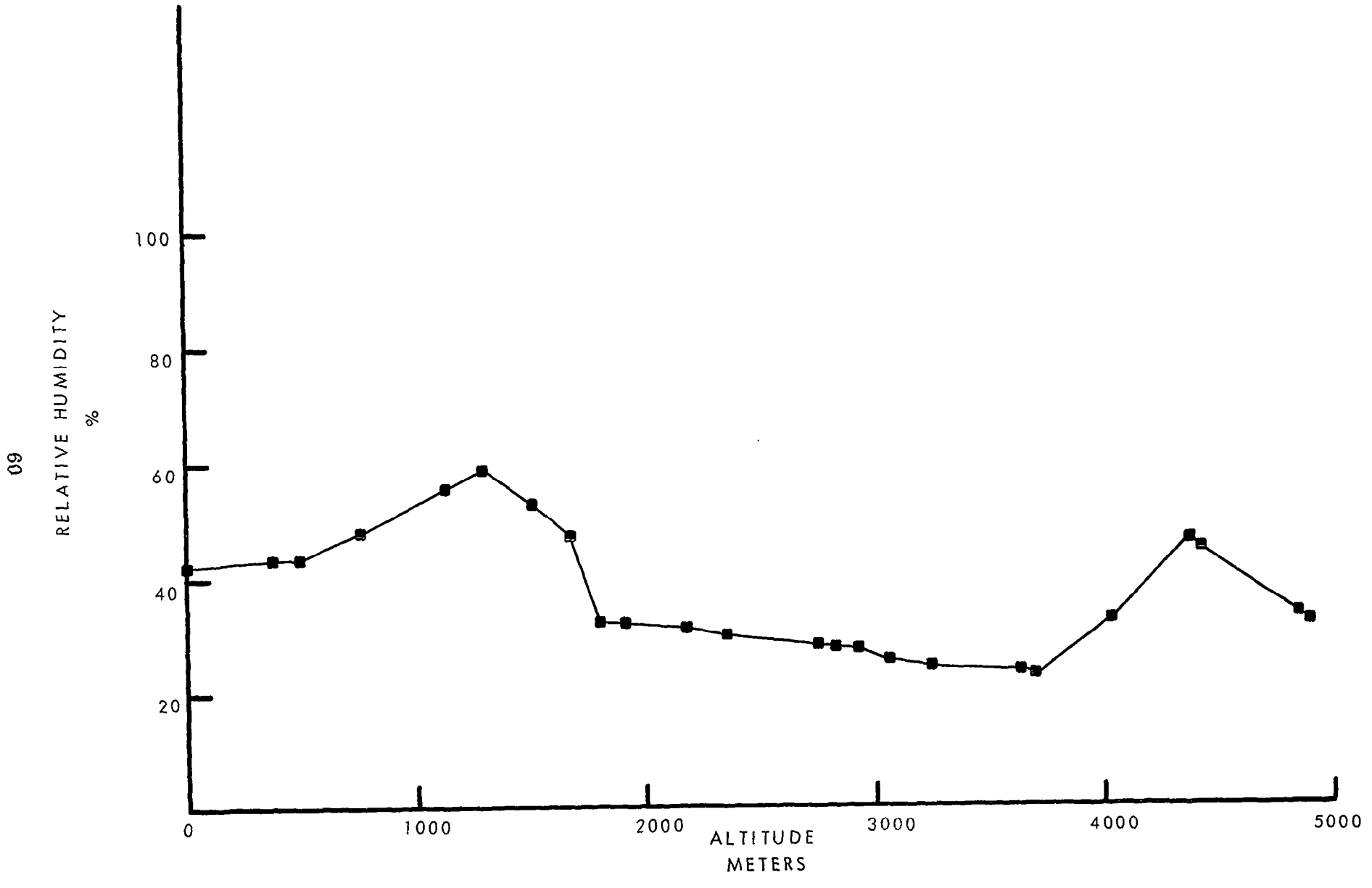

Figure 16. Radiosonde Relative Humidity Sounding.
Firing S-IC-15.

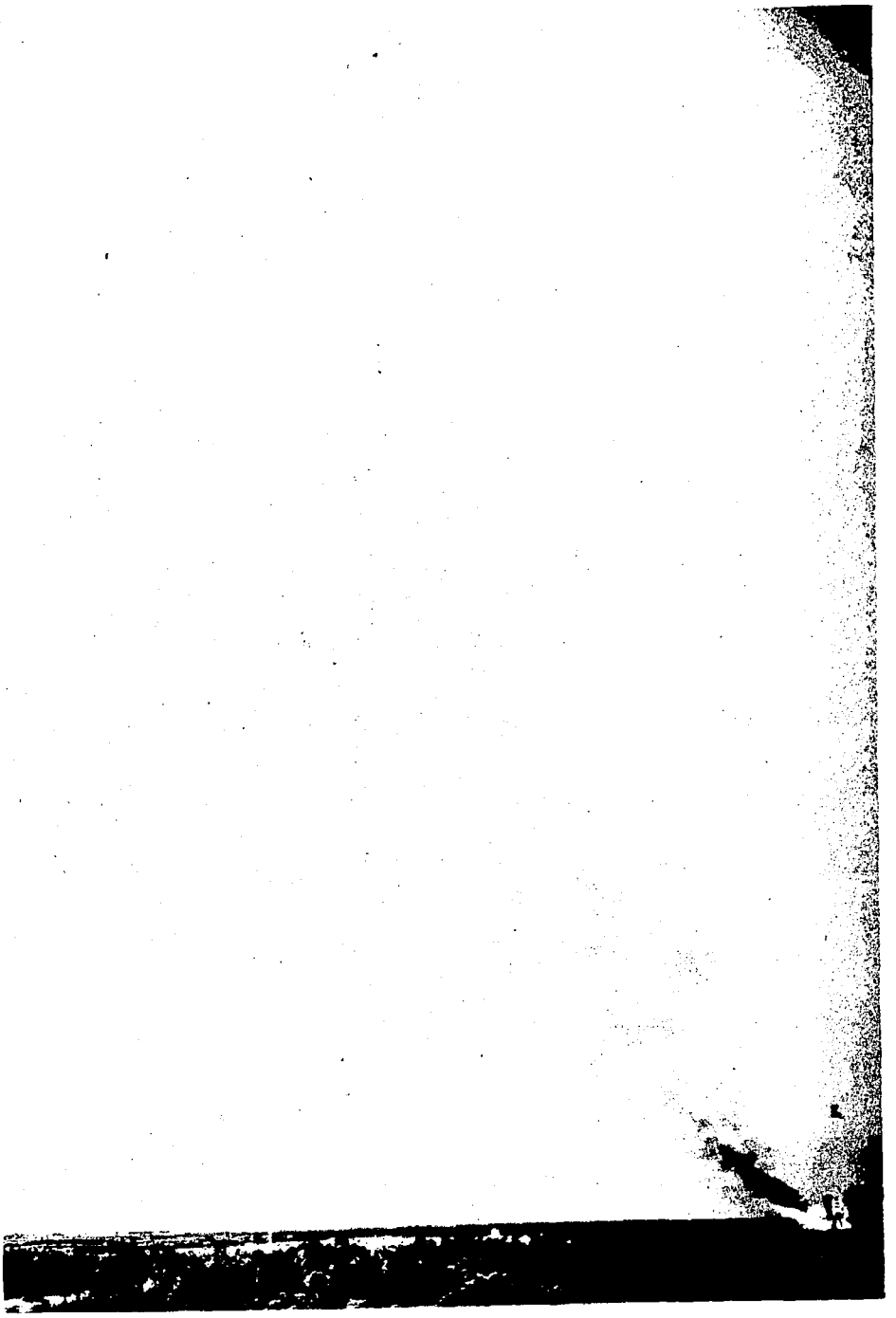

Figure 17. Cloud Photograph 65 Seconds After Ignition. Firing S-IC-15.

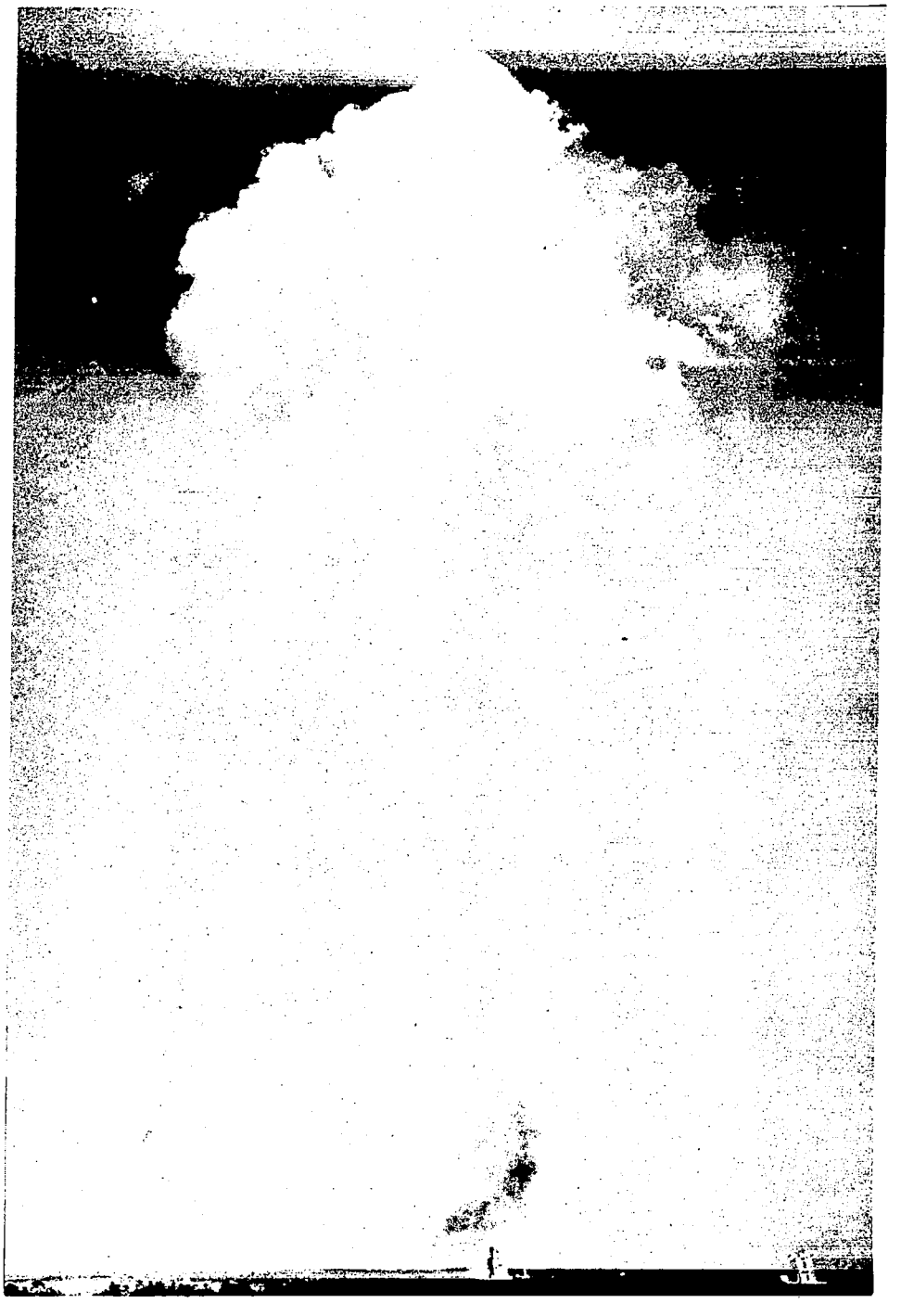

Figure 18. Cloud Photograph 200 Seconds After Ignition. Firing S-IC-15.

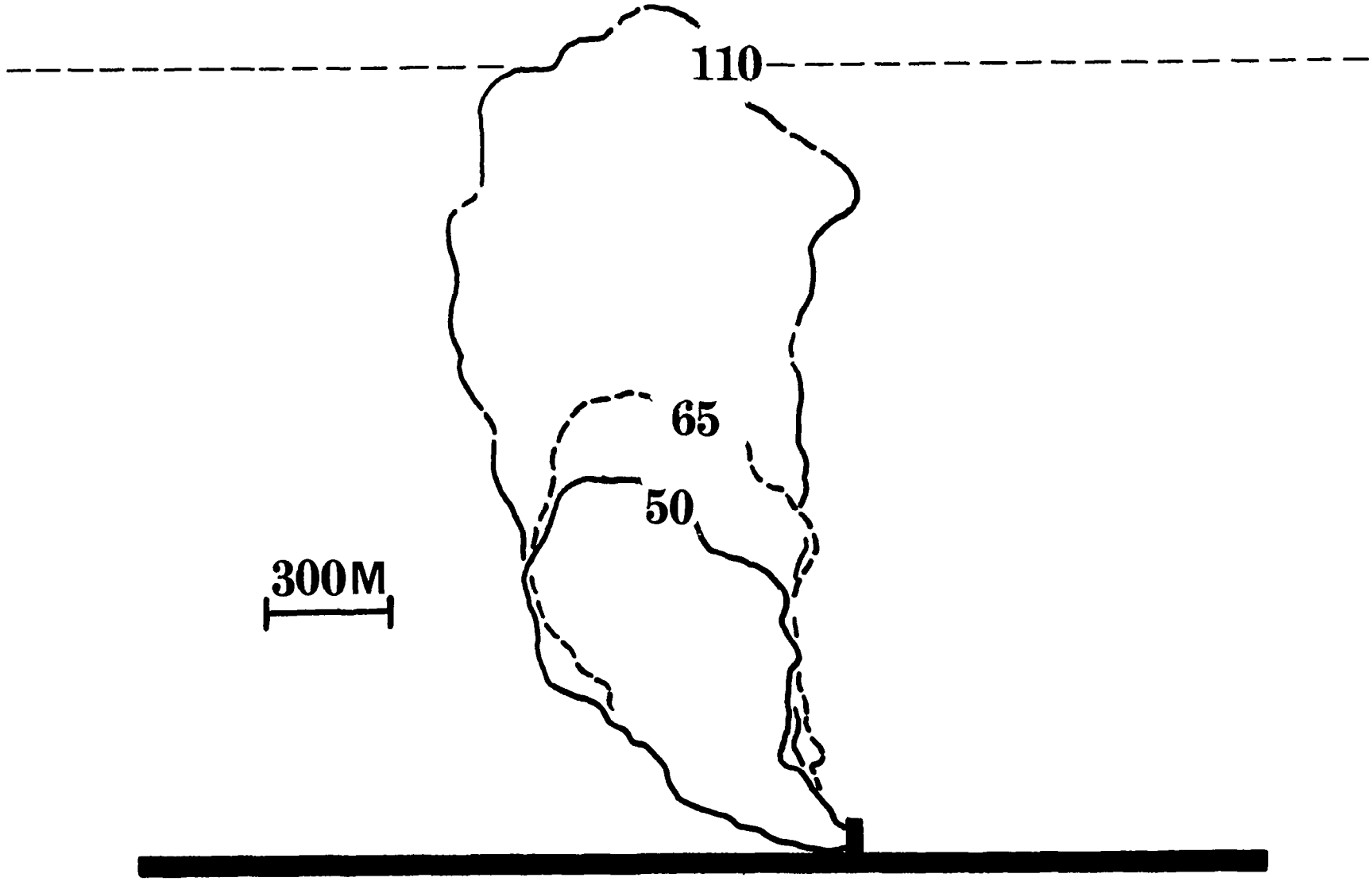

Figure 19. Rectified Cloud Geometry. Firing S-IC-15.

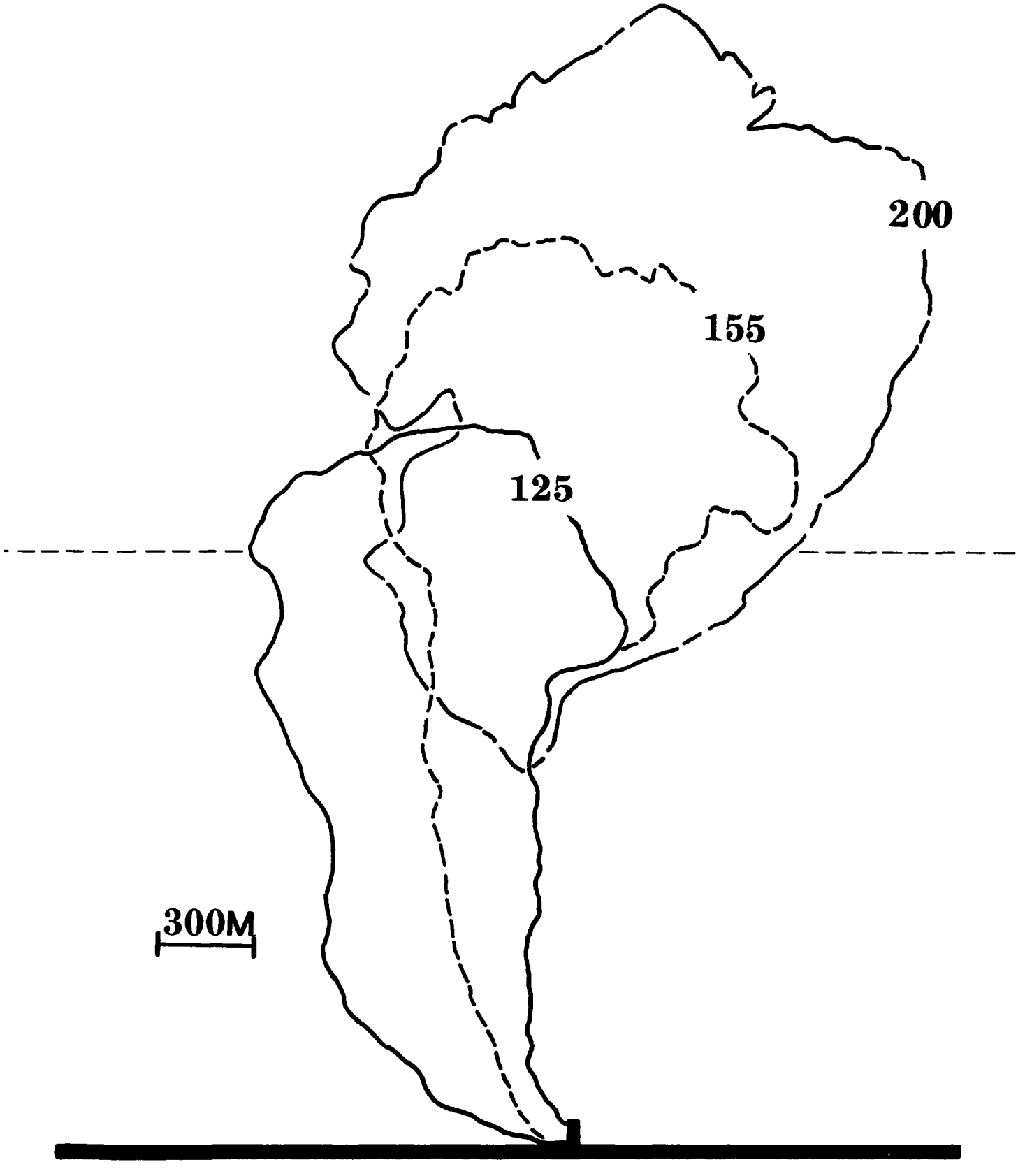

Figure 20. Rectified Cloud Geometry. Firing S-IC-15.

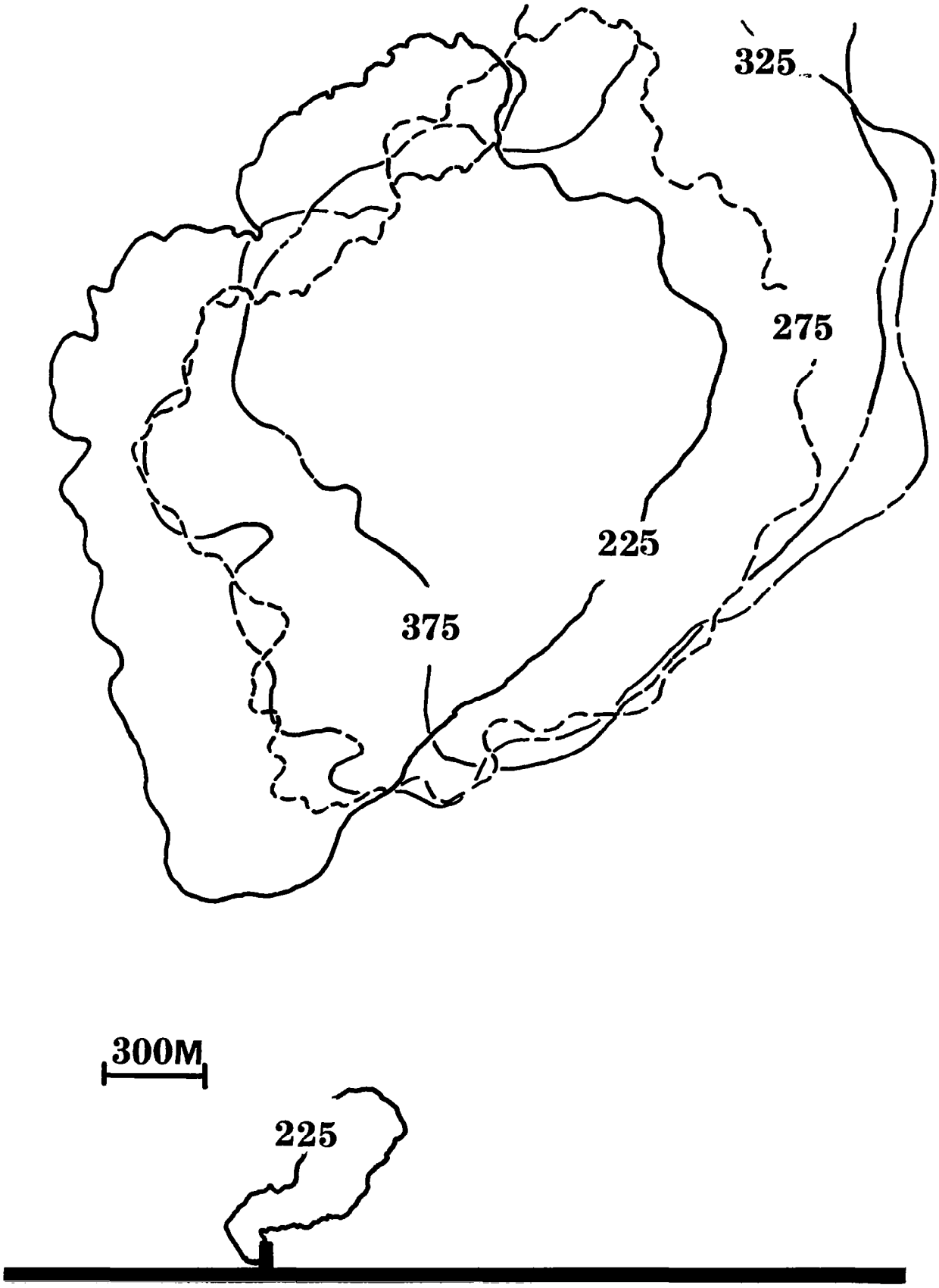

Figure 21. Rectified Cloud Geometry. Firing S-IC-15.

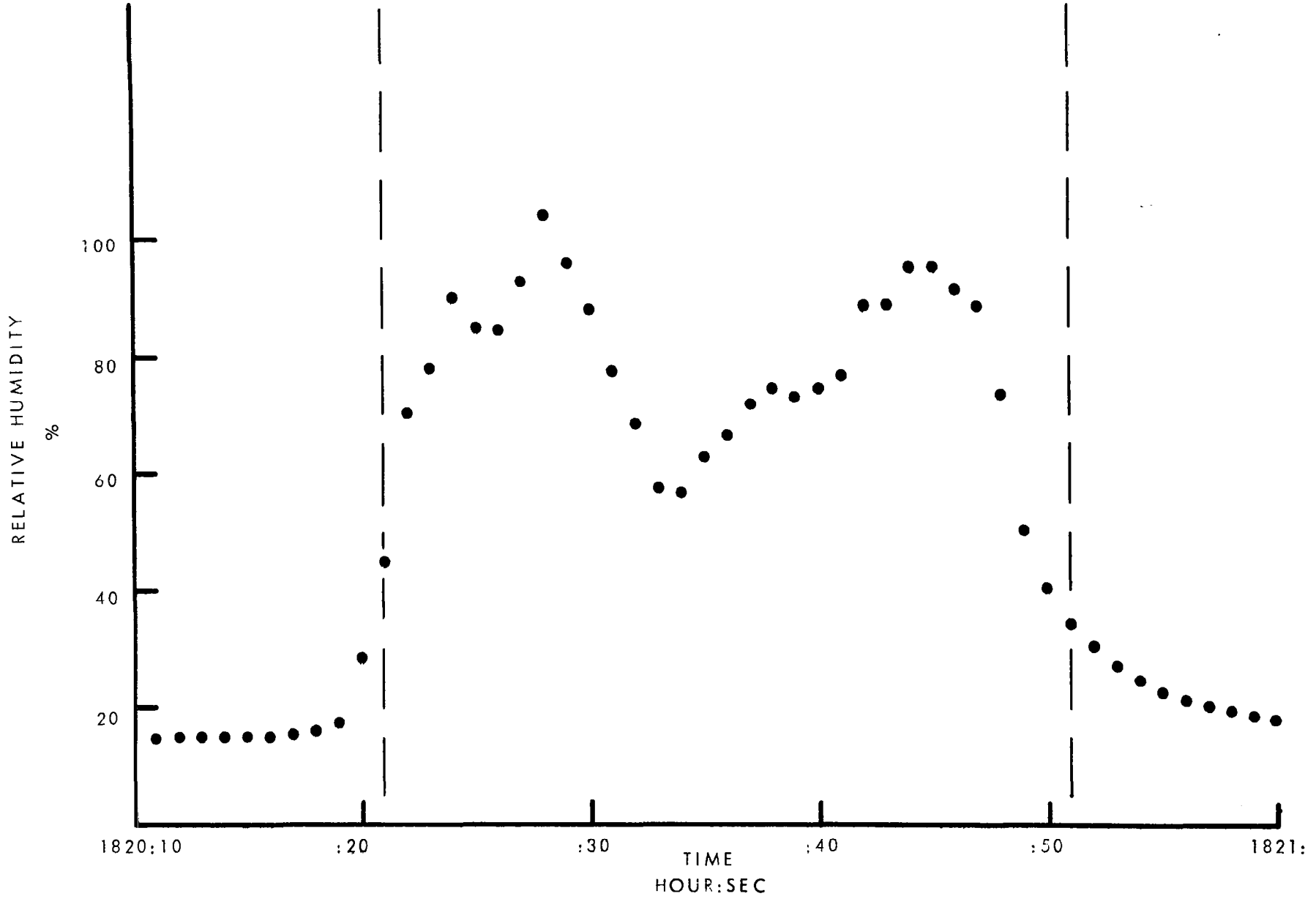

Figure 22. Relative Humidity In Cloud. Pass 1.
Firing S-IC-15. MSU Aircraft.

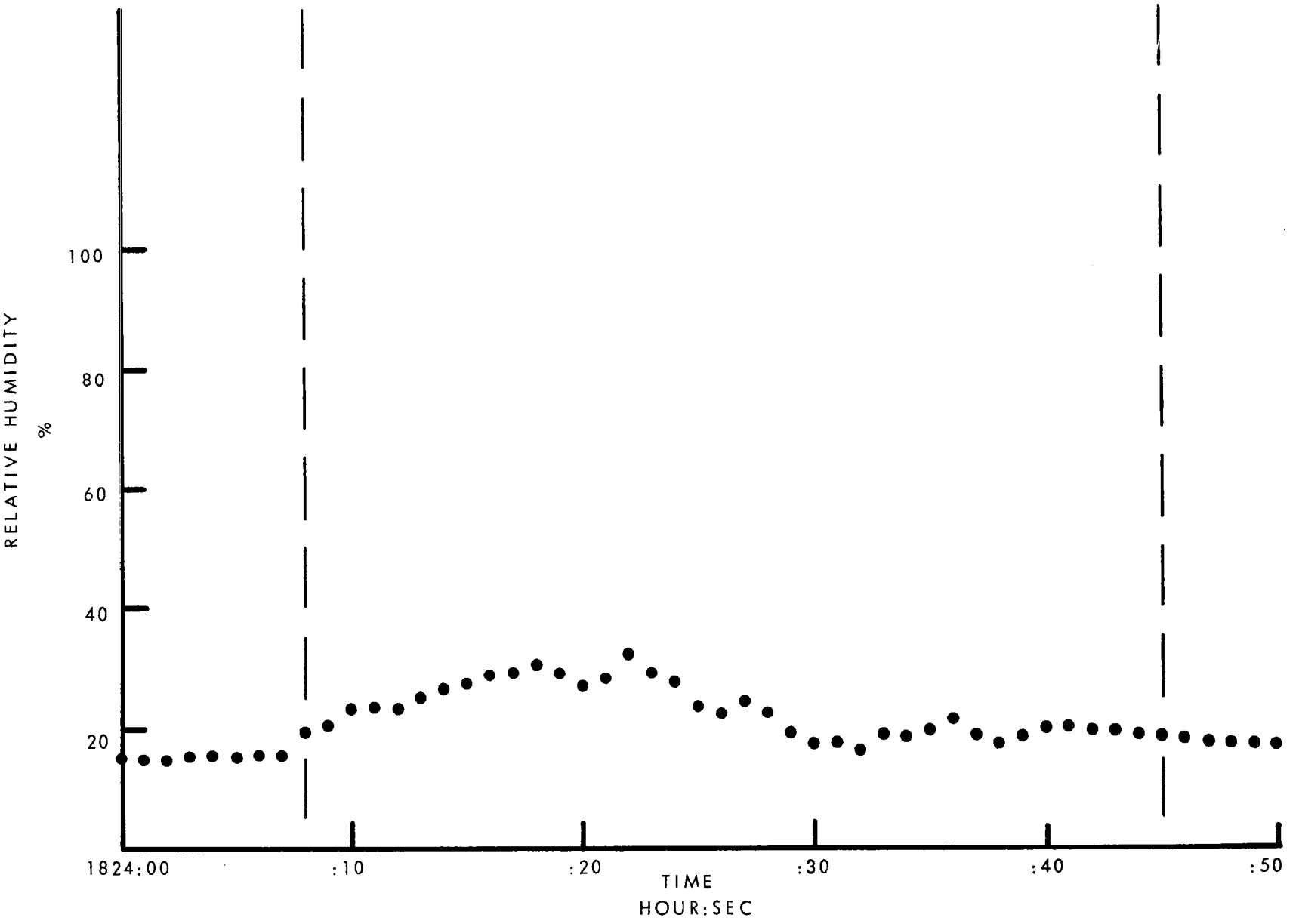

Figure 23. Relative Humidity In Cloud. Pass 2.
Firing S-IC-15. MSU Aircraft.

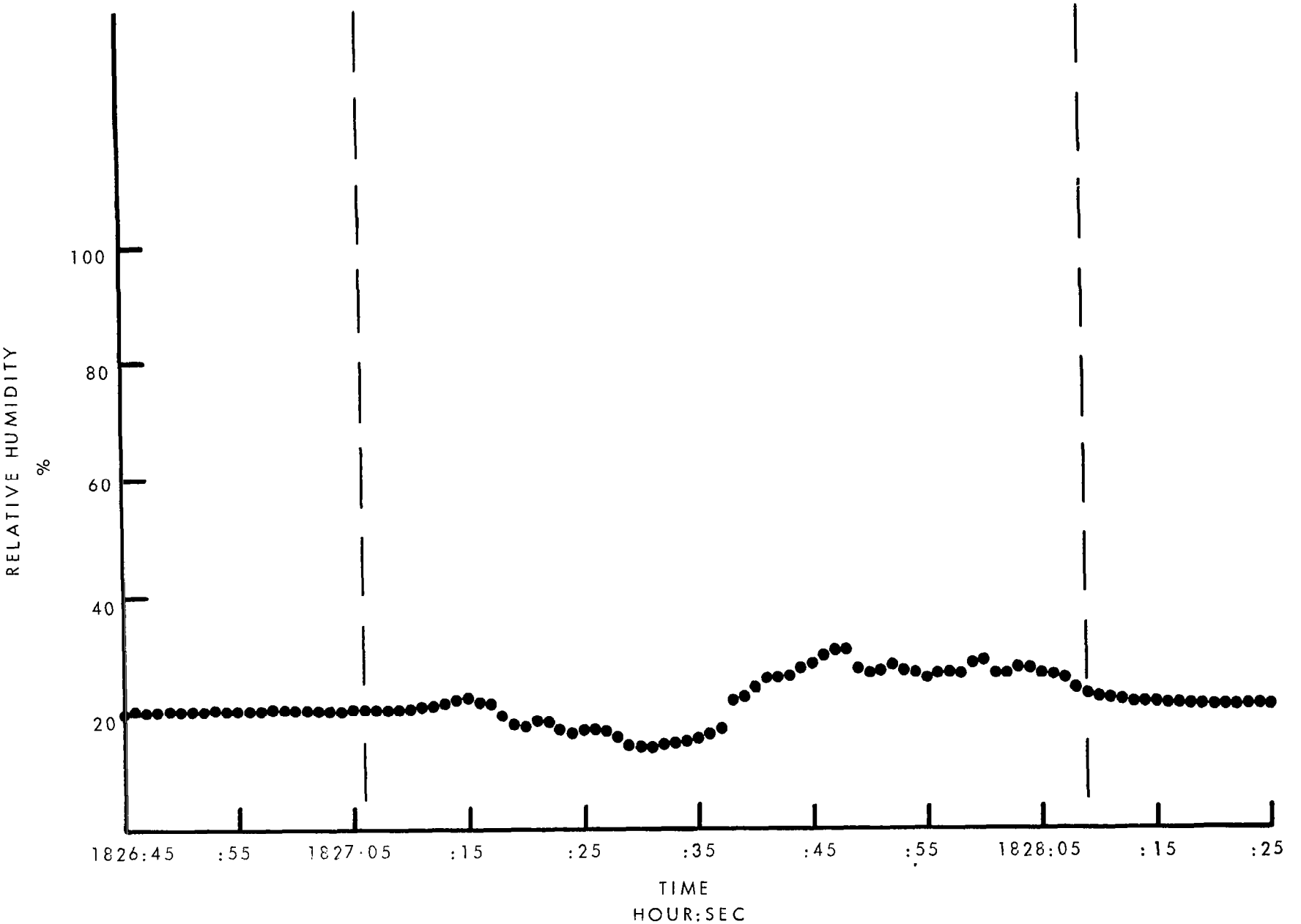

Figure 24. Relative Humidity In Cloud. Pass 3.
Firing S-IC-15. MSU Aircraft.

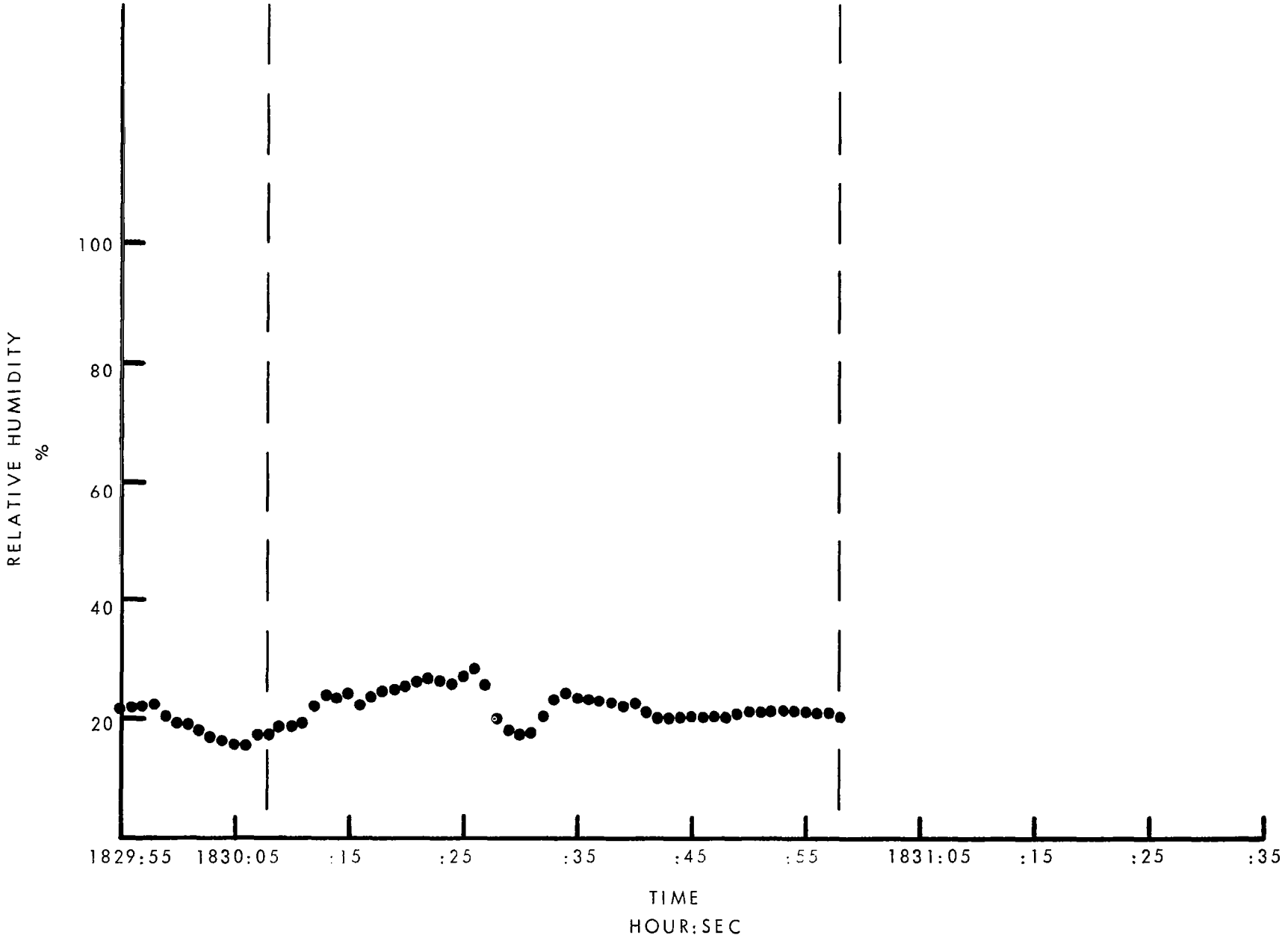

Figure 25. Relative Humidity In Cloud. Pass 4.
Firing S-IC-15. MSU Aircraft.

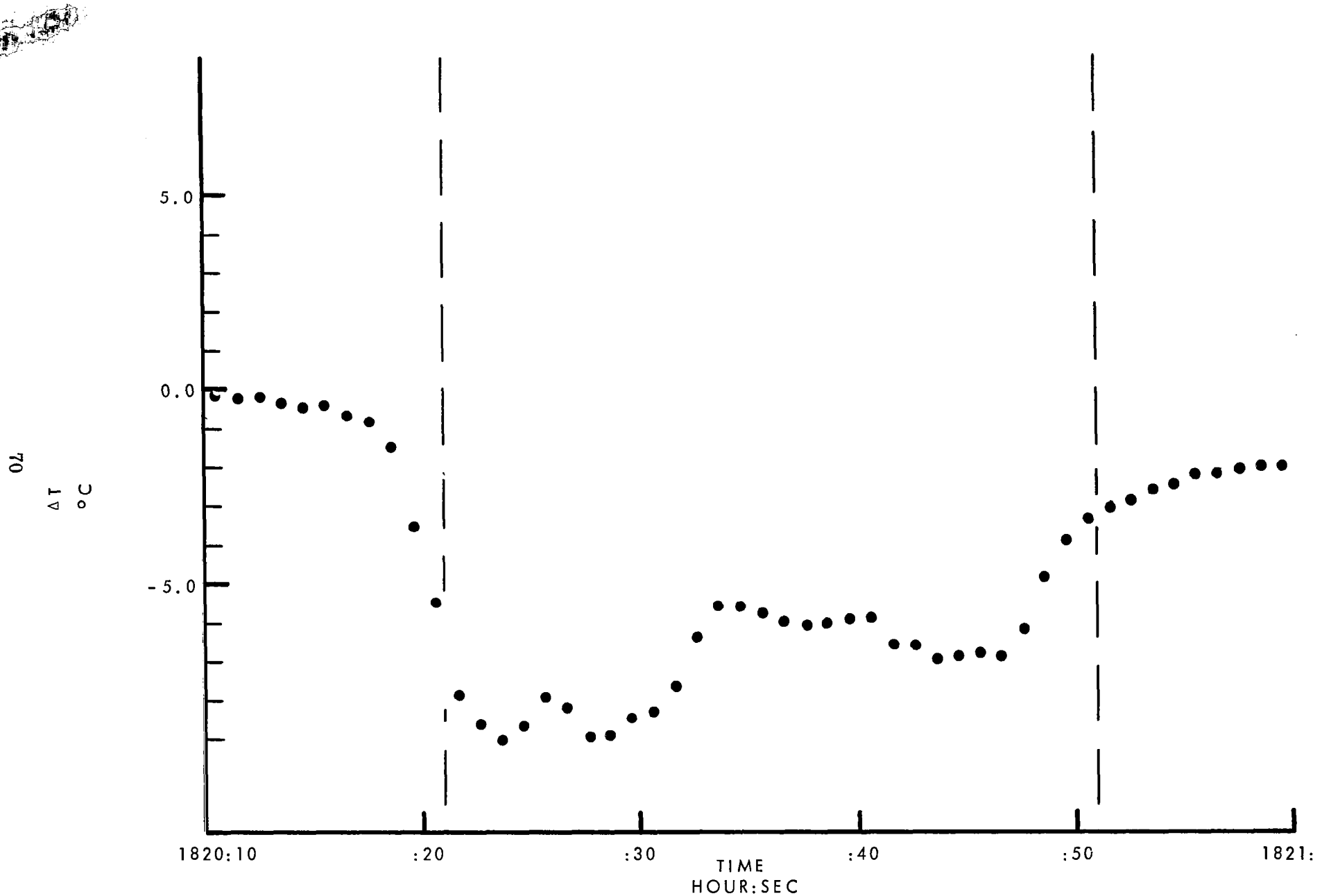

Figure 26. Disturbed Temperature In Cloud. Pass 1.
Firing S-IC-15. MSU Aircraft.

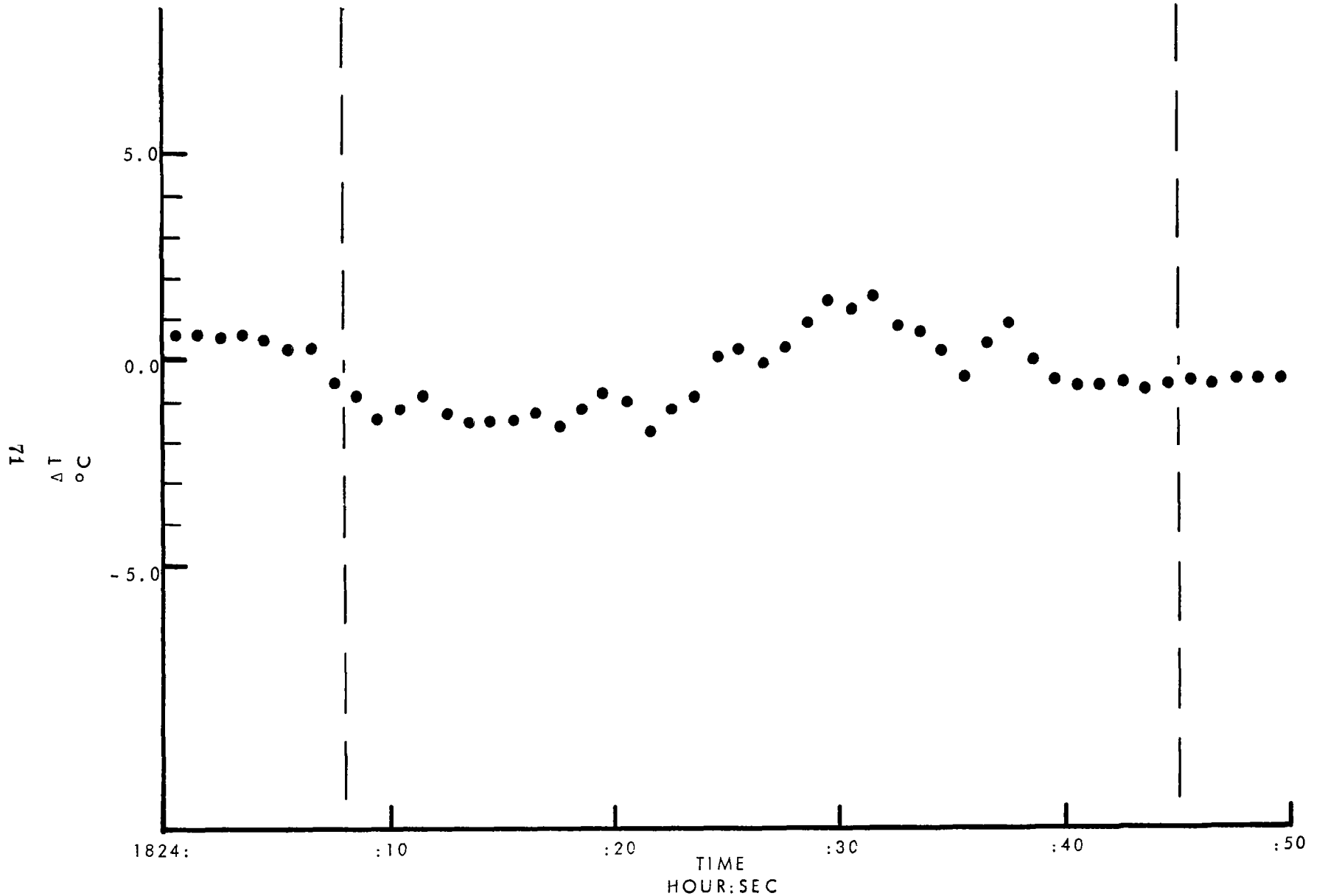

Figure 27. Disturbed Temperature In Cloud. Pass 2.
Firing S-IC-15. MSU Aircraft.

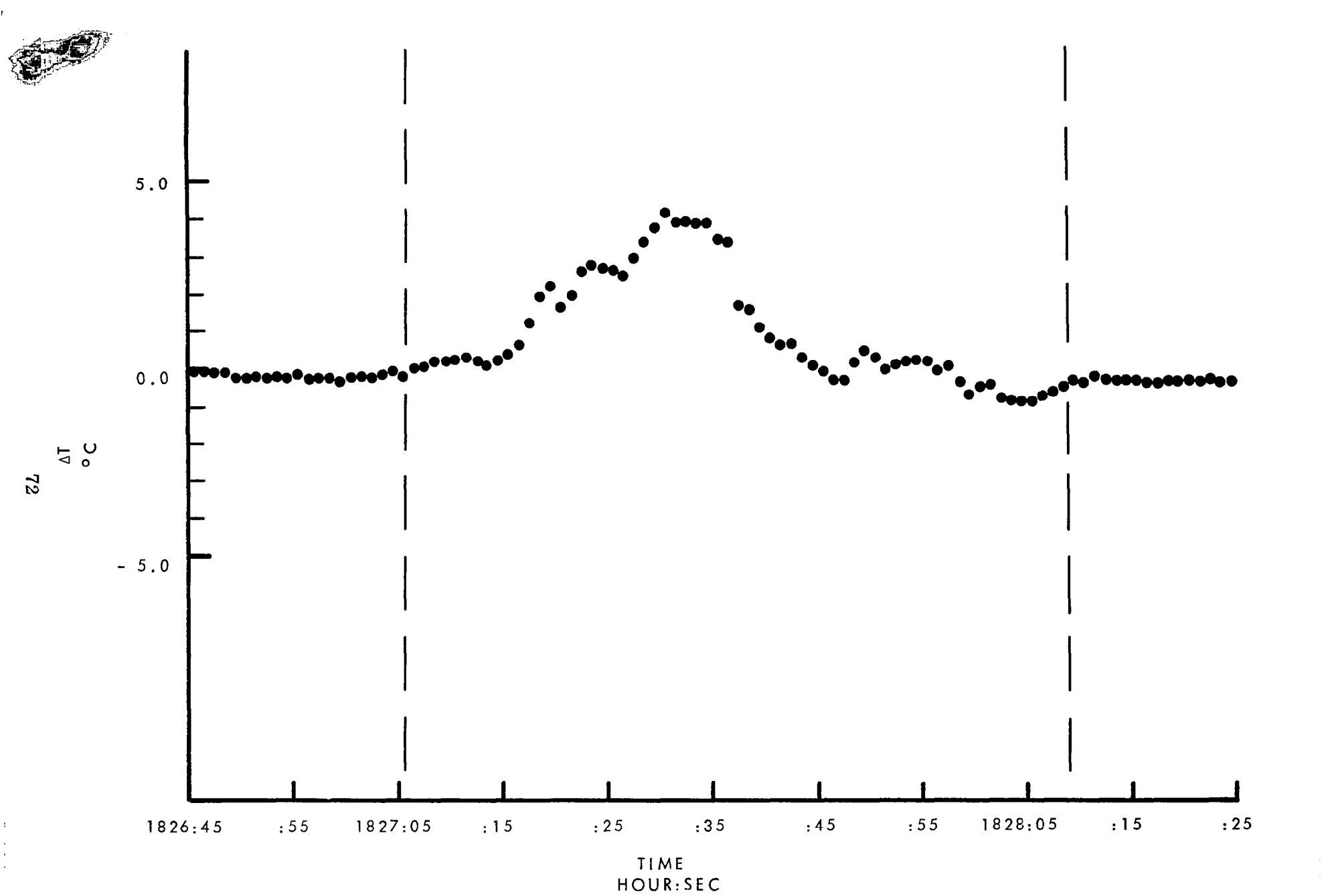

Figure 28. Disturbed Temperature In Cloud. Pass 3.
Firing S-IC-15. MSU Aircraft.

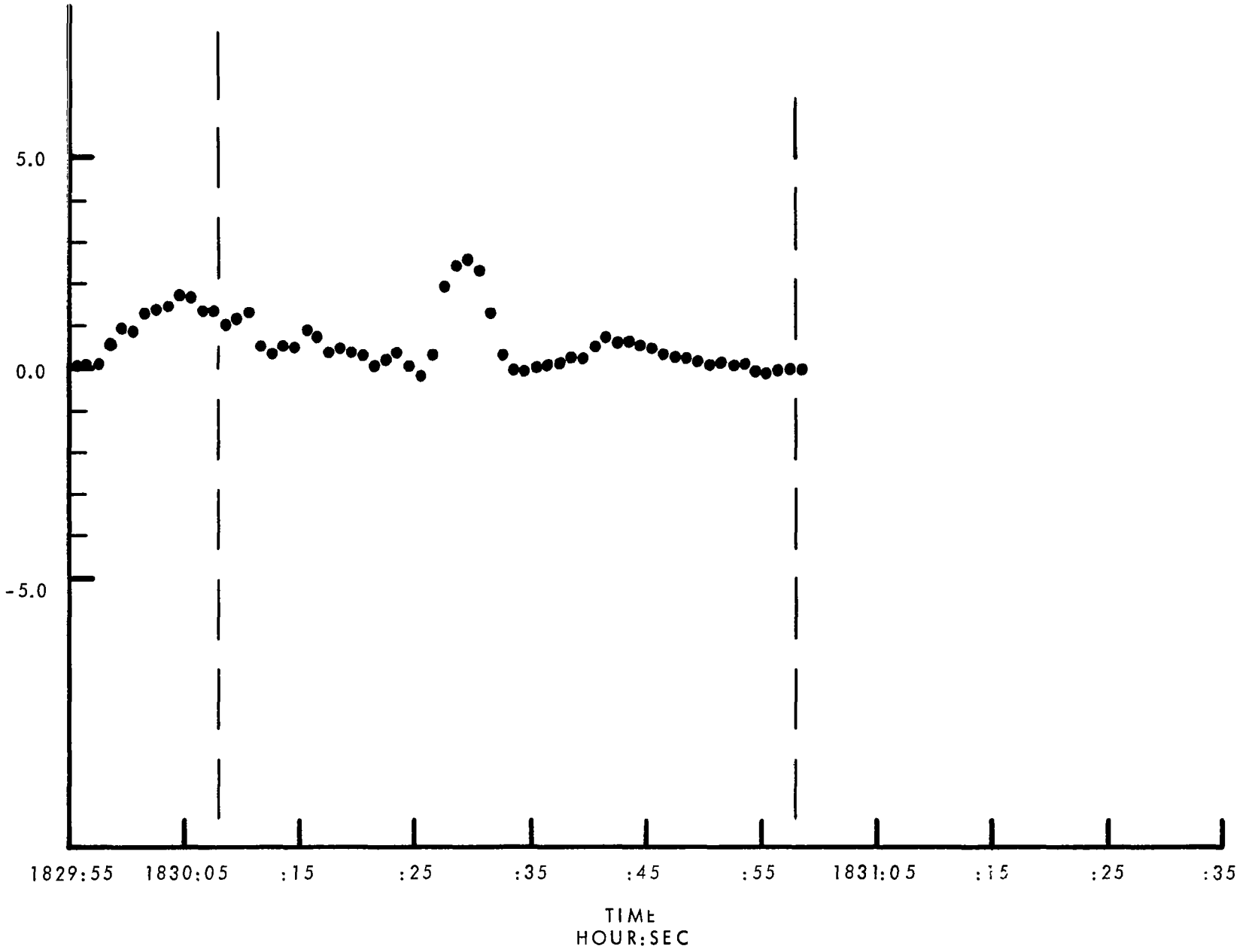

Figure 29. Disturbed Temperature In Cloud. Pass 4.
Firing S-IC-15. MSU Aircraft.

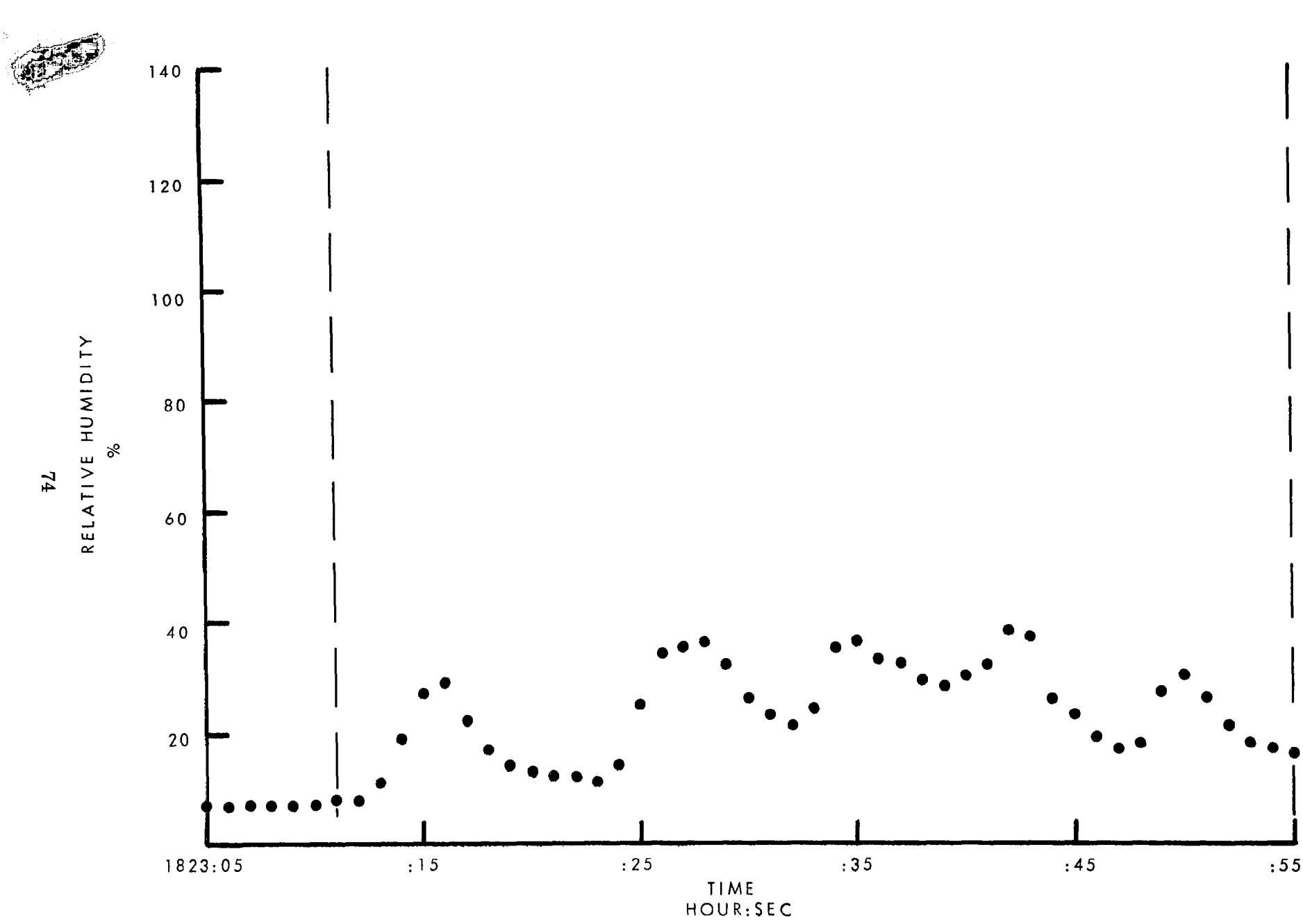

Figure 30. Relative Humidity In Cloud. Pass 1.
Firing S-IC-15. Penn. State Aircraft.

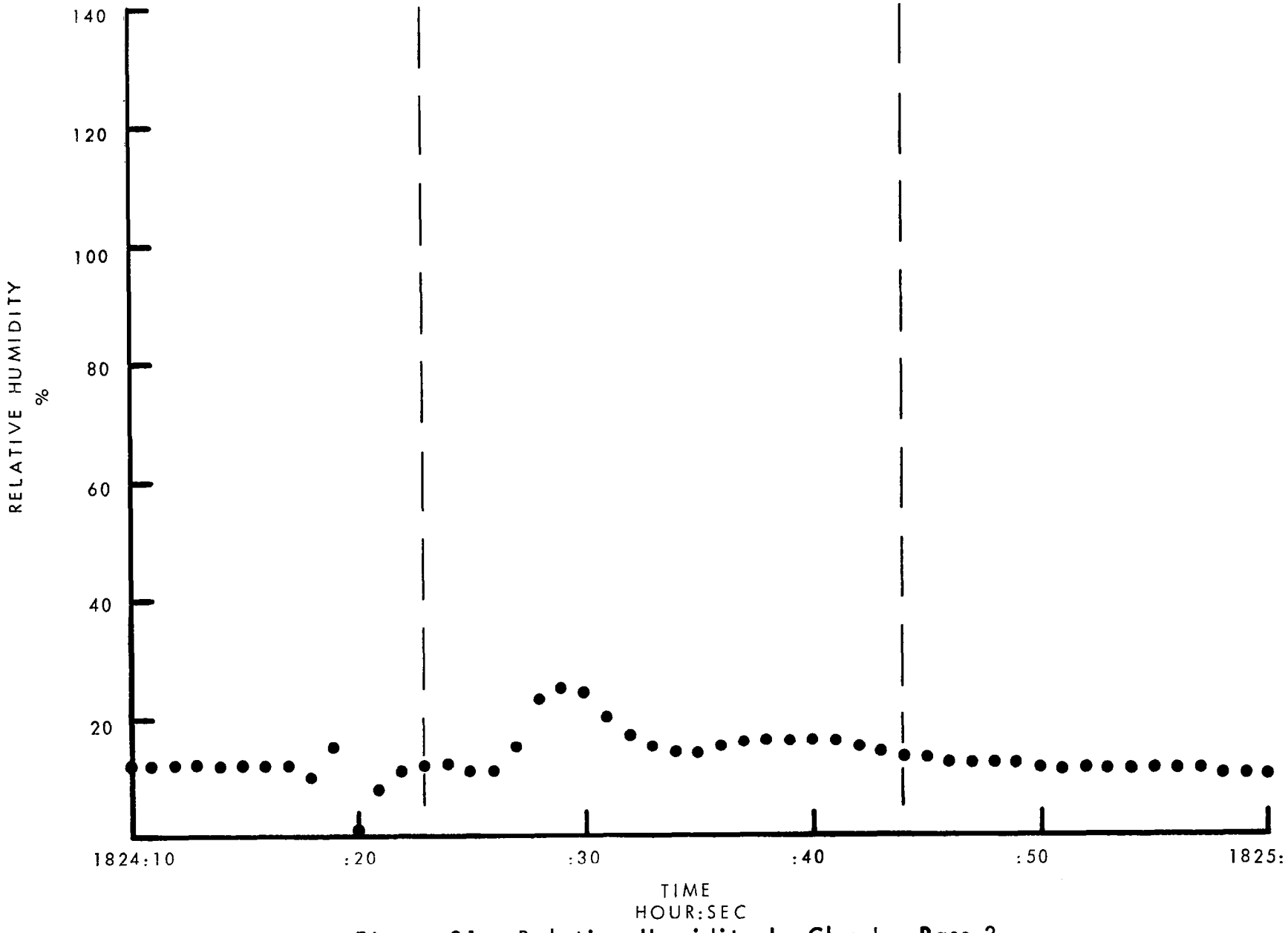

Figure 31. Relative Humidity In Cloud. Pass 2. Firing S-IC-15. Penn. State Aircraft.

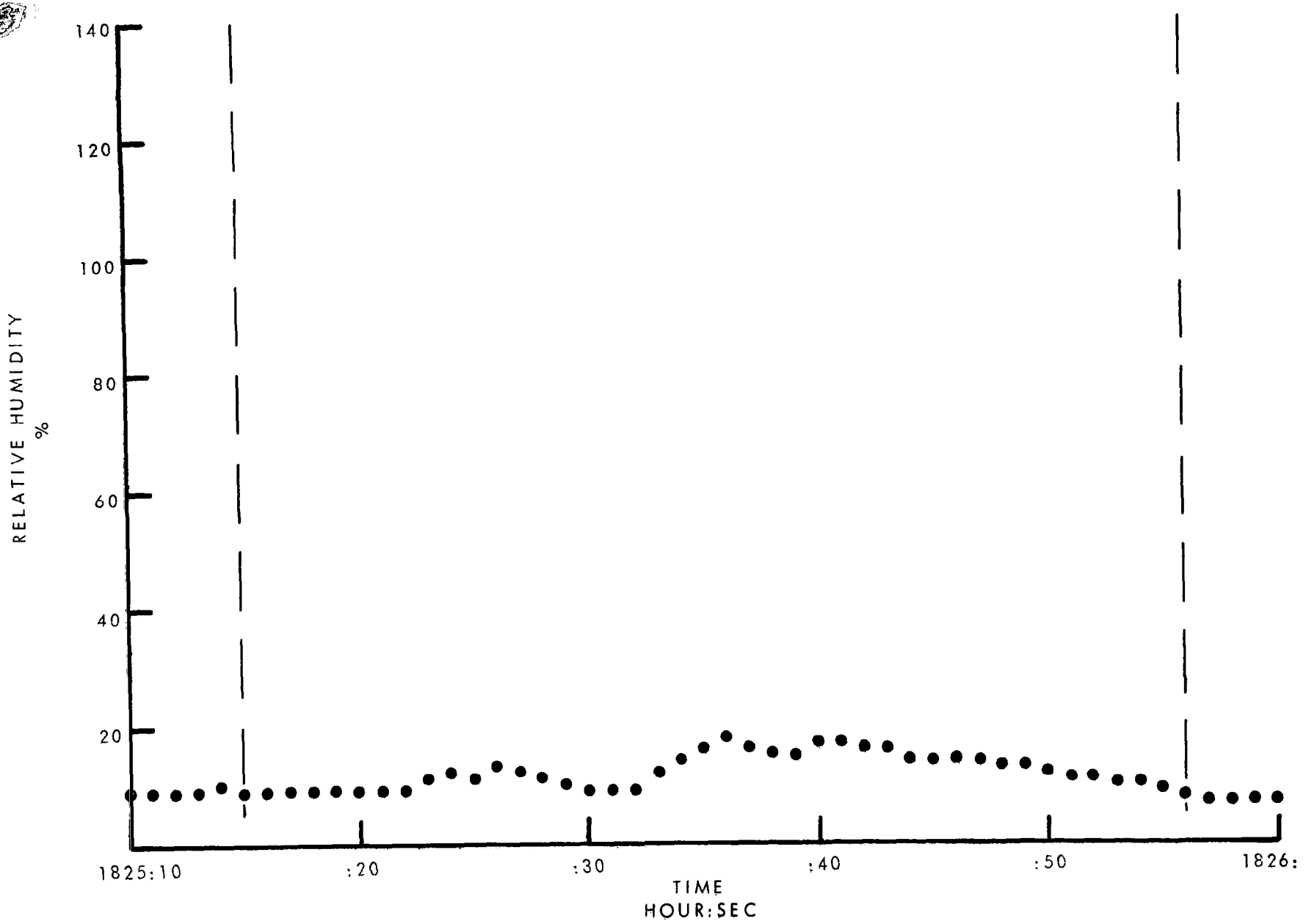

Figure 32. Relative Humidity In Cloud. Pass 3.
Firing S-IC-15. Penn. State Aircraft.

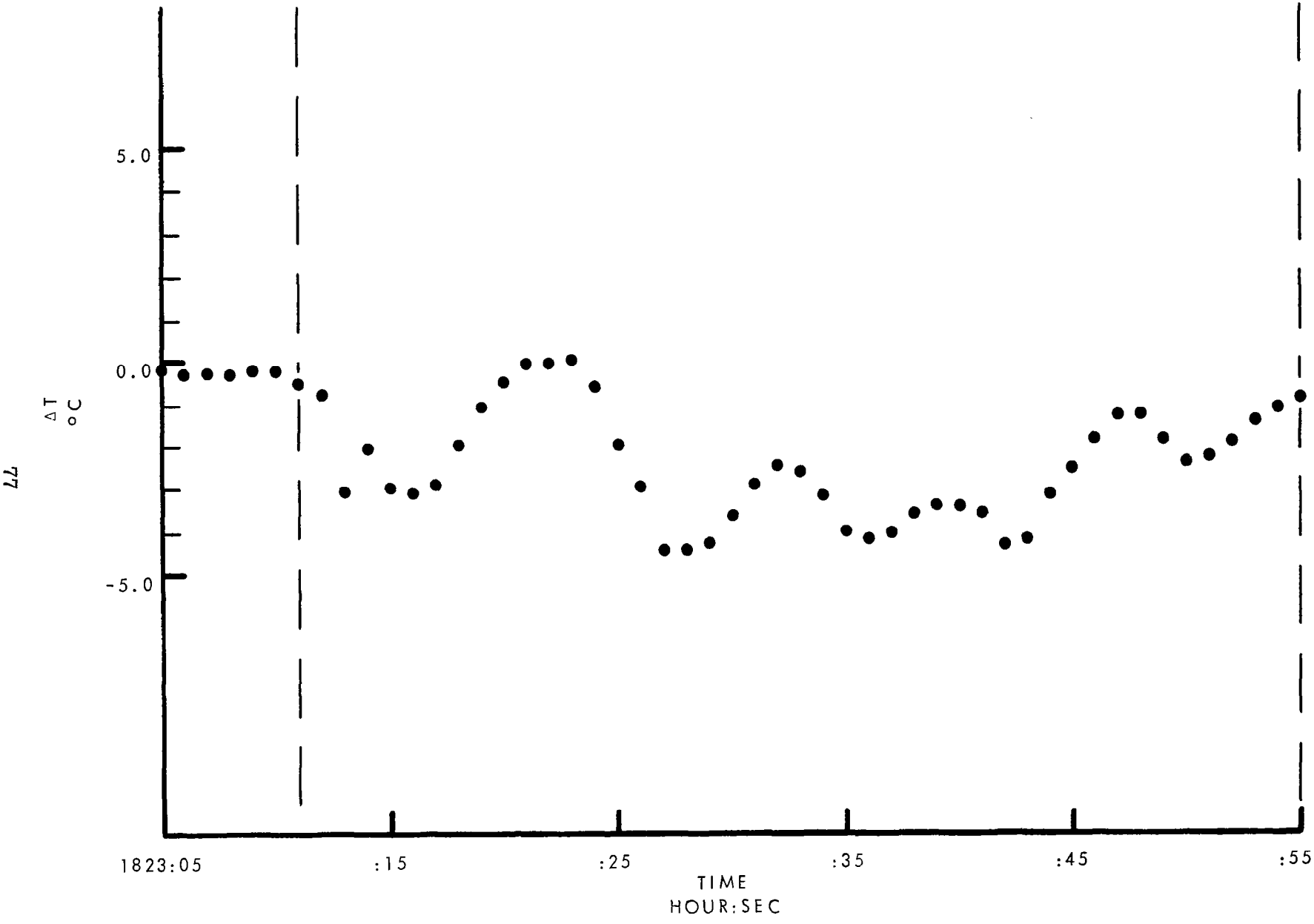

Figure 33. Disturbed Temperature In Cloud. Pass 1.
Firing S-IC-15. Penn. State Aircraft.

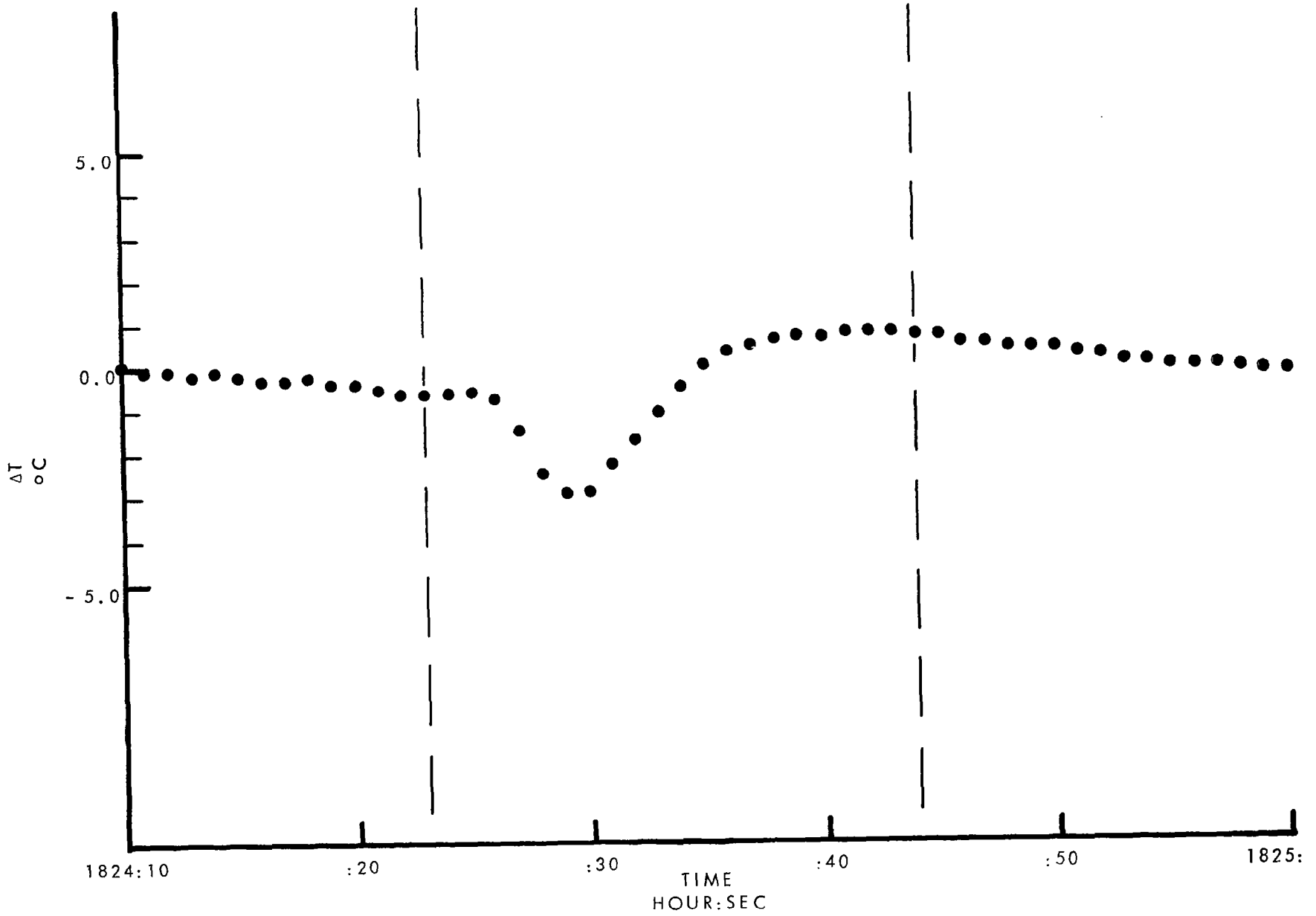

Figure 34. Disturbed Temperature In Cloud. Pass 2.
Firing S-IC-15. Penn. State Aircraft.

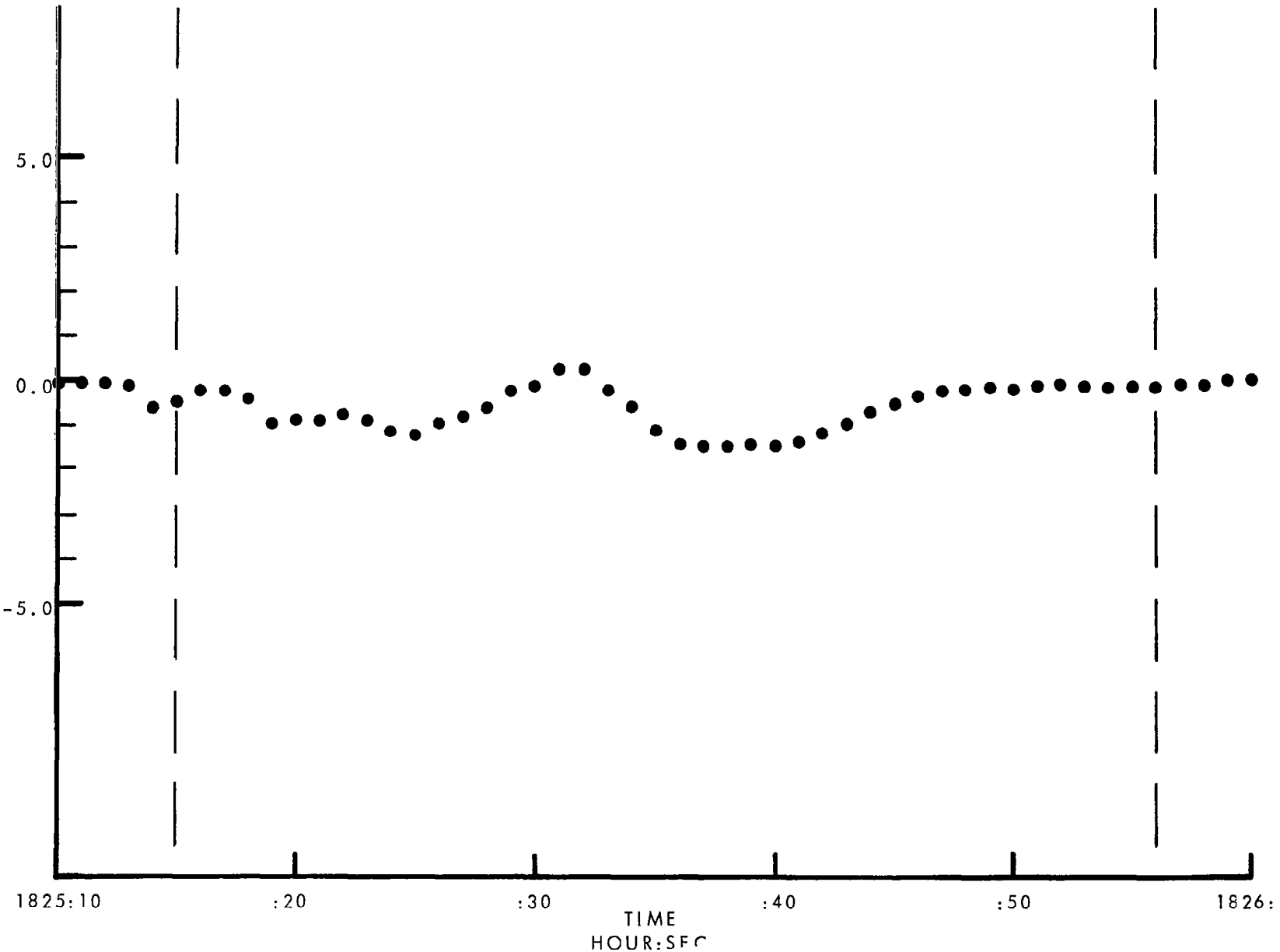

Figure 35. Disturbed Temperature In Cloud. Pass 3.
Firing S-IC-15. Penn. State Aircraft.

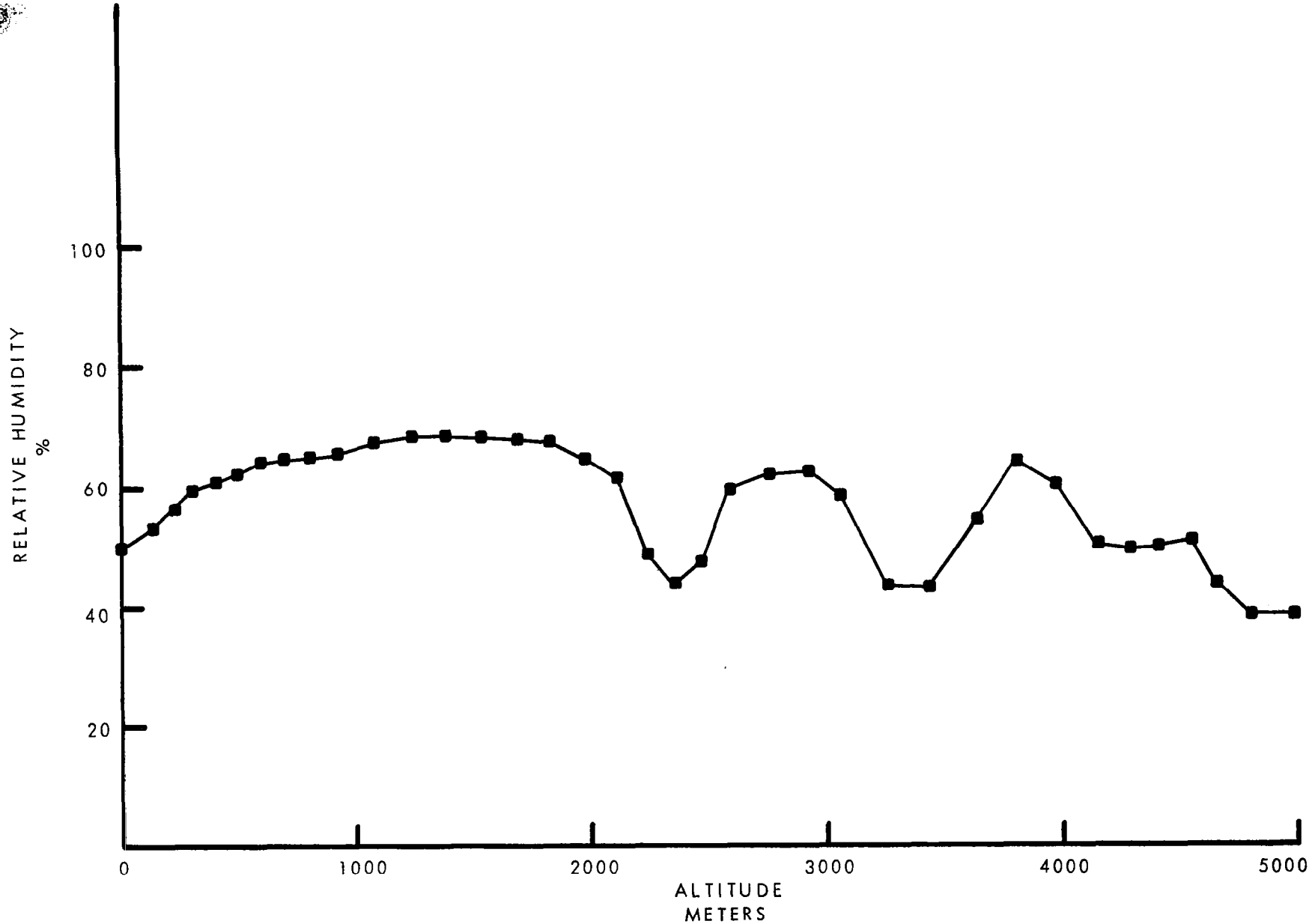

Figure 36. Rediosonde Relative Humidity Sounding.
Firing S-II-14.

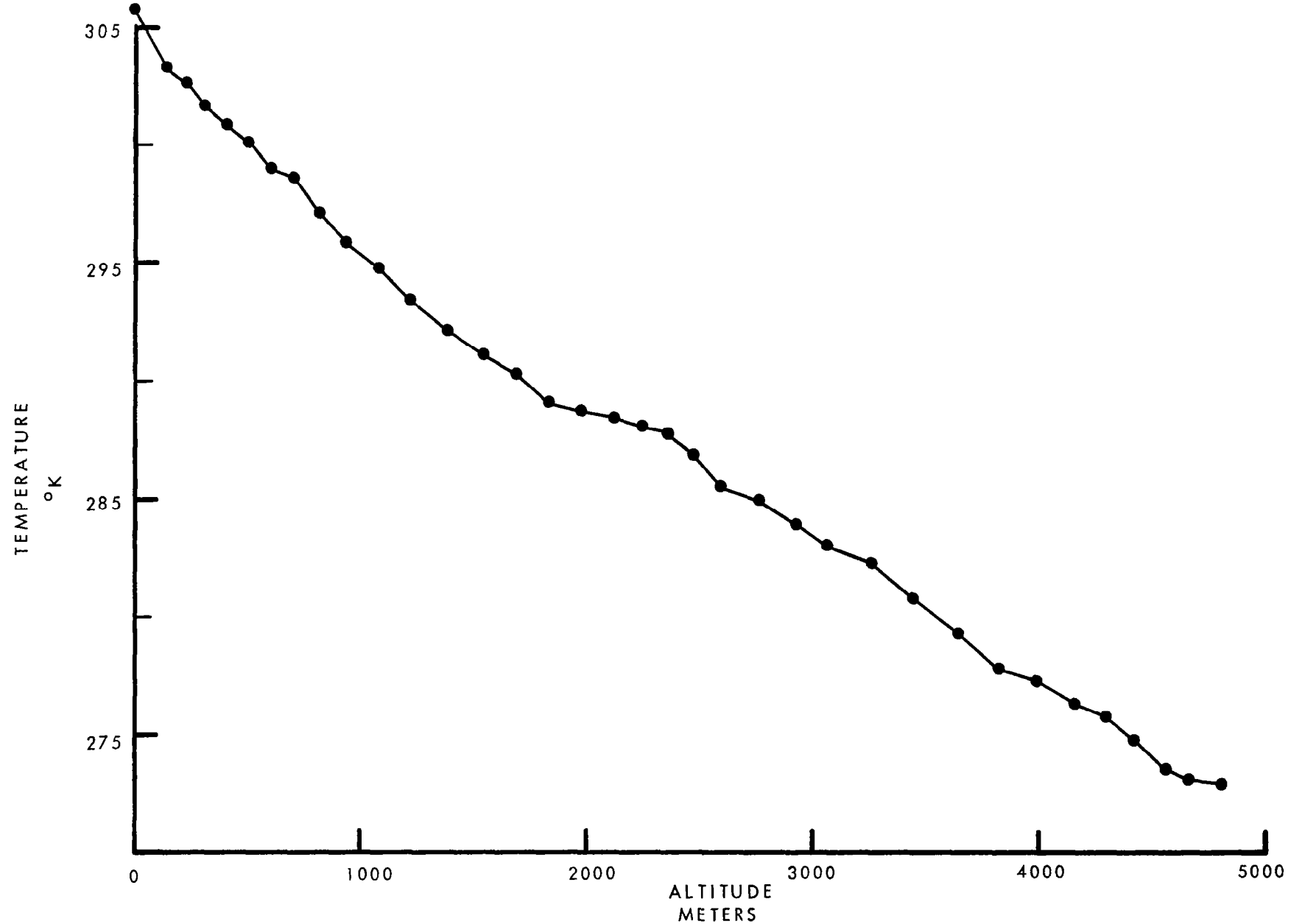

Figure 37. Radiosonde Temperature Sounding.
Firing S-II-14.

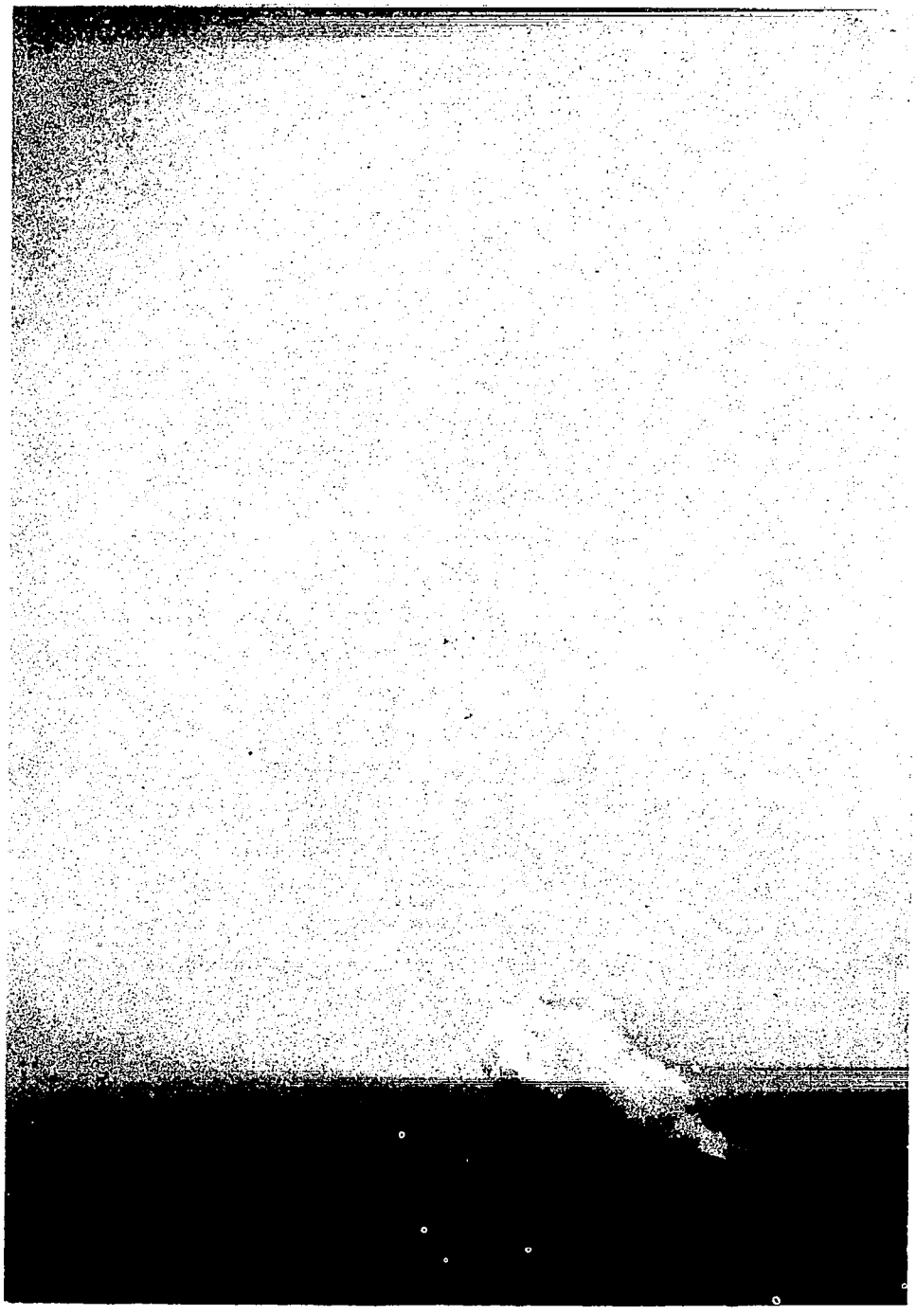

Figure 38. Cloud Photograph 50 Seconds After Ignition. Firing S-II-14.

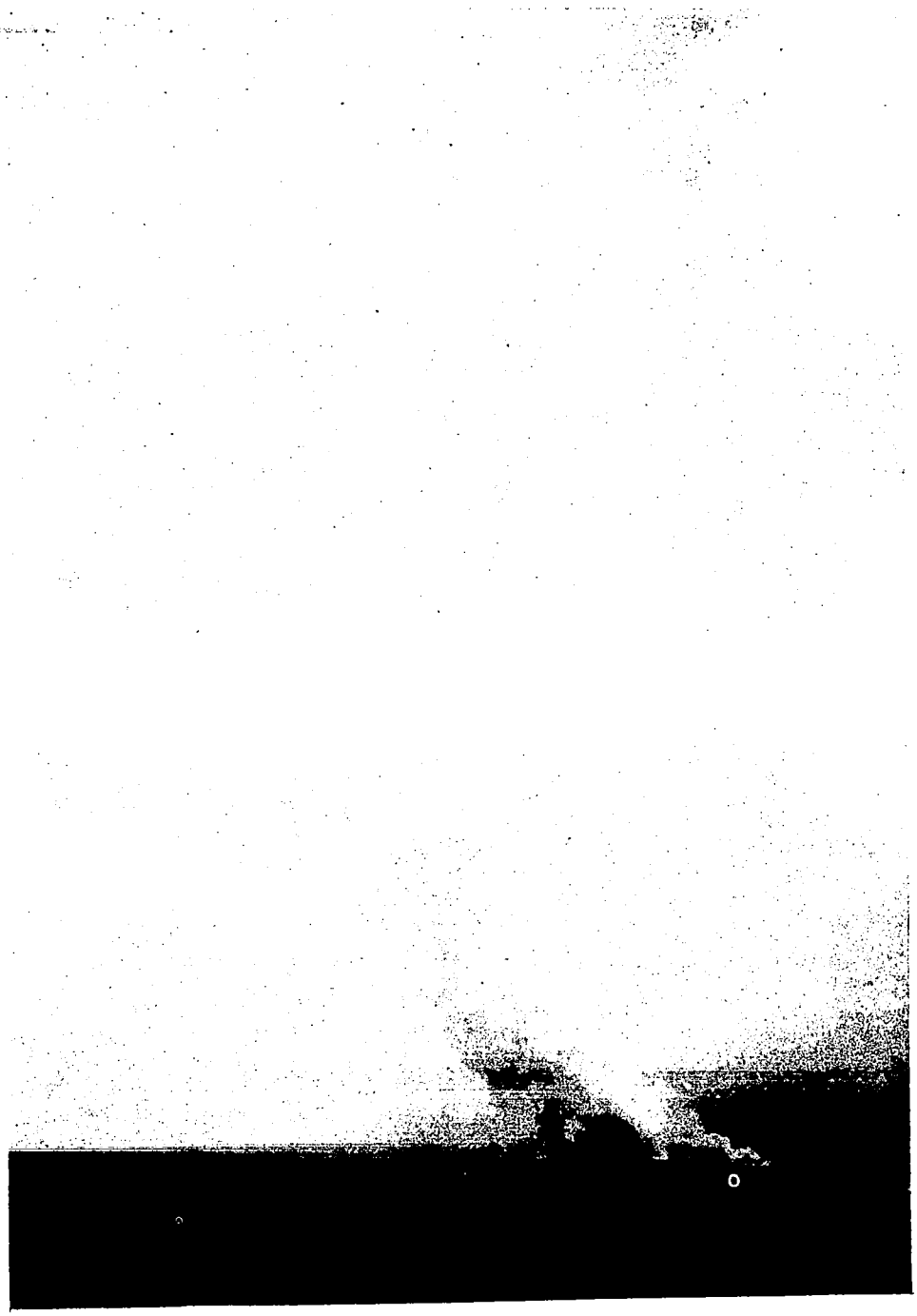

Figure 39. Cloud Photograph 110 Seconds After Ignition. Firing S-II-14.

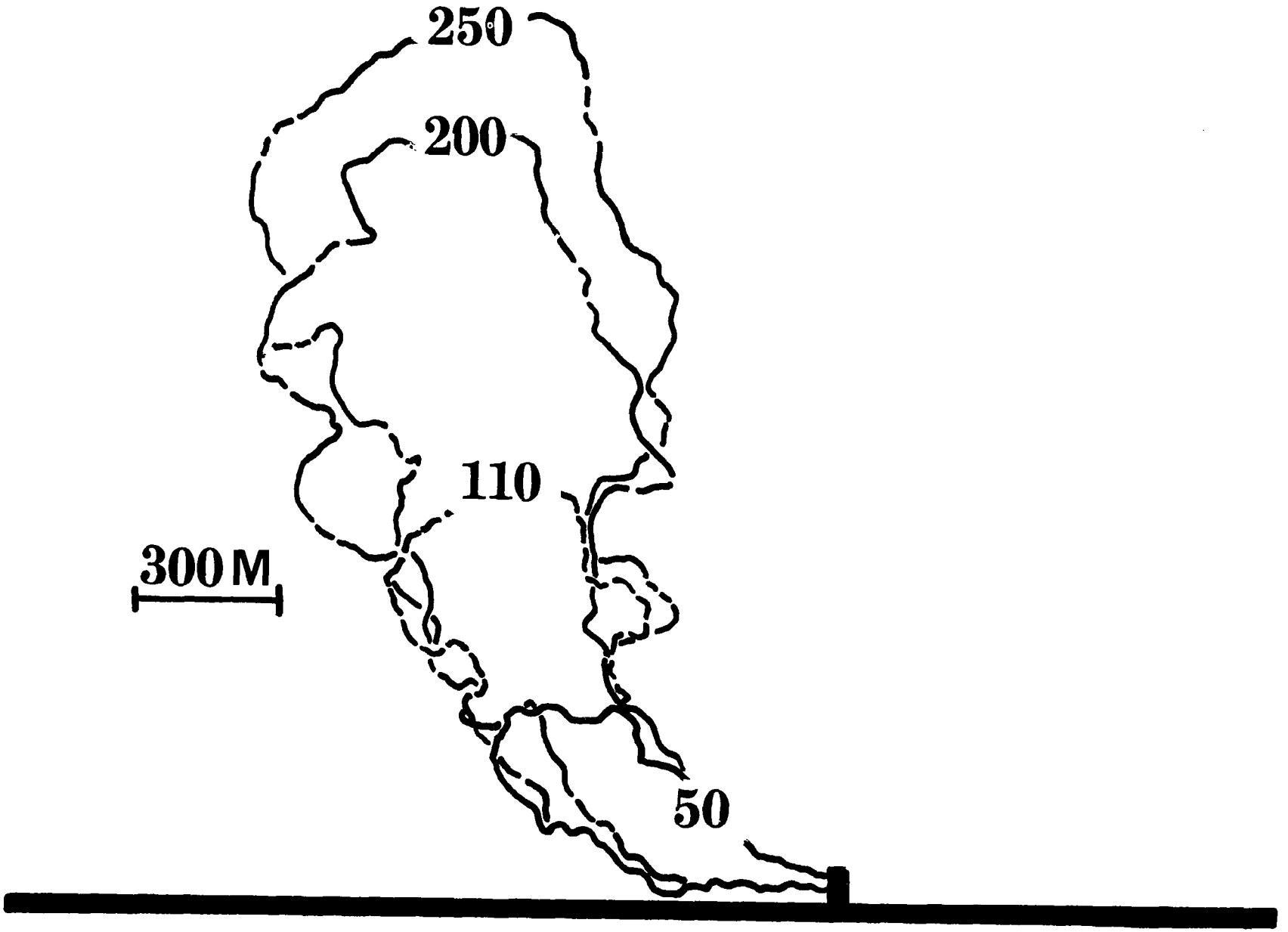

Figure 40. Rectified Cloud Geometry. Firing S-II-14.

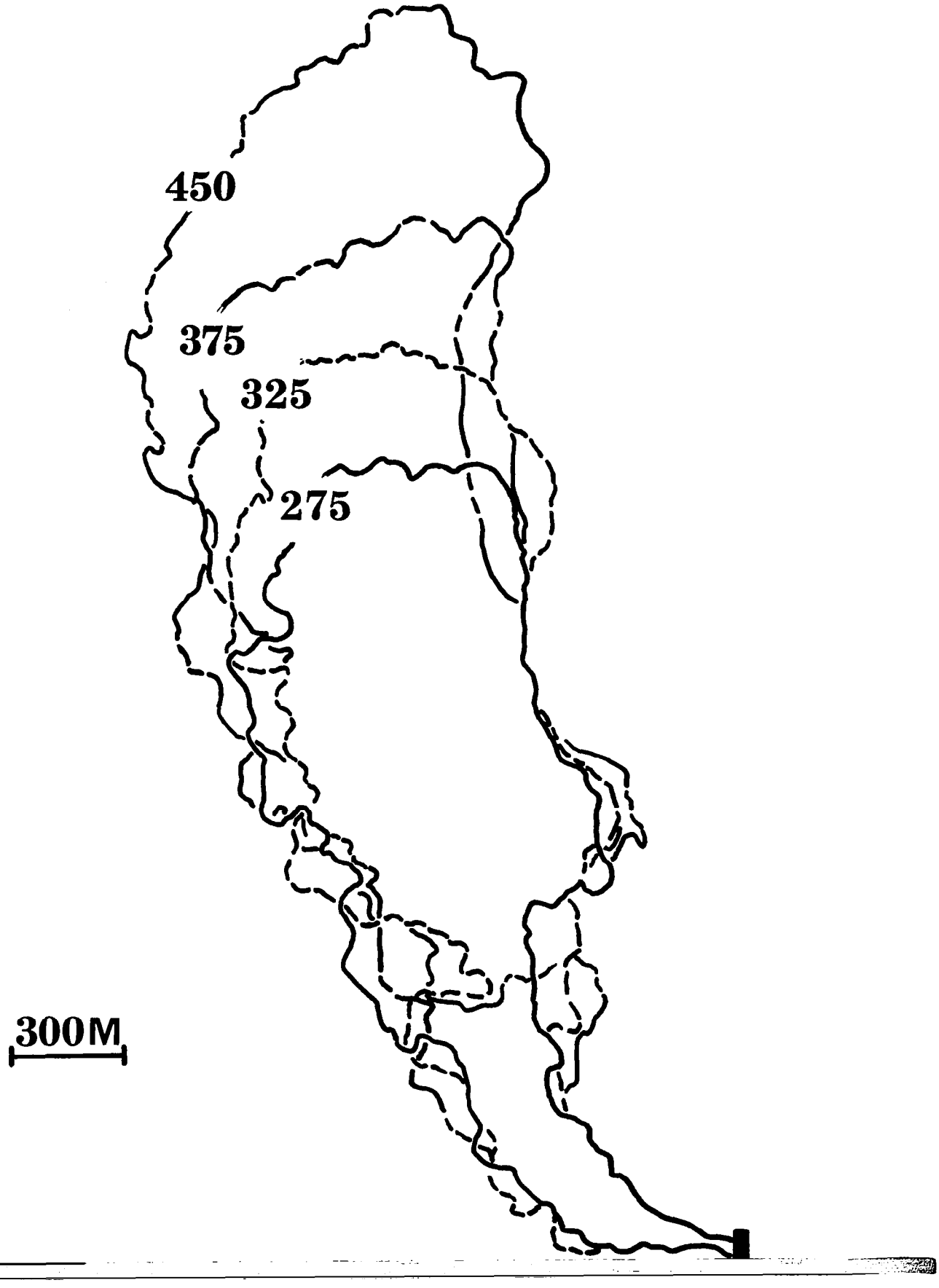

Figure 41. Rectified Cloud Geometry. Firing S-II-14.

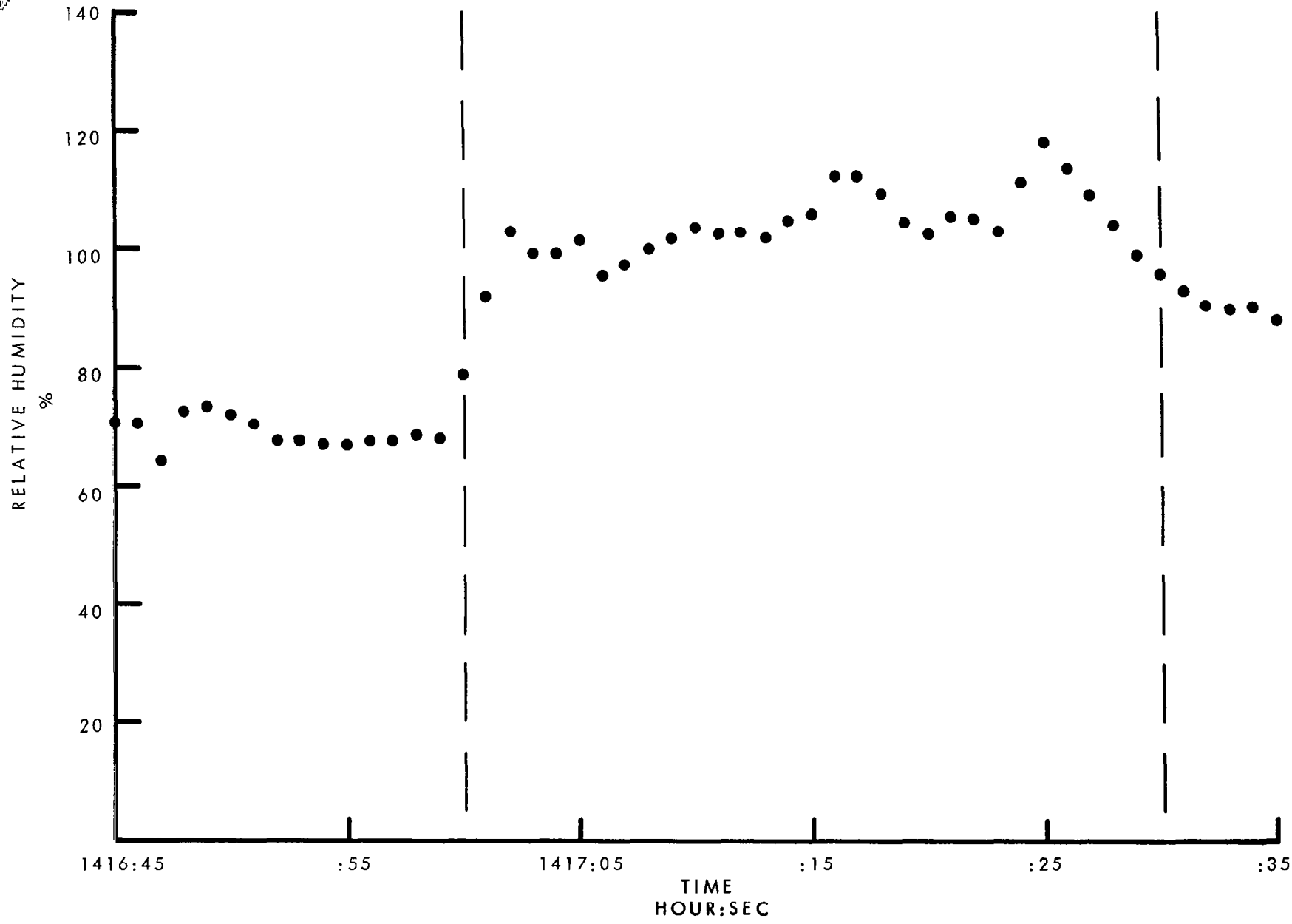

Figure 42. Relative Humidity In Cloud. Pass 1.
Firing S-II-14. MSU Aircraft.

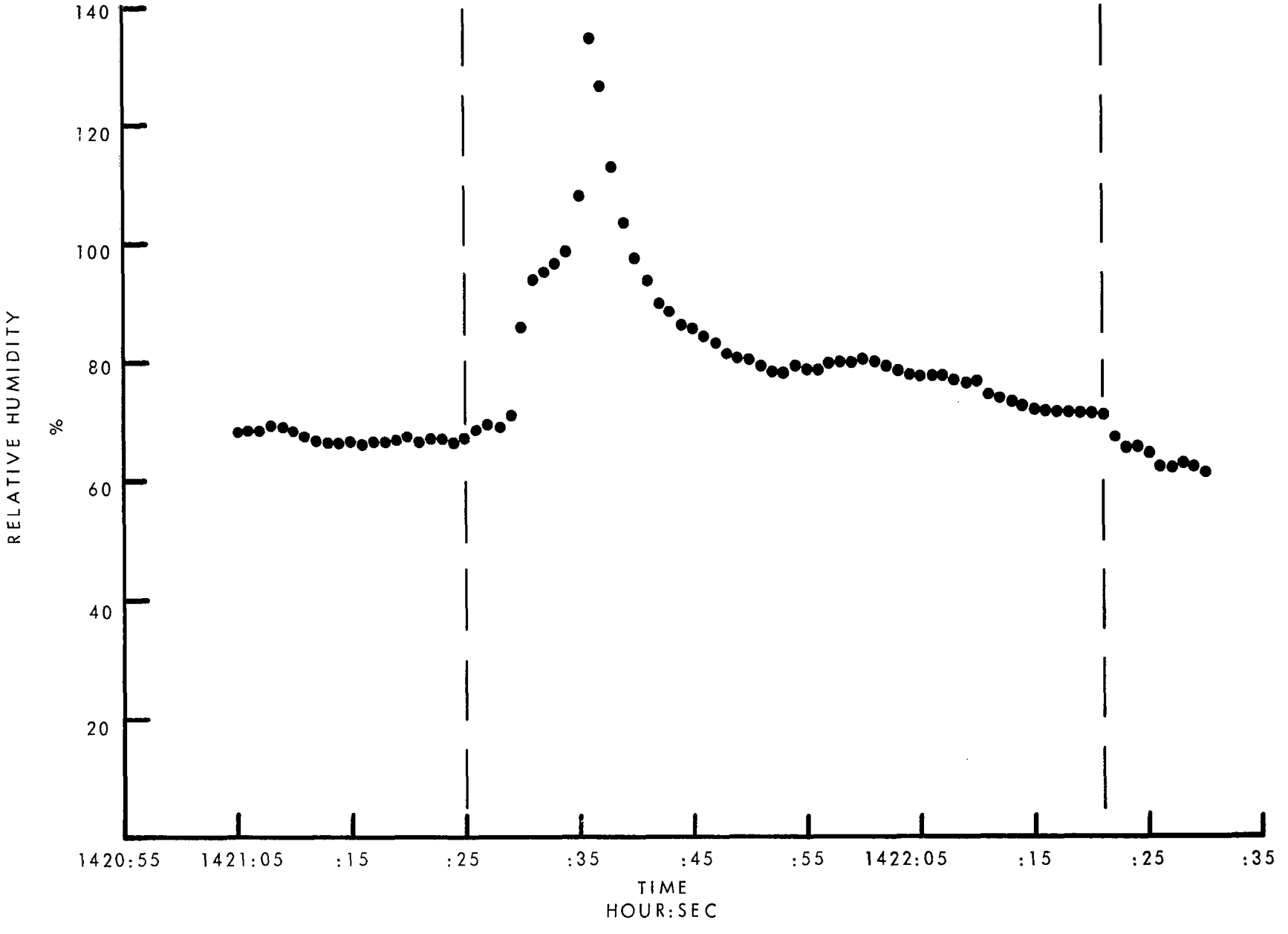

Figure 43. Relative Humidity In Cloud. Pass 2.
Firing S-II-14. MSU Aircraft.

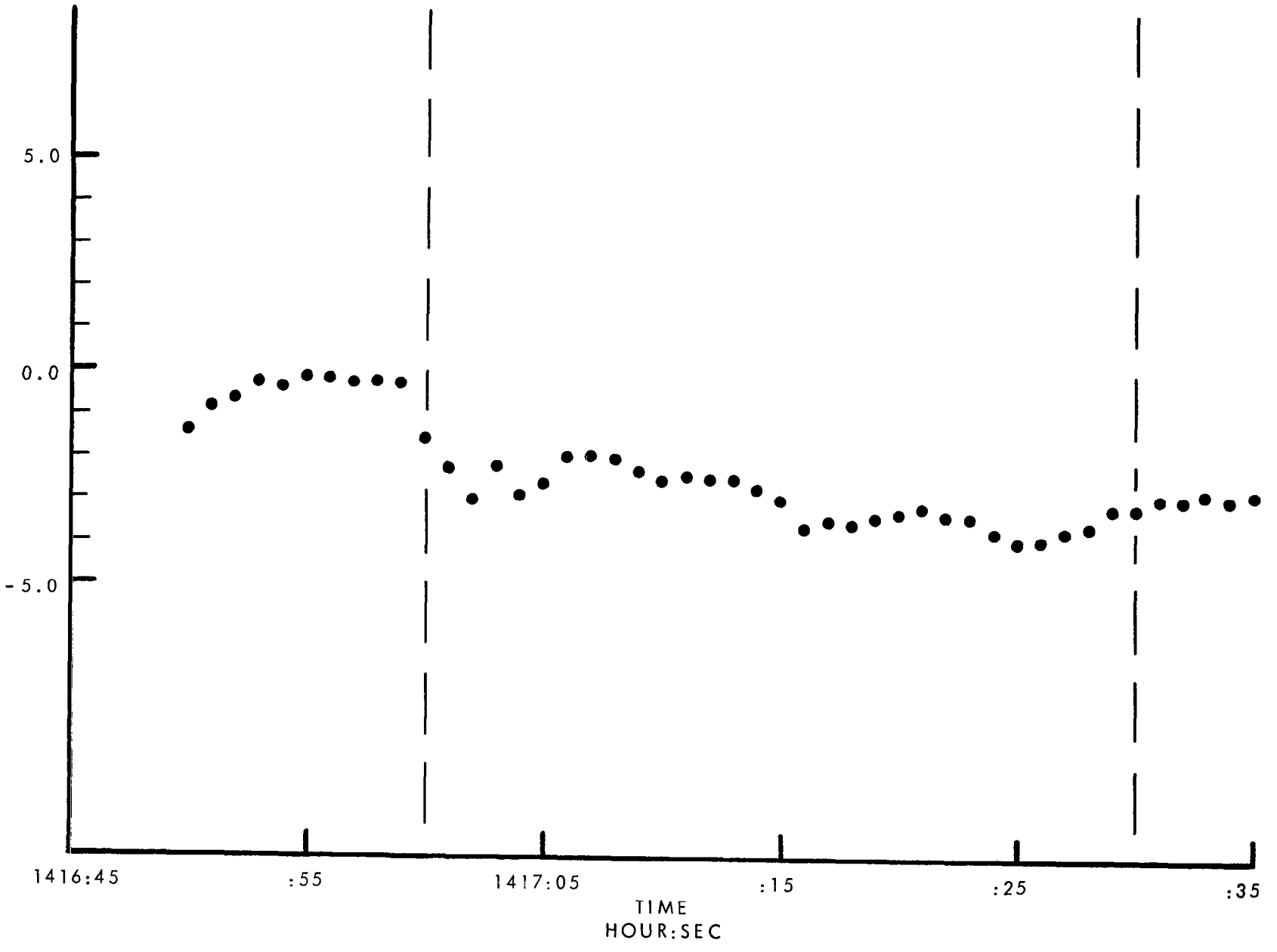

Figure 44. Disturbed Temperature In Cloud. Pass 1.
Firing S-II-14. MSU Aircraft.

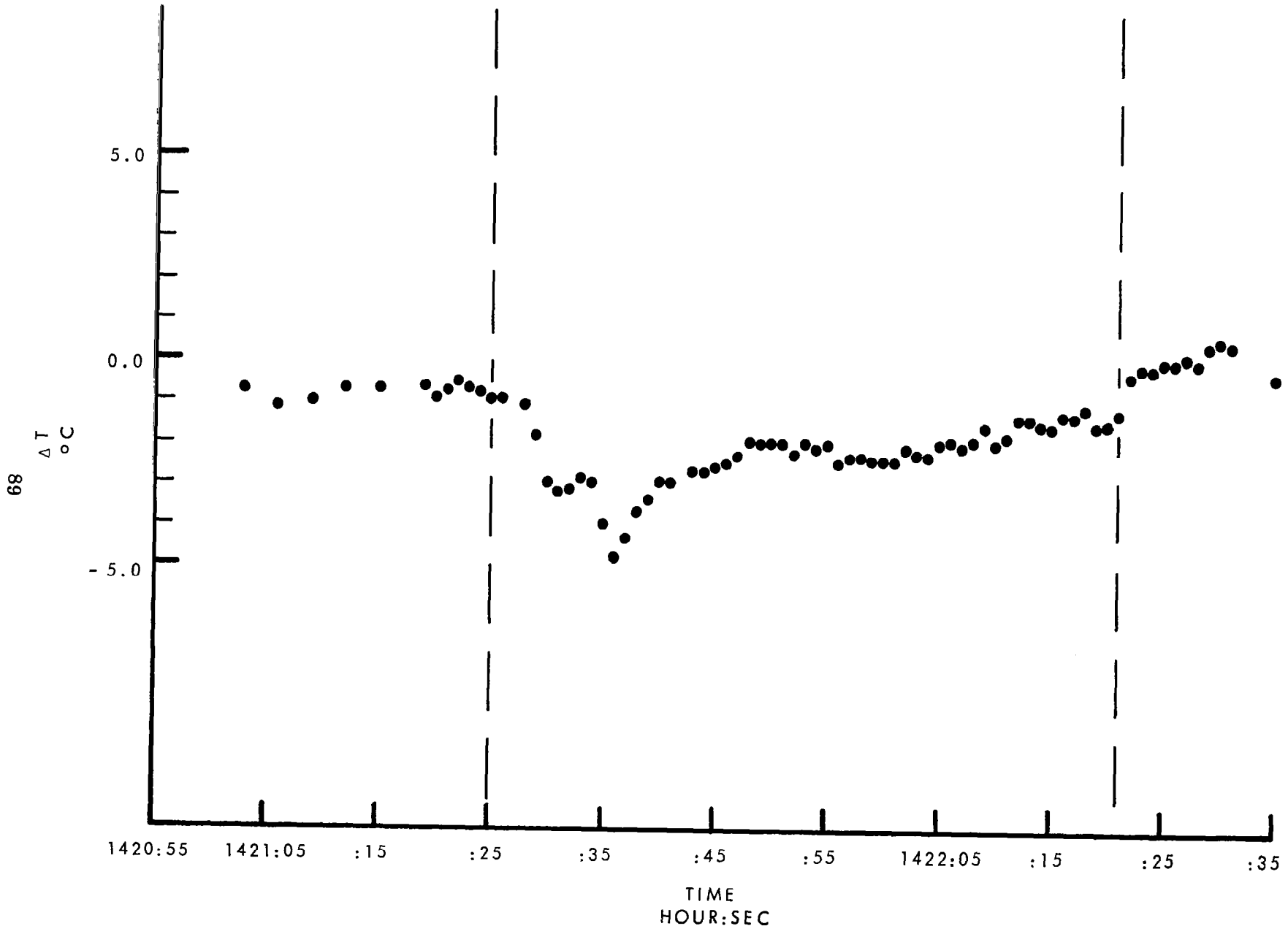

Figure 45. Disturbed Temperature In Cloud. Pass 2.
Firing S-II-14. MSU Aircraft.

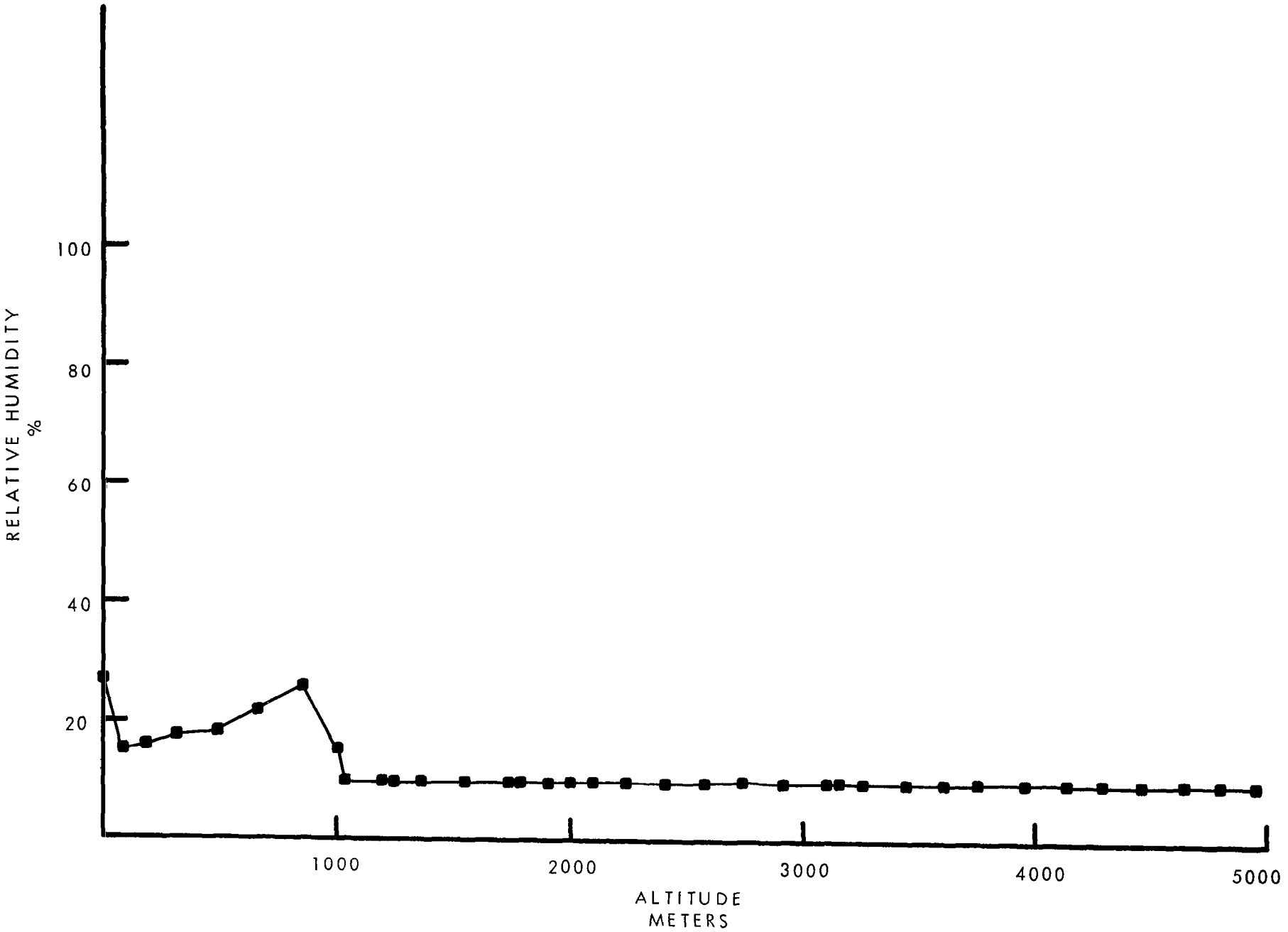

Figure 46. Radiosonde Relative Humidity Sounding.

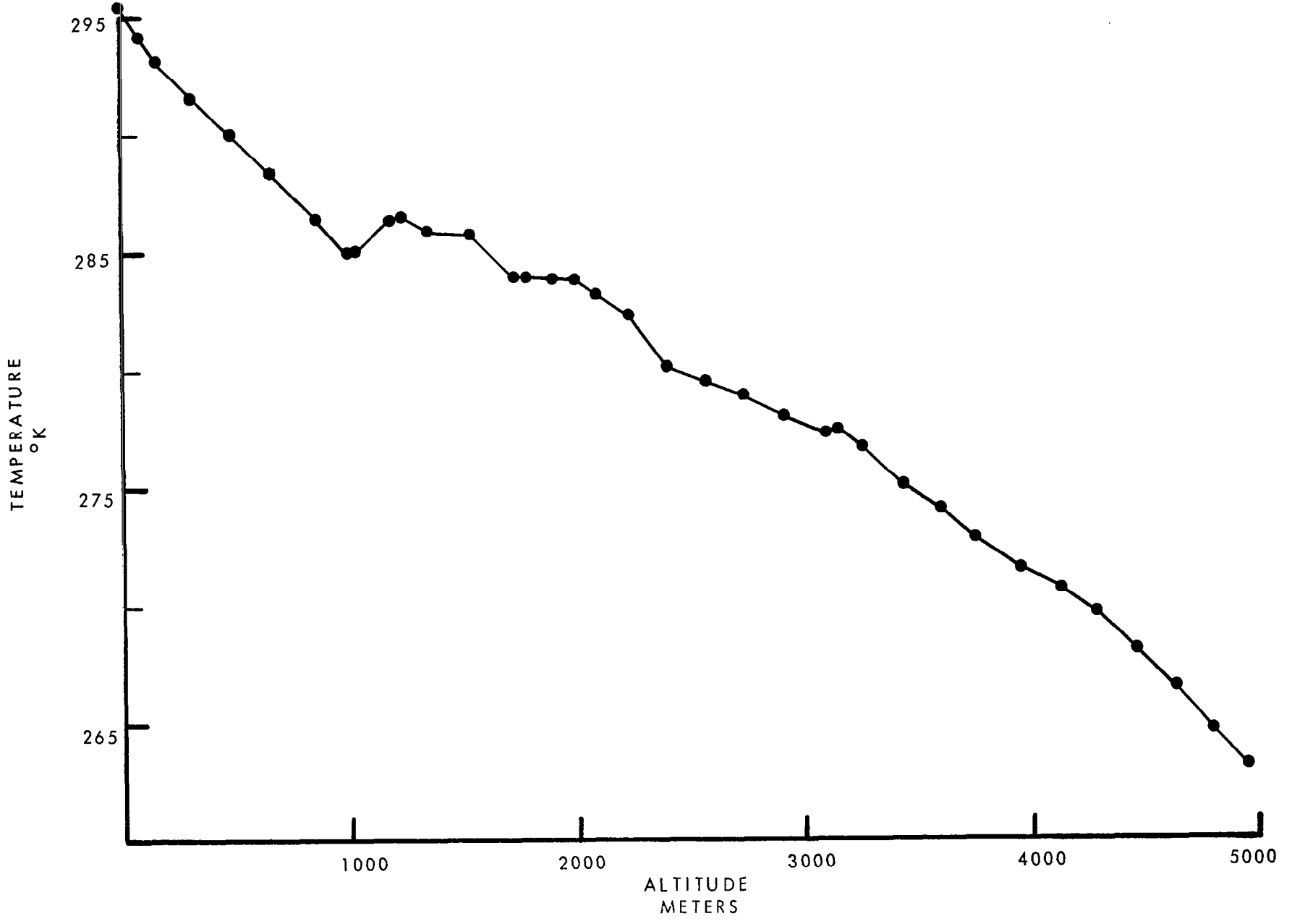

Figure 47. Radiosonde Temperature Sounding
Firing S-II-15.

Figure 48. Cloud Photograph 50 Seconds After Ignition. Firing S-II-15.

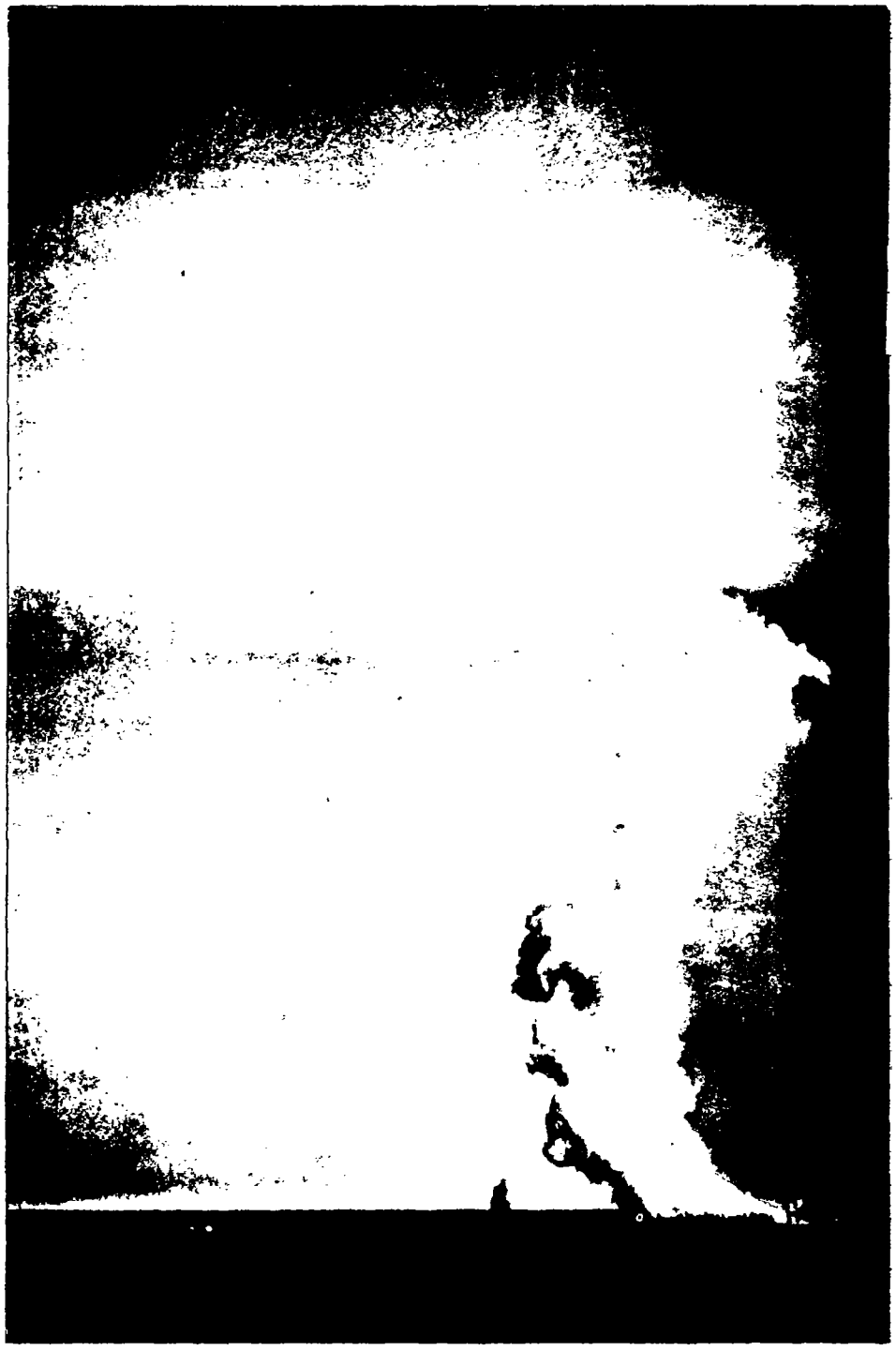

Figure 49. Cloud Photograph 200 Seconds After Ignition. Firing S-II-15.

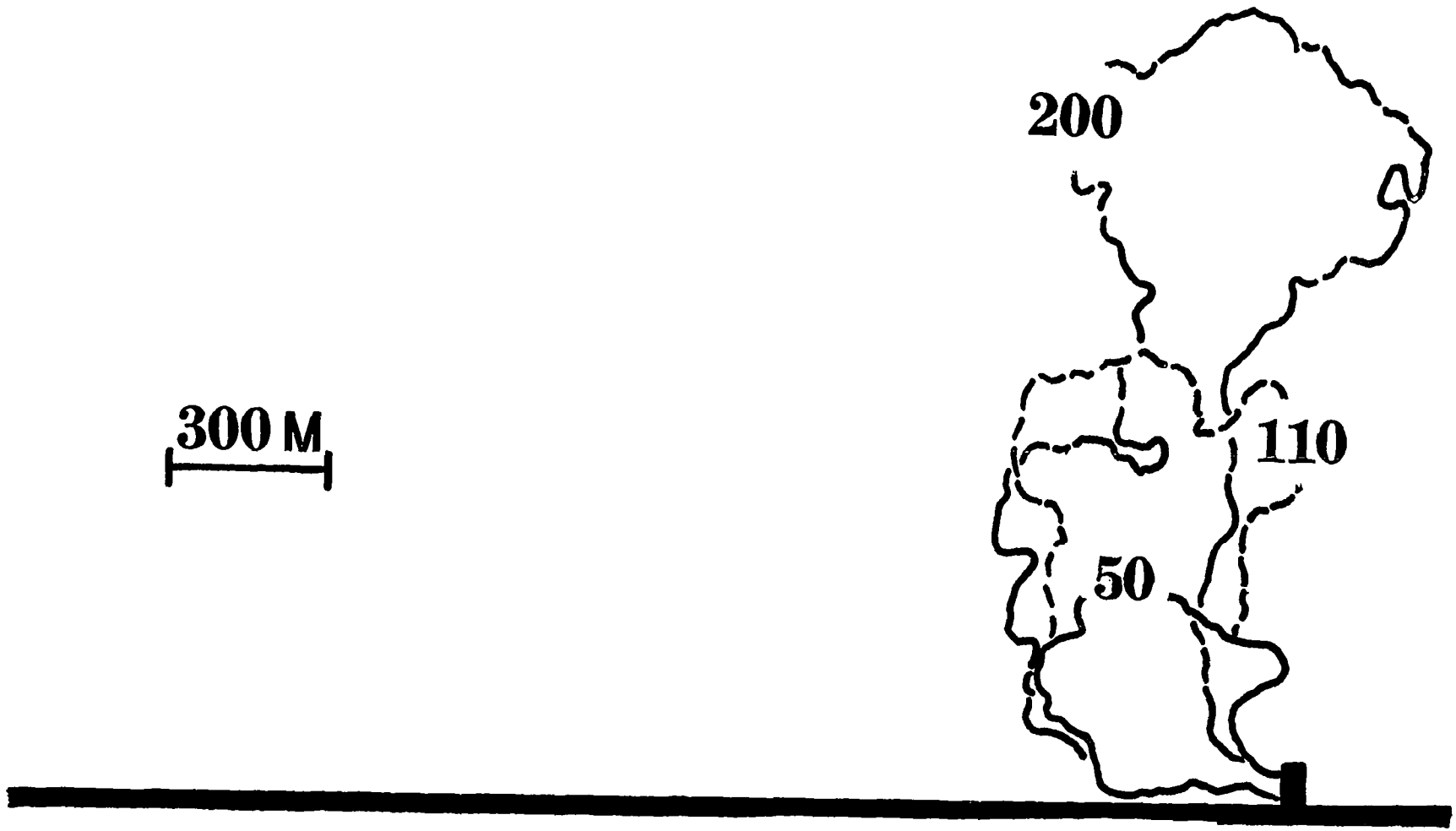

Figure 50. Rectified Cloud Geometry. Firing S-11-15.

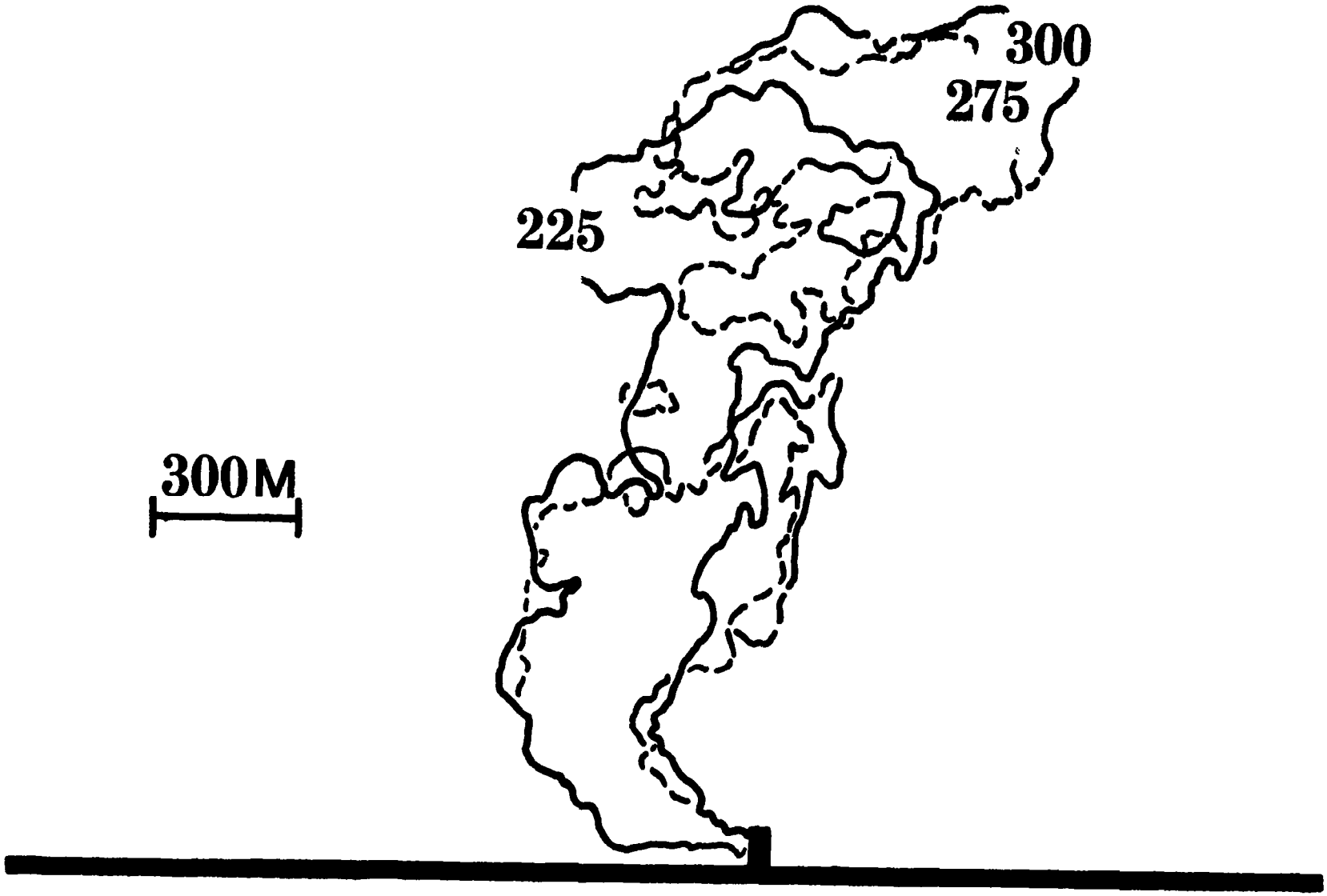

Figure 51. Rectified Cloud Geometry. Firing S-II-15.

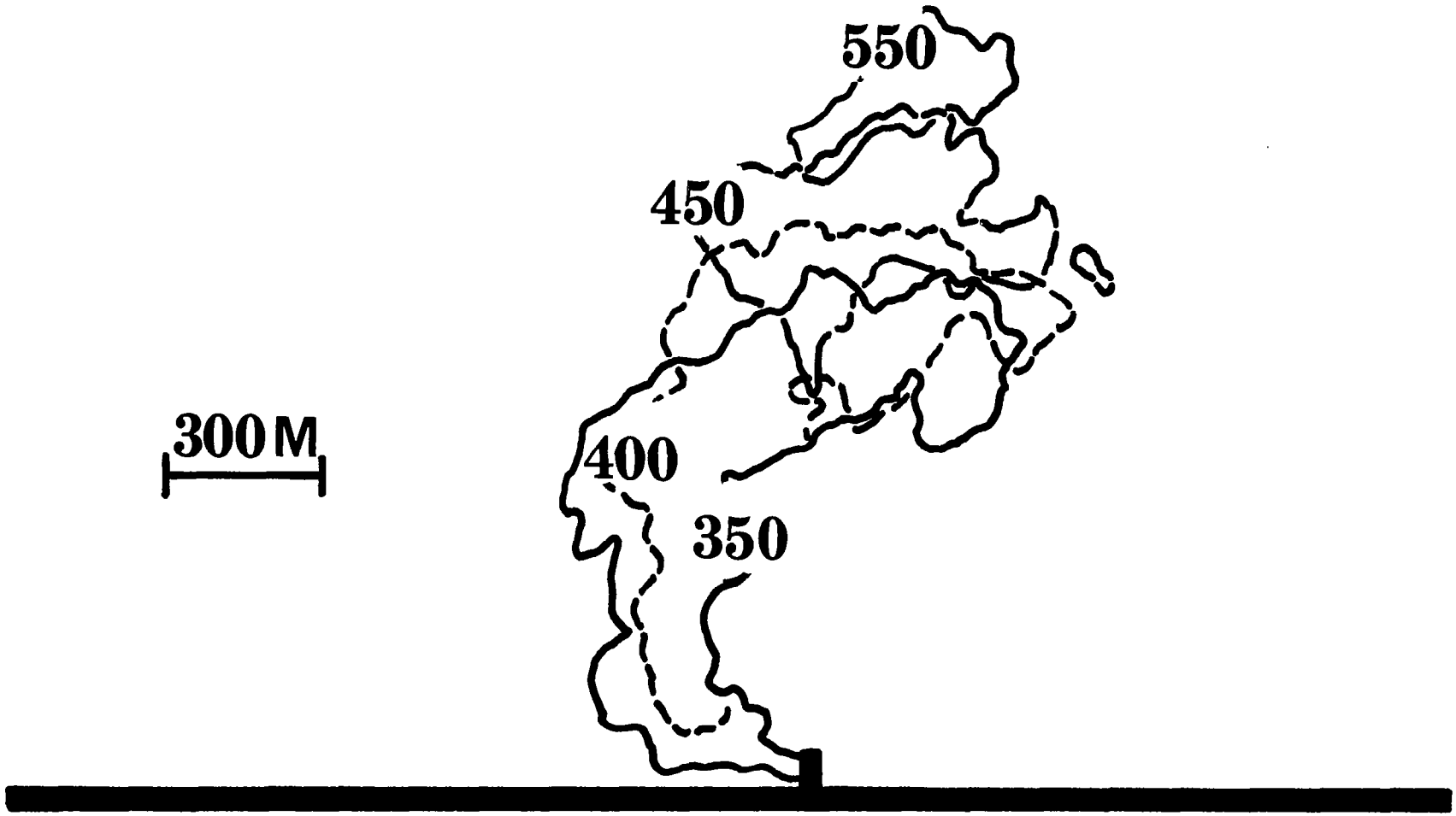

Figure 52. Rectified Cloud Geometry. Firing S-II-15.

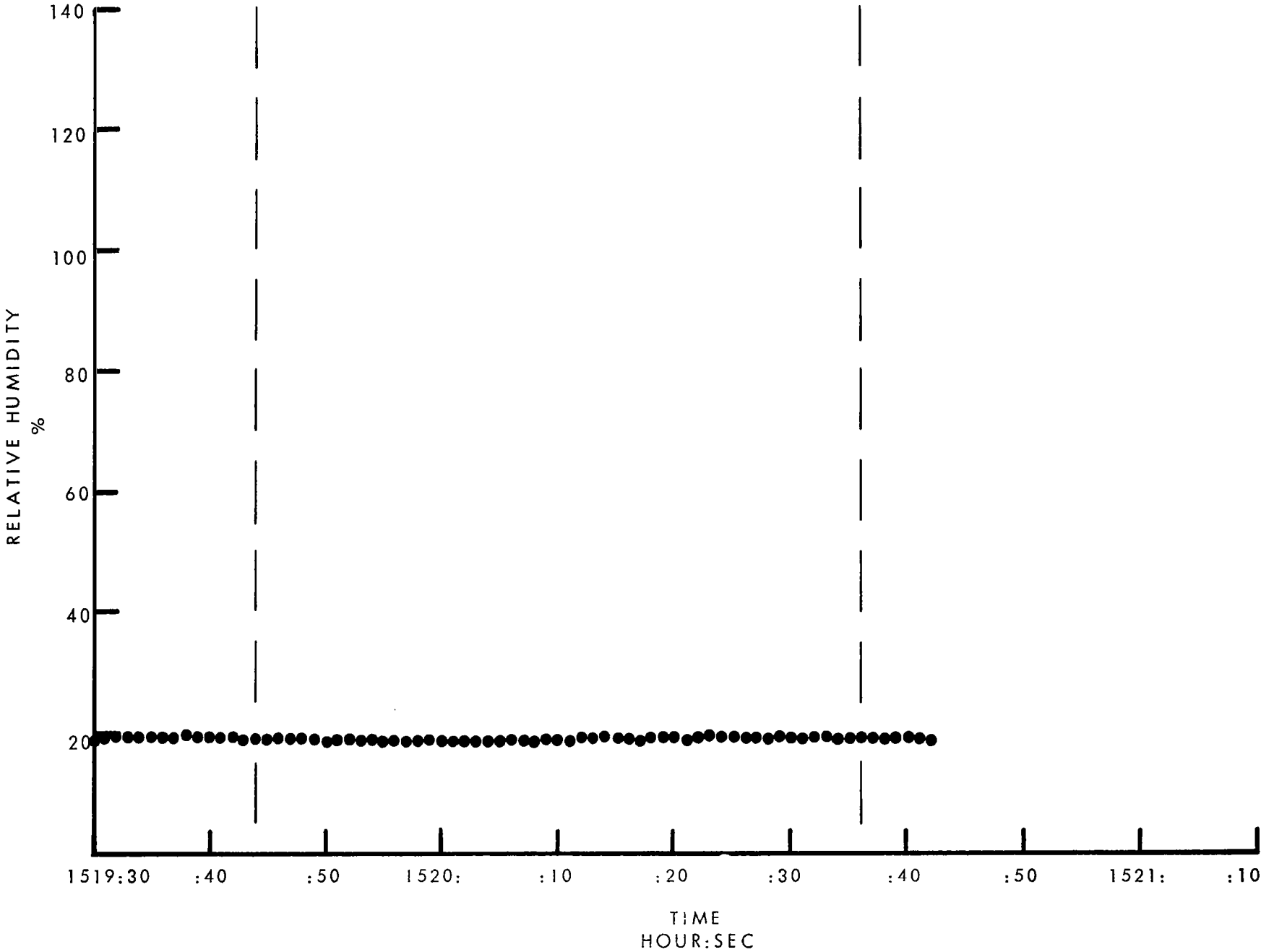

Figure 53. Relative Humidity In Cloud. Pass I.
Firing S-II-15. MSU Aircraft.

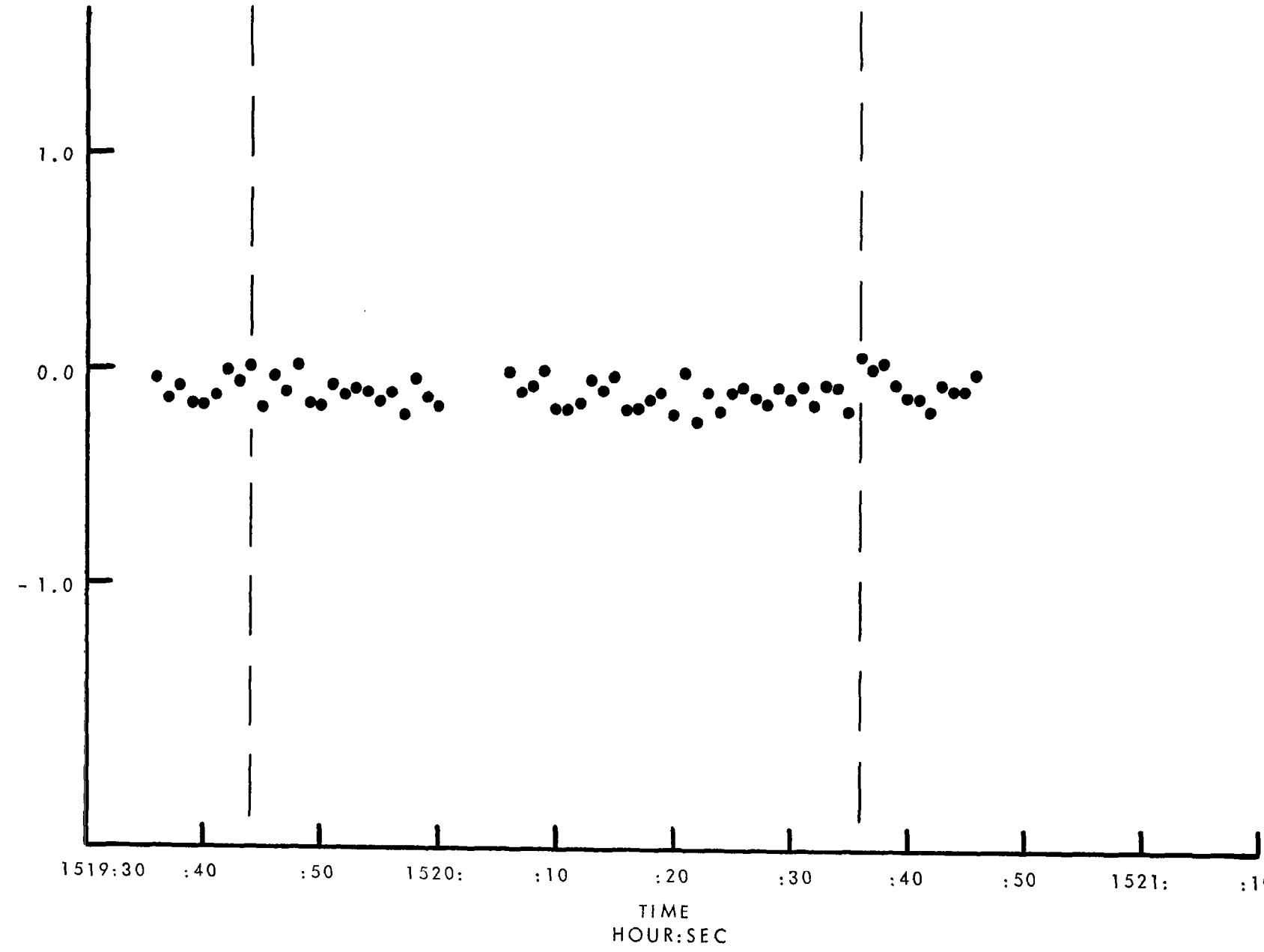

Figure 54. Disturbed Temperature In Cloud. Pass 1. Firing S-II-15. MSU Aircraft.

BIBLIOGRAPHY

(1) Berry, F.A., Bollay, E. and Beers, N.R., Handbook of Meteorology, McGraw-Hill Book Company, New York, 1945.

(2) Smith, M.R. and Johnson, R.A., "Application of Aerospace Data Acquisition Technology to Atmospheric Meteorological Investigations," Technology Utilization Ideas for the 70's and Beyond, Vol. 26, American Astronautical Society, 1970.